T.R.

GEBZE TECHNICAL UNIVERSITY

GRADUATE SCHOOL

PERFORMANCE EVALUATION OF EXISTING RC BUILDINGS IN SIVRICE-PUTURGE SEGMENT CONSIDERING LOCAL SITE CONDITIONS AND FAULT CHARACTERISTICS

FURKAN KANLI

A THESIS OF MASTER OF SCIENCE

DEPARTMENT OF CIVIL ENGINEERING

EARTHQUAKE AND STRTURAL ENGINEERING PROGRAM

ADVISOR: ASST. PROF. DR. ÜLGEN MERT

FEBRUARY 2025

T.R.
GEBZE TECHNICAL UNIVERSITY
GRADUATE SCHOOL

PERFORMANCE EVALUATION OF EXISTING RC BUILDINGS IN SIVRICE-PUTURGE SEGMENT CONSIDERING LOCAL SITE CONDITIONS AND FAULT CHARACTERISTICS

FURKAN KANLI

A THESIS OF MASTER OF SCIENCE
DEPARTMENT OF CIVIL ENGINEERING
EARTHQUAKE AND STRTURAL ENGINEERING PROGRAM

ADVISOR: ASST. PROF. DR. ÜLGEN MERT

FEBRUARY 2025

T.C.
GEBZE TEKNİK ÜNİVERSİTESİ
LİSANSÜSTÜ EĞİTİM ENSTİTÜSÜ

SİVRİCE-PÜTÜRGE SEGMENTİ ÜZERİNDEKİ MEVCUT BETONARME BİNALARIN YEREL ZEMİN KOŞULLARI VE FAY KARAKTERİSTİKLERİNE GÖRE PERFORMANS DEĞERLERLENDİRMESİ

FURKAN KANLI

YÜKSEK LİSANS TEZİ
İNŞAAT MÜHENDİSLİĞİ ANABİLİM DALI
DEPREM VE YAPI MÜHENDİSLİĞİ PROGRAMI

DANIŞMAN: DR. ÖĞR. ÜYESİ ÜLGEN MERT

FEBRUARY 2025

MASTER of SCIENCE JURY APPROVAL FORM

A thesis submitted by Furkan KANLI, defended on 21/02/2025 before the jury formed with the 03/02/2025 date and 2025/08 numbered decision of the GTU Graduate Administration Board, has been accepted as a MASTER of SCIENCE thesis in the Department of Civil Engineering, Earthquake and Structural Engineering Program.

JURY

MEMBER
(THESIS ADVISOR) : Asst. Prof. Dr. Ülgen MERT

MEMBER : Asst. Prof. Dr. Ebru HARMANDAR

MEMBER : Asst. Prof. Dr. Ahu KÖMEÇ

APPROVAL

Gebze Technical University Graduate Administration Board

…..…/…..…/..…..… date and ………/……... numbered decision.

SIGNATURE/SEAL

Beni bugünlere taşıyan
aileme ve her koşulda
sarsılmaz iradesiyle varlığını
sürdüren aziz Türk
milletine, bilimsel bir katkı
sunma dileğiyle…

ABSTRACT

Since ancient times, construction has been a cornerstone of civilizations, continually adapting to natural disasters, especially earthquakes. In response, engineering advancements have strengthened seismic resilience, shaping modern building design based on scientific research and regulations.

Turkey, situated on the highly active Alp-Himalayan Seismic Belt, frequently experiences earthquakes. Its seismicity is shaped by the North Anatolian Fault Zone (NAFZ), the East Anatolian Fault Zone (EAFZ), and extensional tectonic regimes in Western Anatolia.

Within this study, one of the two major fault zones affecting Malatya, the Malatya-Ovacık Fault Zone (MOFZ), specifically its Sivrice-Pütürge segment, was examined. Due to seismic uncertainties, the entire fault zone was analyzed, modeled using open-source Geographic Information Systems (GIS) software, and subjected to Probabilistic Seismic Hazard Analysis (PSHA). This analysis produced a seismic hazard map illustrating peak ground acceleration (PGA) values and an elastic spectrum with a 10% probability of exceedance in 50 years. Then a design spectrum was developed for the DD-2 Earthquake Ground Motion Level in accordance with the Turkish Building Earthquake Code (TBEC-2018), using soil classification data from nearby AFAD accelerometer stations. This design spectrum was compared with the seismic hazard spectrum, and the one with higher acceleration values was selected for further analysis. Earthquake records were selected based on the Simple Scaling Method defined in TBEC-2018, and these records were scaled according to the determined spectrum. A total of 11 real earthquake records, including those representing near-fault effects that could impact Malatya, were identified. The selected records were further amplified for directivity effects considering their influence on Malatya Airport and surrounding potential settlement areas, ultimately forming two sets of earthquake records for analysis.

The seismic performance assessment of structures was conducted using the Nonlinear Time History Analysis Method. Three reinforced concrete buildings in Malatya were selected for the analyses, and their numerical models were created in a computational environment. The investigated buildings included a low-rise public library, a mid-rise public office building, and a high-rise residential building. According to the structural system classification defined in TBEC-2018, these buildings were evaluated as structures either with only moment-resisting reinforced concrete frames or with a combination of frames and reinforced concrete shear walls.

As a result of the conducted analyses, all obtained data were processed, and the effects of directivity on structures with different story levels and natural vibration periods were identified.

Keywords: Probabilistic Seismic Hazard Analysis (PSHA), Nonlinear Time History Analysis, Directivity Effects, Simple Scaling Method, Malatya-Ovacık Fault Zone (MOFZ)

ÖZET

Milattan yüzyıllar öncesine dayanan ve günümüzde hâlâ medeniyetlerin kuruluşu, gelişimi ve ilerlemesinde temel bir unsur olan yapı inşası, insanlığın tarih boyunca karşılaştığı doğal afetler, özellikle depremler karşısında sürekli bir evrim geçirmiştir. Bu süreçte, yapıların sismik dayanıklılığını artırmaya yönelik çeşitli mühendislik yaklaşımları geliştirilmiş ve bilimsel çalışmalar ile yönetmelikler doğrultusunda modern yapı tasarım kriterleri oluşturulmuştur.

Türkiye, Alp-Himalaya Sismik Kuşağı üzerinde yer almakta olup, dünyanın en aktif deprem bölgelerinden biri olması nedeniyle sık sık depremler meydana gelmektedir. Türkiye'nin sismotektonik yapısını belirleyen ana unsurlar arasında Kuzey Anadolu Fay Zonu (KAFZ), Doğu Anadolu Fay Zonu (DAFZ) ve Batı Anadolu'daki genişlemeli tektonik rejimler bulunmaktadır.

Bu çalışma kapsamında, öncelikle Malatya ilini etkileyen iki büyük fay zonundan biri olan Malatya-Ovacık Fay Zonu'nun (MOFZ) Sivrice-Pütürge segmenti incelenmiş, segmentteki sismik belirsizlikler nedeniyle fay zonunun tamamı kapsamlı bir şekilde ele alınmış ve açık kaynaklı Coğrafi Bilgi Sistemleri (CBS) yazılımları kullanılarak modellenmiş, ardından Olasılıksal Sismik Tehlike Analizi (PSHA) gerçekleştirilmiştir. Bu analizler sonucunda, fay bazlı en büyük yer ivmesi (PGA) değerlerini gösteren bir deprem tehlike haritası oluşturulmuş ve 50 yılda aşılma olasılığı %10 olan deprem yer hareketi düzeyi için bir elastik spektrum elde edilmiştir. Daha sonra, Malatya-Merkez'de belirlenen bir lokasyon ve lokasyona en yakın AFAD ivmeölçer istasyonlarından alınan yerel zemin sınıfı verileri baz alınarak, TBDY-2018 yönetmeliği doğrultusunda, DD-2 Deprem Yer Hareketi Düzeyi esas alınarak bir tasarım spektrumu oluşturulmuştur. Bu spektrum ile sismik tehlike analizinden elde edilen spektrum karşılaştırılmış ve daha yüksek ivmelere sahip spektrum temel alınarak analizler gerçekleştirilmiştir.

TBDY-2018'de tanımlanan Basit Ölçeklendirme Yöntemi ile deprem kayıtları seçilmiş ve belirlenen spektruma göre ölçeklenmiştir. Malatya ilinde etkili olabilecek yakın saha etkilerini içeren deprem kayıtları dikkate alınarak toplamda 11 gerçek deprem kaydı belirlenmiştir. Seçilen kayıtlar, Malatya Havalimanı ve çevresindeki olası yerleşim alanları için doğrultu etkisi ile arttırılmış ve sonuç olarak analizler için iki takım deprem kaydı hazırlanmıştır.

Yapıların sismik performans değerlendirmesi, Zaman Tanım Alanında Doğrusal Olmayan Analiz Yöntemi kullanılarak gerçekleştirilmiştir. Malatya'da bulunan üç adet betonarme bina analiz için seçilmiş ve bilgisayar ortamında nümerik modelleri oluşturulmuştur. İncelenen binalar, az katlı bir devlet kütüphanesi, orta katlı bir kamu kurumu binası ve yüksek katlı bir konut yapısı olup, TBDY-2018'de yapılan taşıyıcı sistem sınıflandırmasına göre, yalnızca moment aktaran betonarme çerçevelere sahip olan yapılar ile hem çerçeve hem de betonarme perde içeren sistemler kapsamında değerlendirilmiştir.

Gerçekleştirilen analizler sonucunda, elde edilen tüm veriler işlenmiş ve doğrultu etkisinin farklı kat seviyelerine ve doğal titreşim periyotlarına sahip yapılar üzerindeki etkileri belirlenmiştir.

Anahtar Kelimeler: Olasılıksal Sismik Tehlike Analizi (PSHA), Zaman Tanım Alanında Doğrusal Olmayan Analiz, Doğrultu Etkisi, Basit Ölçeklendirme Yöntemi, Malatya-Ovacık Fay Zonu (MOFZ)

ACKNOWLEDGEMENTS

I extend my deepest gratitude and appreciation to my esteemed advisor, Dr. Ülgen MERT, who has guided me throughout my studies and illuminated my path with his academic knowledge and expertise. His patience, mentorship, and unwavering support have been invaluable to me.

I would also like to sincerely thank Assoc. Prof. Dr. Abdullah Can ZÜLFİKAR, an expert in Seismic Hazard and Risk Assessments, for his continuous support and patience throughout my coursework, as well as for enabling me to work on the *REDACt* project and obtain a scholarship.

My heartfelt thanks go to Mr. Kemal Burak HANOĞLU, a highly respected senior in my profession and my professional mentor, whose perspectives and principles have greatly influenced me and who has always been generous in sharing his knowledge and experience.

I am deeply grateful to Ms. Yeter APAYDIN, my first teacher, who taught me the true importance of discipline, respect, and lifelong learning.

Lastly, I express my endless gratitude to my mother, Emine KANLI, who has supported me at every stage with her unwavering dedication, my father, Metin KANLI, whose sacrifices and guidance have always led me forward, and my sister, İrem Çağla KANLI SANDIK, whose presence has been a constant source of motivation.

TABLE OF CONTENTS

LIST OF SYMBOLS AND ABBREVIATIONS

M_w	:	Earthquake Magnitude
V_{s30}	:	The average shear wave velocity in the top 30 meters of soil
PGA	:	Peak Ground Acceleration
$S_{0.3}$	:	Short-period spectral acceleration
$S_{1.0}$	:	1.0-second period spectral acceleration
S_{DS}	:	Short-period design spectral acceleration coefficient
S_{D1}	:	Design spectral acceleration coefficient at a 1.0-second period
T_A	:	First Corner Period in Elastic Spectrum
T_B	:	Second Corner Period in Elastic Spectrum
T_L	:	Long Period in Elastic Spectrum
T_p	:	Fundamental period of a structure
K	:	Curvature of a frame member
Lp	:	Plastic Hinge Length
θ_p	:	Plastic Rotation
C	:	Damping matrix
α	:	Mass-proportional damping coefficient
β	:	Stiffness-proportional damping coefficient
M	:	Mass matrix
K	:	Stiffness matrix

LIST OF FIGURES

LIST OF TABLES

1. INTRODUCTION

Earthquakes are among the most devastating natural disasters, causing significant loss of life and property worldwide. This study examines the impact of earthquakes, particularly in regions located near active fault lines. Malatya Province is one of the areas with a high seismic risk due to its geographical location and proximity to active faults. In this context, assessing the seismic performance of public buildings in Malatya is of critical importance to ensure their safety during and after potential earthquakes.

The objective of this study is to evaluate the seismic performance of public buildings in Malatya, assess their compliance with current seismic regulations (TBEC-2018), and propose necessary measures to enhance their earthquake resilience. To achieve this, the study first analyzes the geological characteristics and fault structures of the region. Then, probabilistic seismic hazard analyses (PSHA) are conducted to assess local earthquake risks, identifying key parameters that influence the seismic behavior of structures.

The scope of this research focuses on seismic performance assessment procedures for reinforced concrete structures, linear and nonlinear analysis methods, soil properties, damage limits of structural components, and performance levels. Throughout the study, analyses will be performed based on the criteria outlined in TBEC-2018, providing a comprehensive assessment of the existing condition of these structures. Consequently, this study aims to outline a roadmap for enhancing the seismic safety of buildings in earthquake-prone areas.

Ultimately, this research is expected to offer a new perspective on seismic performance assessments and serve as a reference for future studies in this field. The findings obtained from the case study of Malatya will contribute to the development of applicable measures both locally and in other earthquake-prone regions.

2. SEISMIC HAZARD ANALYSIS FOR MALATYA PROVINCE

2.1. Geographical Background of Malatya Province and Fault / Seismicity Characteristics

2.1.1. Geographical Features of Malatya Province

Malatya, situated in the Eastern Anatolia Region of Turkey, experiences significant seismic activity. The region's geological structure has been shaped by the influence of the Alpine Orogeny and encompasses a diverse range of soil types. During the Alpine Orogeny, fractures and folds led to both tectonic uplifts and subsidence plains in the area. These characteristics have directly influenced the seismic behavior and soil properties of the region.

Soil Characterization

Quaternary-aged alluvial sediments in Malatya consist of materials transported by major rivers such as the Tohma River and the Euphrates. These soils are typically characterized by loose sand, gravel, and silt layers, which have low bearing capacity and high liquefaction potential. Fluvial sediments, predominantly found in floodplain areas, are fine-grained and exhibit high heterogeneity, often presenting weak engineering properties. Additionally, volcanic-origin tuffs and limestones, formed through volcanic activity, are present in certain areas. These layers display moderate-to-high strength, but tuffs can exhibit brittle characteristics with extensive crack networks.

Seismic Hazard and Earthquake Risk

Malatya faces a considerable seismic hazard due to its location near the East Anatolian Fault Zone. Data obtained from earthquake observation stations established by Turkey’s Disaster and Emergency Management Authority (AFAD) indicate the high seismic activity in the region. Particularly, shallow-focus earthquakes pose a significant risk of surface damage. Additionally, the effects of soil amplification can increase seismic wave amplitudes, causing greater damage to structures.

Dynamic soil properties play a critical role in understanding seismic behavior. Shear modulus (*G*), which measures the stiffness of the soil against seismic motion, ranges between 30−100 MPa at the surface, as revealed by MASW, **Figure 2.1**, tests conducted in the Battalgazi region. The damping ratio, indicating energy dissipation in soils, has been measured between 2−5% in silty and sandy soils. Furthermore, V_{s30} (seismic wave velocity), a key parameter for soil classification, generally falls between 200−400 m/s in the Malatya region. These values indicate that most soils in the area are classified as "D" class, representing moderate to loose soils.

As a result of this literature review, although the local soil class can be determined as ZD according to TBEC-2018, in future studies, accelerometer stations near the Malatya-Center location will be scanned from the AFAD database, and the appropriate local soil class will be selected.

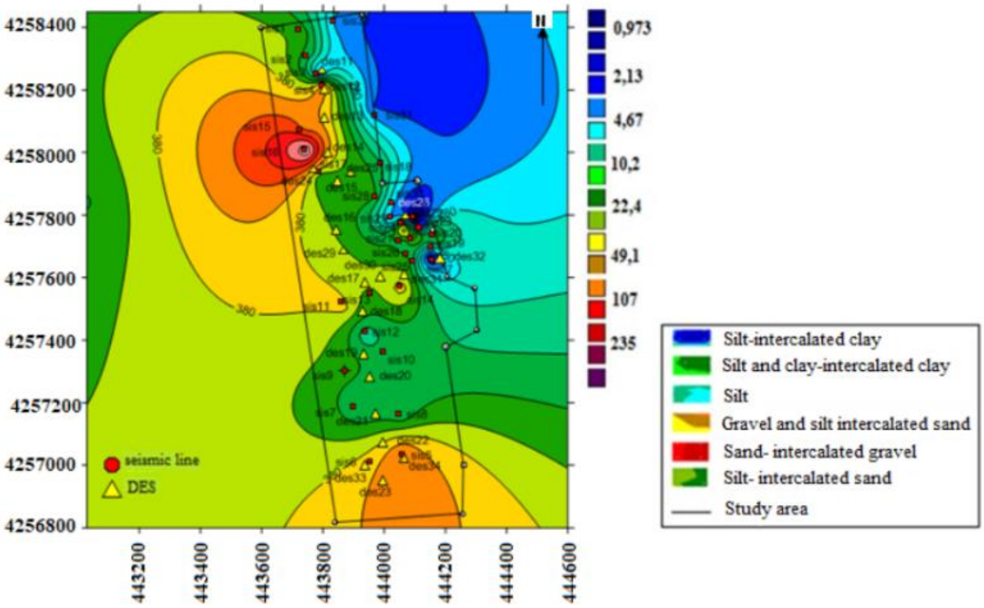

Figure 2.1: The lithological distribution of the study area according to the MASW test results.

Soil Properties

The soil characteristics of Malatya exhibit significant diversity because of geological processes. Specifically, Brown Forest Soils and Non-Calcareous Brown Soils are prominent soil types in the province. In volcanic areas, high amounts of limestone and tuff are observed, which also influences soil properties **(Ö. Yıldız, 2022)**.

Local site conditions pose certain engineering challenges. Site amplification is a notable concern in alluvial soils, where low shear wave velocities amplify seismic wave amplitudes, increasing the potential for structural damage. Settlement problems are also prevalent in soft alluvial soils, necessitating careful settlement analyses to prevent differential settlements that could compromise structural stability. In addition, high-plasticity clays in some areas exhibit swelling behavior when they absorb water. This swelling can lead to stress and deformation in building foundations, posing long-term risks to structural integrity **(Önal & Ceylan, 2020)**.

2.1.2. Characteristics of Malatya-Ovacık Fault Zone (MOFZ)

The Malatya-Ovacık Fault Zone (MOFZ), the primary seismic source of the region, will be utilized in this study. The results of the Probabilistic Seismic Hazard Analysis (PSHA) will be applied to Nonlinear Structural Performance Analyses.

In a study conducted by Sevimli and Ünlügenç in 2022, the Yazıhan Segment of the Malatya-Ovacık Fault Zone (MOFZ) was examined, focusing on its seismic risk and seismotectonic characteristics. The study assessed the recurrence interval and earthquake probability of past events using statistical analysis methods. The average recurrence interval for large earthquakes in this segment was estimated to be approximately 2000 years, indicating its long-term potential for generating major earthquakes.

However, according to Gamma and Weibull distribution models, the likelihood of a significant earthquake within the next 50 years is low. Nevertheless, seismic risk cannot be entirely disregarded, as the segment has shown prolonged energy accumulation.

A TÜBİTAK project conducted by Karabacak and Sançar between 2015 and 2018 focused on the Malatya Fault (Malatya-Ovacık Fault Zone), investigating its geological slip rate, paleoseismic history, and seismic potential. The annual slip rate of the Malatya Fault was calculated to be approximately 1.2–1.5 mm/year. Although this rate is lower than that of the East Anatolian Fault Zone (EAFZ), it demonstrates the fault's potential for long-term energy accumulation.

At least 3–4 major earthquakes have been identified along the fault in the past. The most recent major earthquake is estimated to have occurred between 965–549 BCE. The average recurrence interval for earthquakes was calculated to be 2275 ± 605 years.

The deformation characteristics of the Malatya Fault indicates its long-term activity. Surface ruptures observed along its segments support the potential for major earthquakes.

Another significant study was conducted by Zabcı et al. between 2014 and 2017, aiming to understand the past seismic behavior and deformation characteristics of the fault. The annual slip rate in the zone was estimated to range between 1.0–1.4 mm/year, indicating the fault's potential for accumulating energy and generating significant earthquakes over the long term.

At least three major earthquakes have been identified along the fault in the past. The most recent major earthquake occurred approximately 2000 years ago, with a recurrence interval estimated to be around 2000–2500 years.

The geomorphic features observed along the fault zone (e.g., channel offsets, ridges) confirm its activity. The deformation characteristics of the fault segments reveal that past major earthquakes caused surface ruptures **(D. Y. Yıldız et al., 2023)**.

For this fault zone, a probabilistic seismic hazard analysis will be conducted, and the results for the selected coordinates in Malatya-Center will be compared with those derived from the Turkish Interactive Seismic Hazard Map. The most critical scenario will be identified, and earthquake records to be utilized in the structural performance analysis will be selected based on this scenario.

2.1.3. Directivity Effect

Within the scope of this study, structures located in Malatya city center will be hypothetically relocated to the potential settlement area near the airport, which lies within the boundaries of directivity effects (the distance of the nearest fault rupture to the potential settlement area near the airport is 8 km.), **Figure 2.2**, and their performance under these effects will also be examined. Detailed information regarding the structures and city center will be provided in subsequent sections.

Figure 2.2: The distance of Malatya city center and the potential settlement area near the airport to the nearest fault rupture.

The directivity effect is a phenomenon observed during fault rupture, where seismic energy becomes concentrated in the direction of rupture propagation. This effect impacts the amplitude, frequency content, and duration of seismic waves, leading to stronger ground motions in certain directions compared to others **(Mavroeidis & Papageorgiou, 2003)**.

In the directions where the fault's directivity effect is concentrated, higher peak ground acceleration (PGA) values are observed in acceleration records. This is a result of energy being focused on that direction **(Somerville et al., n.d.)**.

The directivity effect is particularly significant in directions parallel to the fault plane (e.g., in structures located at close distances), where it causes a pronounced velocity pulse. Such velocity pulses are critical sources of loading for structures.

The propagation of this effect along with the fault can be categorized into two types: Forward Directivity and Backward Directivity.

Forward Directivity: In this case, the fault rupture generates high-amplitude and short-duration seismic waves in the direction of motion. These waves often produce a pulse with large energy content, which can be particularly damaging to structures, **Figure 2.3**.

Backward Directivity: In this case, when the fault rupture propagates away from the direction of motion, it generates seismic waves with lower amplitude and longer duration.

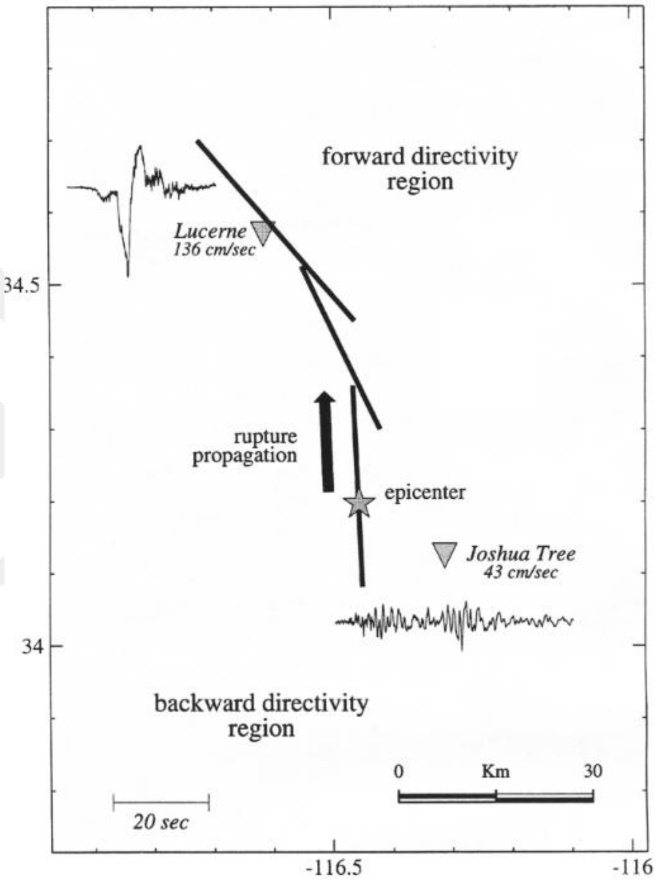

Figure 2.3: 1992 Landers Earthquake, the forward and backward directivity effects relative to the earthquake epicenter and their differences as reflected in velocity/time graphs (Somerville et al., n.d.).

In the Malatya-Ovacık Fault Zone, which exemplifies a fault generating directivity pulses, the strike-normal component (motion perpendicular to the fault) tends to be more pronounced than the strike-parallel component (motion parallel to the fault) under forward directivity conditions. This difference becomes particularly significant at periods of 0.6 seconds and above. The destructive impact of such earthquake accelerations is more pronounced on medium- and high-rise buildings.

In the study conducted by Moghimi and Akkar (2017), the effects of directivity on earthquake acceleration records were investigated, and models used for determining amplification ratios were developed. The study emphasized that pulse-type ground motions with directivity effects cause significant amplification in medium to long period ranges, increasing the inelastic demands on structures **(Vassiliou & Makris, 2011)**.

Deterministic and Probabilistic Seismic Hazard Analyses (DSHA and PSHA) were employed to evaluate various earthquake scenarios, and amplification ratios were examined based on these scenarios. The analyses explored the role of parameters such as source-to-site geometry, slip rate, and fault magnitude on directivity effects. A regular grid was established around the fault, and scenarios involving faults ranging from 20 to 300 km in length with magnitudes between Mw=6.25 and Mw=7.5 were considered.

Table 2.1: Maximum and median amplification level at T=4 sec for the faults with SR=0.5, 1 and 2cm/year CHS-13 model **(Moghimi & Akkar, 2017)**.

	10% in 50 year exceedance (475 year RP)		2% in 50 year exceedance (2475 year RP)	
	AMP_{max}(T=4sec)	AMP_{median}(T=4sec)	AMP_{max}(T=4sec)	AMP_{median}(T=4sec)
SR=0.5	1.45	1.13	1.52	1.15
SR=1.0	1.47	1.14	1.5	1.15
SR=2.0	1.52	1.15	1.53	1.15

The CHS-13 model utilizes the Direct Point Parameter (DPP) for determining directivity effects and is adapted from the Chiou and Youngs (2014) Ground Motion Prediction Equation, which is one of the recommended ground motion prediction equations for use in Turkey. Because of this, based on the seismic hazard analyses conducted in the study, amplification ratios were computed for various slip rates and ground motion levels, with the results specifically presented for the CHS-13 model, **Table 2.1**.

For the smallest slip rate (SR=0.5 cm/year), the average amplification ratios of both models were evaluated across all ground motion levels, because, according to the data obtained from the Malatya Ovacık Fault Zone (MOFZ), even the highest slip rate is lower than 0.5 cm/year. Consequently, an amplification ratio of 13% was decided to be applied to the selected earthquake records.

2.2. Probabilistic Seismic Hazard Analysis (PSHA)

Probabilistic Seismic Hazard Analysis (PSHA) is a statistical method used to determine the potential effects of earthquakes in a region in terms of magnitude, frequency, and intensity. This analysis estimates the probability of a structure exceeding a specific ground acceleration level within a given time frame by considering earthquakes of various magnitudes and their probabilities. PSHA is a critical tool in assessing seismic risks and defining design standards in engineering and urban planning.

Seismic Hazard Analyses were performed using the R-CRISIS v20.3.0 software, developed by Instituto de Ingeniería – Universidad Nacional Autónoma de México and Evaluación de Riesgos Naturales (ERN).

R-CRISIS is a Windows-based software designed for conducting probabilistic seismic hazard analysis through a fully probabilistic methodology. It enables the computation of results in various forms, such as exceedance probability curves and stochastic event sets.

Seismic Hazard Analysis starts with defining the seismotectonic region, identifying active faults, fault mechanisms, lengths, and slip rates to model seismic hazards accurately.

2.2.1. Turkey Map and Generation of City Coordinates

In this study, the Turkey map data was obtained in Geographic Information Systems (GIS)-compatible shape file (.shp) format from the SimpleMaps.com™ platform for use in seismic hazard analysis. The platform provides interactive and customizable HTML5 and JavaScript ®-based maps and offers a comprehensive database containing up-to-date and accurate data on cities and towns worldwide.

The coordinates of city centers in Turkey were assigned using Google Maps® and Google Earth® service providers. These coordinates were integrated into the R-CRISIS software by creating a file in ASCII File (.asc) format.

The Turkey map and city coordinates used for seismic hazard analysis are presented in **Figure 2.4**.

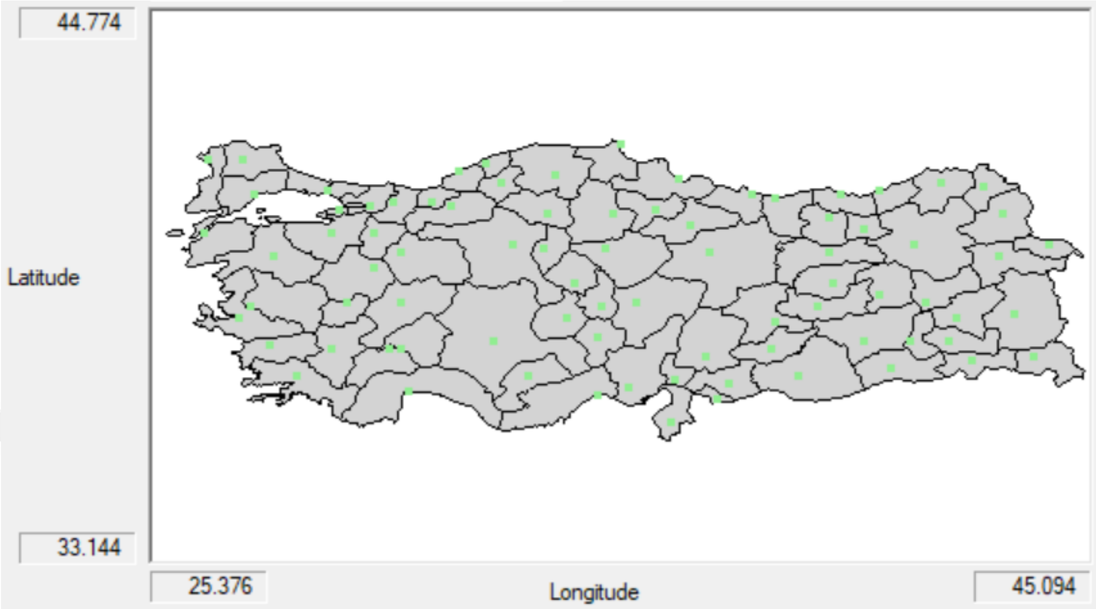

Figure 2.4: The Turkey map and city coordinates

2.2.2. The Active Faults of Eurasia Database (AFEAD)

The Active Faults of Eurasia Database (AFEAD) is a large-scale geospatial dataset that comprehensively compiles active fault systems across the Eurasian continent and is structured for spatial analysis. AFEAD contains 48,205 active fault records, providing spatial resolution suitable for mapping at a 1:1,000,000 scale. Each fault entry is detailed with parameters such as fault type, confidence level in activity, slip rate, last movement age, total displacement amount, and references to source publications **(Zelenin et al., 2022)**.

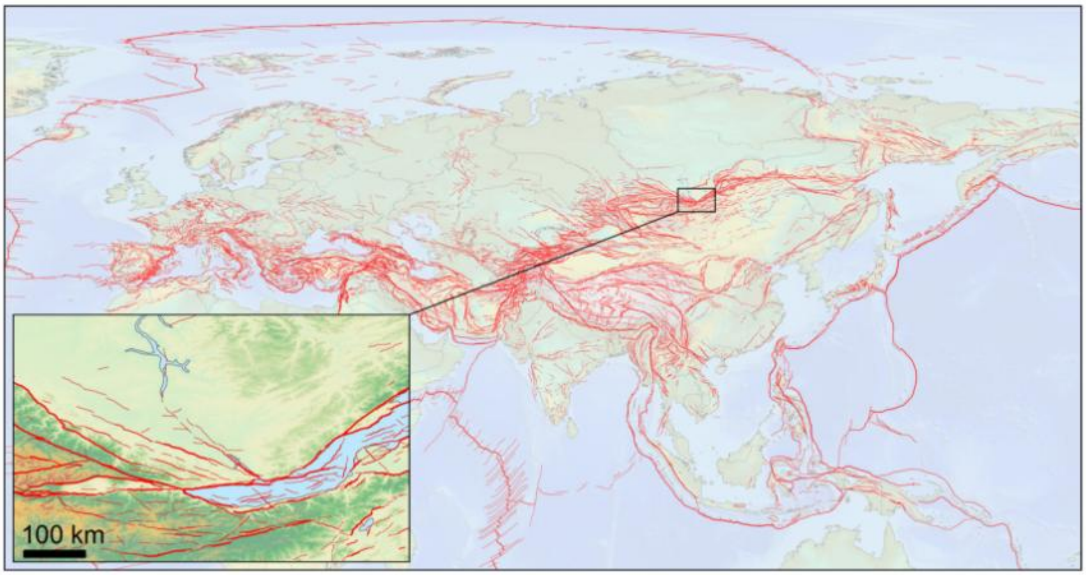

Figure 2.5: Overview and detailed exploration of the Active Faults of Eurasia Database (AFEAD).

The data have been compiled from 612 published sources, including regional maps, academic research, national and international databases, and field studies. Covering the entirety of the Eurasian continent, this study specifically aims to fill gaps in less-studied regions such as Central and Northern Asia by incorporating Russian-language sources and printed maps containing information on active faults, **Figure 2.5**.

AFEAD is provided in shapefile format, compatible with Geographic Information Systems (GIS), ensuring the positional accuracy of each fault through satellite imagery, SRTM digital elevation models, Landsat 7 ETM+ data, and geophysical studies. The fault movement direction, slip rate, and seismicity relationship have been determined by comparing regional studies and past field observations, allowing the classification of faults based on confidence levels.

The confidence level of fault activity in AFEAD is categorized into four levels based on the quality of available scientific evidence, **Figure 2.6**:

- Level A: Faults that have been proven active through historical, instrumental, or paleoseismological evidence.
- Level B: Faults with clear surface deformation but no directly confirmed fault movement.

- Level C: Faults with limited evidence of activity, where seismic activity and surface deformation are weak.
- Level D: Faults that have been previously reported as active but lack sufficient evidence or are considered questionable.

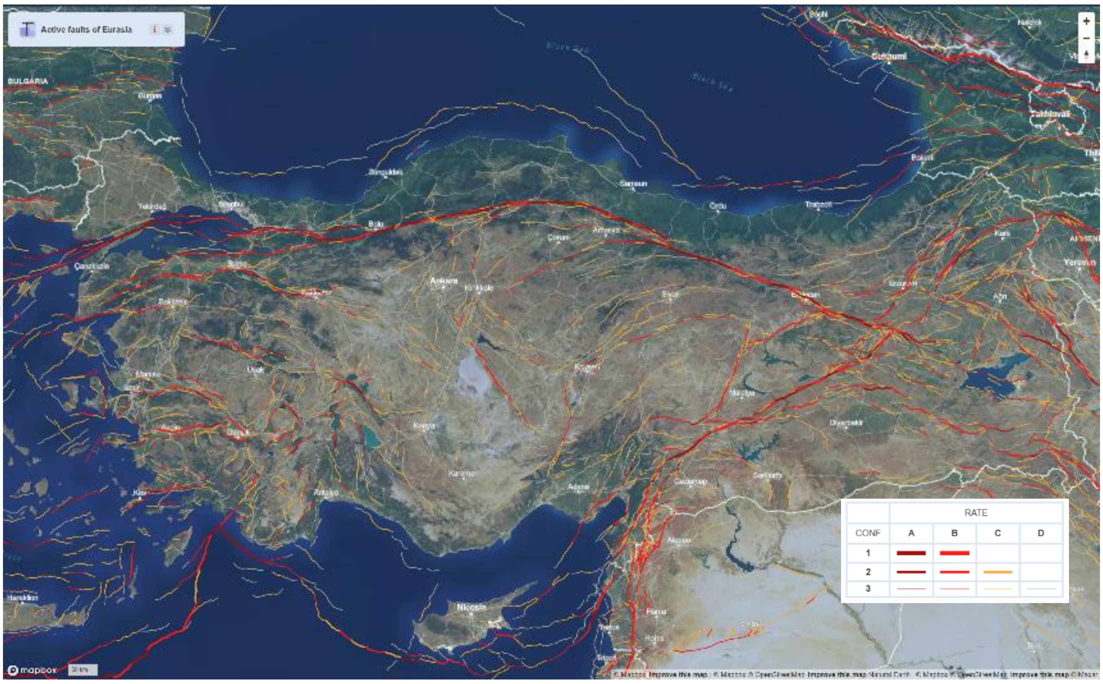

Figure 2.6: The confidence levels of active faults in the geography of Turkey.

Based on fault movement rates, deformation rates are classified into three categories:

- Level 1: Faults with a high activity level, exhibiting a slip rate greater than 5 mm/year.
- Level 2: Faults with a moderate activity level, characterized by a slip rate ranging between 1–5 mm/year.
- Level 3: Faults with a low activity level or undetermined slip rates, where the slip rate is less than 1 mm/year or remains unspecified.

The data extracted from the AFEAD database in dBase (.dbf) format was initially loaded into QGIS software, **Figure 2.7**. QGIS is a free and open-source Geographic Information System (GIS) software designed for spatial data analysis, visualization, and management. It supports various vector, raster, and database formats, offering advanced cartographic and geoprocessing tools.

In this process, the data related to the Malatya-Ovacık Fault Zone, which will be used in seismic hazard analysis, was identified and extracted from the dataset. The separated fault data was then processed in the R-CRISIS program and converted into a format compatible with the software.

The dataset used in the hazard analyses and all processed fault data are presented in the **Figure 2.7**.

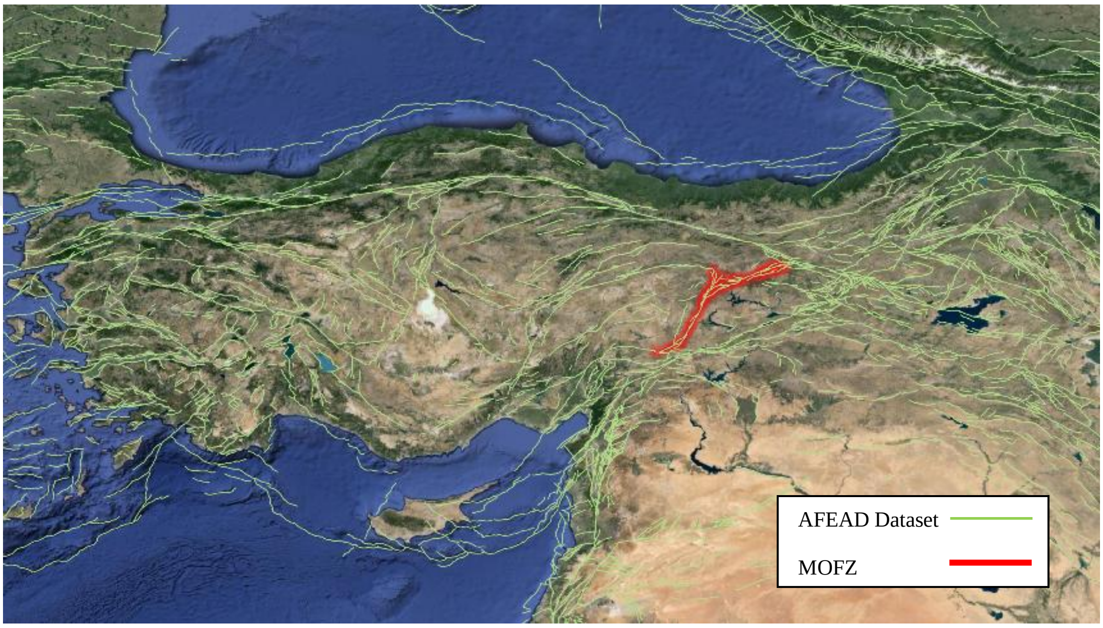

Figure 2.7: The AFEAD dataset prepared for Turkey and the Malatya-Ovacık Fault Zone (MOFZ).

2.2.3. Used Spectral Ordinates

The data obtained from the Horizontal Elastic Design Spectrum, which will be further detailed in the subsequent sections based on various selection parameters, have been utilized as spectral ordinates in hazard analyses. The rationale behind this approach lies in the fact that structures with different natural periods respond differently to seismic excitation. Short-period structures (e.g., low-rise buildings) are more affected by high-frequency ground motion, whereas long-period structures (e.g., high-rise buildings) experience significant displacement at lower frequencies.

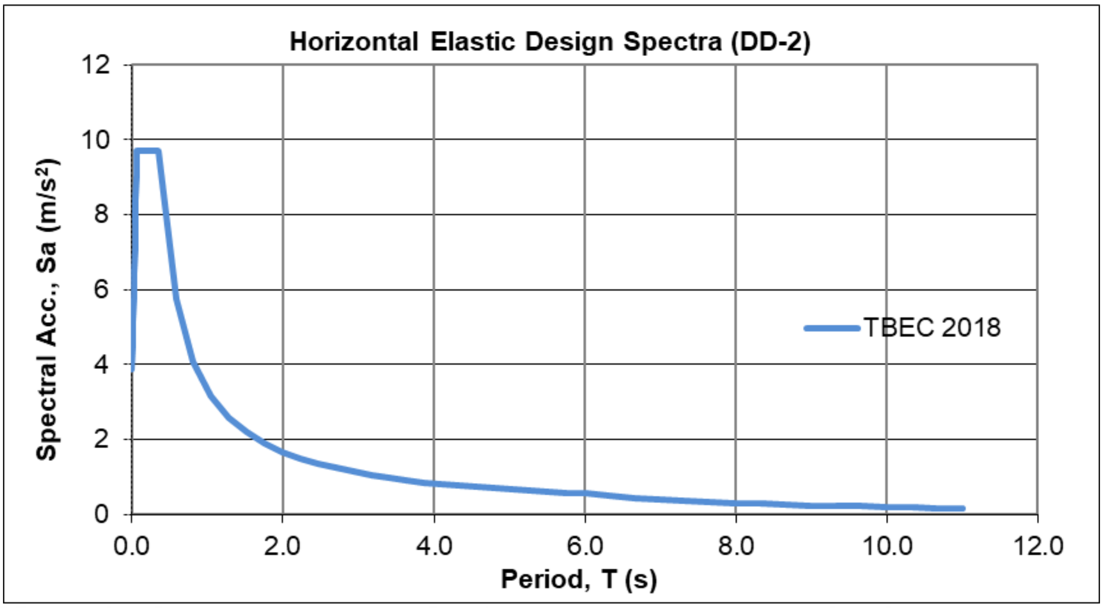

Figure 2.8: The Horizontal Elastic Design Spectrum used in hazard analyses.

Therefore, it is essential to determine spectral accelerations corresponding to specific periods in the analysis. The defined spectrum is presented in **Figure 2.8**.

2.2.4. Gutenberg-Richter Seismic Model

In order to understand the Gutenberg-Richter relationship, seismic data for the region were obtained from the AFAD Earthquake Catalog, covering a total of 709 recorded earthquakes since the year 1900. The selected dataset represents a wide range of magnitudes, from M 4.0 to M 7.6. Among these events, the Elbistan (Kahramanmaraş) Earthquake that occurred on February 6, 2023, is also included in the dataset, **Figure 2.9**.

Simple Linear Regression Analysis was performed using the Least Squares Method, establishing the best-fitting linear model between the observed earthquake data and the logarithmically expressed magnitude-frequency equation.

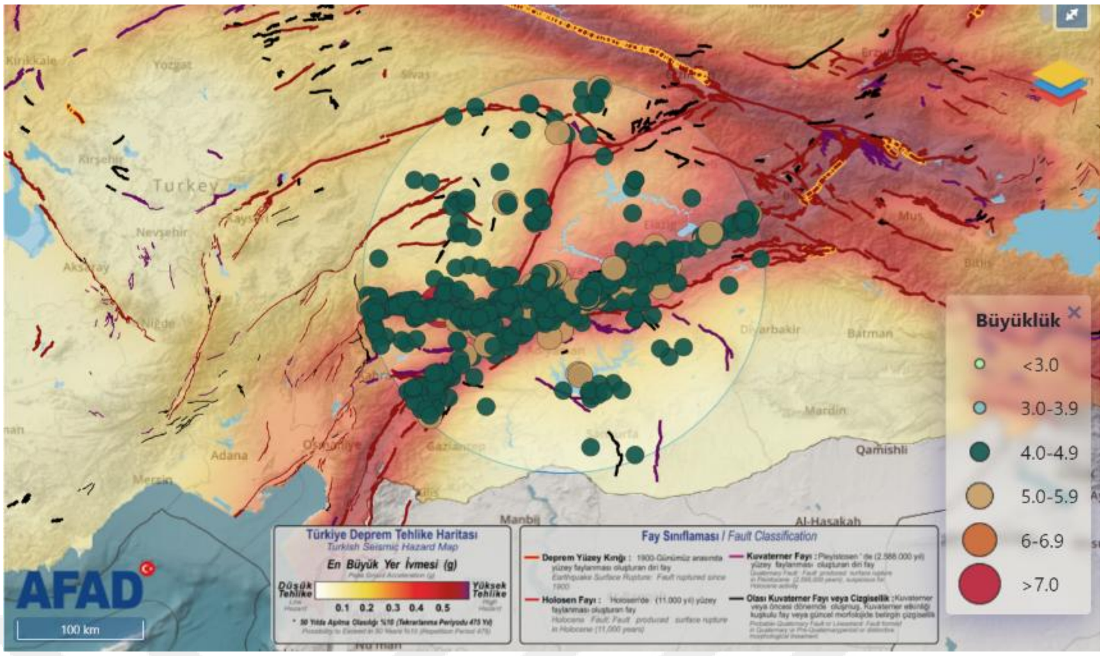

Figure 2.9: Distribution of earthquake epicenters and active faults on the 2018 Turkish Seismic Hazard Map.

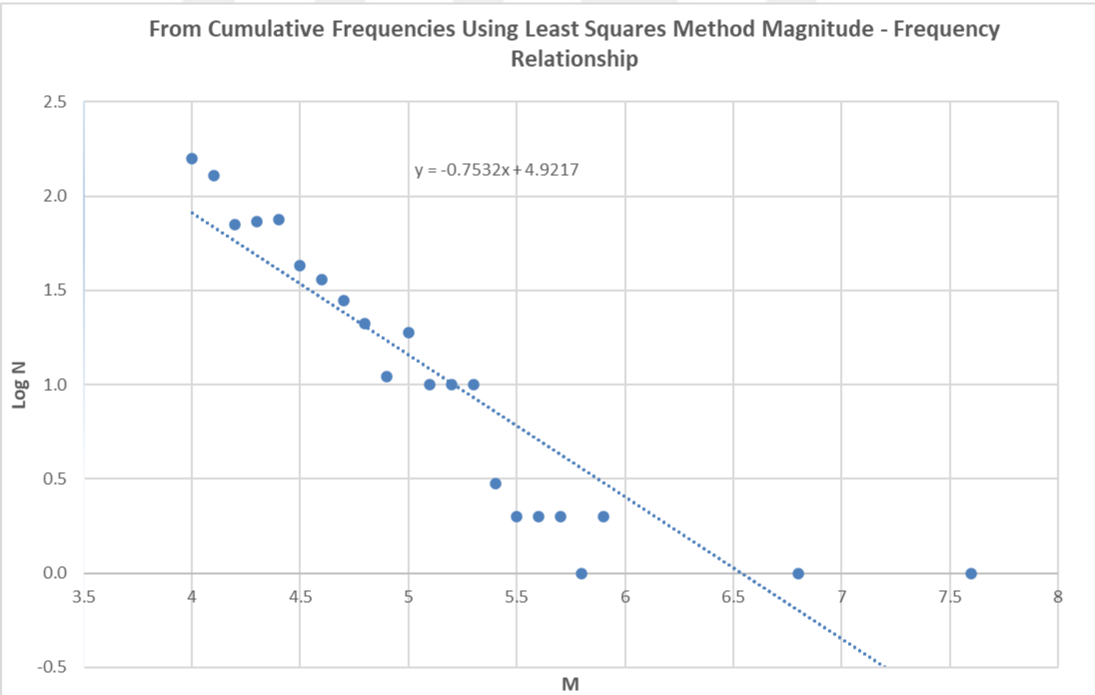

Figure 2.10: Magnitude–frequency relationship obtained from cumulative earthquake data using the least squares method.

The primary objective of this method is to calculate the annual exceedance probabilities and recurrence intervals of earthquakes with a given magnitude. Within the scope of Probabilistic Seismic Hazard Analysis (PSHA), estimated recurrence rates (λ) for earthquakes of different magnitudes are determined, serving as a fundamental data source for the development of seismic hazard maps.

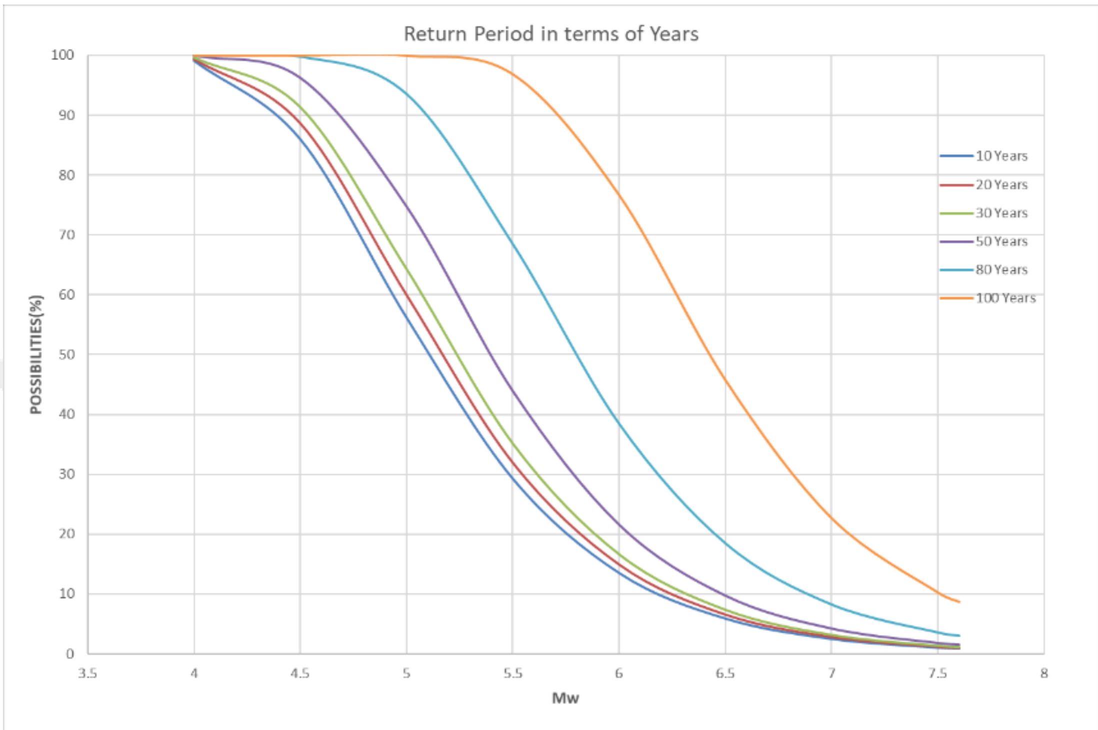

Figure 2.11: Probability of earthquake occurrence for different magnitudes (Mw) over various return periods ranging from 10 to 100 years.

Probability distributions of earthquake magnitudes and distances were calculated, and the occurrence probabilities of earthquakes with return periods of 10, 20, 30, 50, 80, and 100 years are presented in **Figure 2.11**.

As a result, an earthquake with a magnitude of 4.5 M_w was selected as the Threshold Magnitude for use in the analyses, and its occurrence probability was calculated as λ = 20%.

2.2.5. Regional Applicability of Ground Motion Prediction Equations (GMPEs) for Turkey

In earthquake engineering and seismology, attenuation relationships are empirical or semi-empirical equations used to predict expected ground motion parameters for a given earthquake magnitude and distance. These relationships are developed for estimating seismic parameters such as spectral acceleration, peak ground velocity, and peak ground acceleration, playing a critical role in seismic hazard analyses and structural design processes.

In general, attenuation relationships are based on the following key parameters:

1. Earthquake Magnitude (M_w): A measure of the energy released by the seismic source.
2. Fault-to-Site Distance (R): The distance between the rupture source and the observation point, typically expressed as the hypocentral distance or the closest distance to the fault surface.
3. Site Conditions (V_{s30}): A parameter representing surface geology and soil conditions that influence seismic wave propagation. The average shear-wave velocity over the top 30 meters (V_{s30}) is commonly used to model site effects (Borcherdt, 1994).
4. Fault Mechanism: The type of faulting (e.g., strike-slip, reverse, normal) influences the intensity and spectral characteristics of ground motion.

Ground Motion Prediction Equations (GMPEs) are advanced versions of attenuation relationships, considering not only distance-dependent attenuation but also additional factors such as site conditions, fault mechanisms, and rupture directivity. GMPEs are statistical models developed using large datasets and are employed to estimate seismic hazard at regional or global scales **(Boore et al., 2014)**.

Modern GMPEs have been developed under the NGA-West1 (2008) and NGA-West2 (2014) projects, making them adaptable to different tectonic settings. Models proposed by Abrahamson et al. (2014), Boore et al. (2014), Campbell & Bozorgnia (2014), and Chiou & Youngs (2014) have been refined for active crustal regions, improving their accuracy through extensive data calibration.

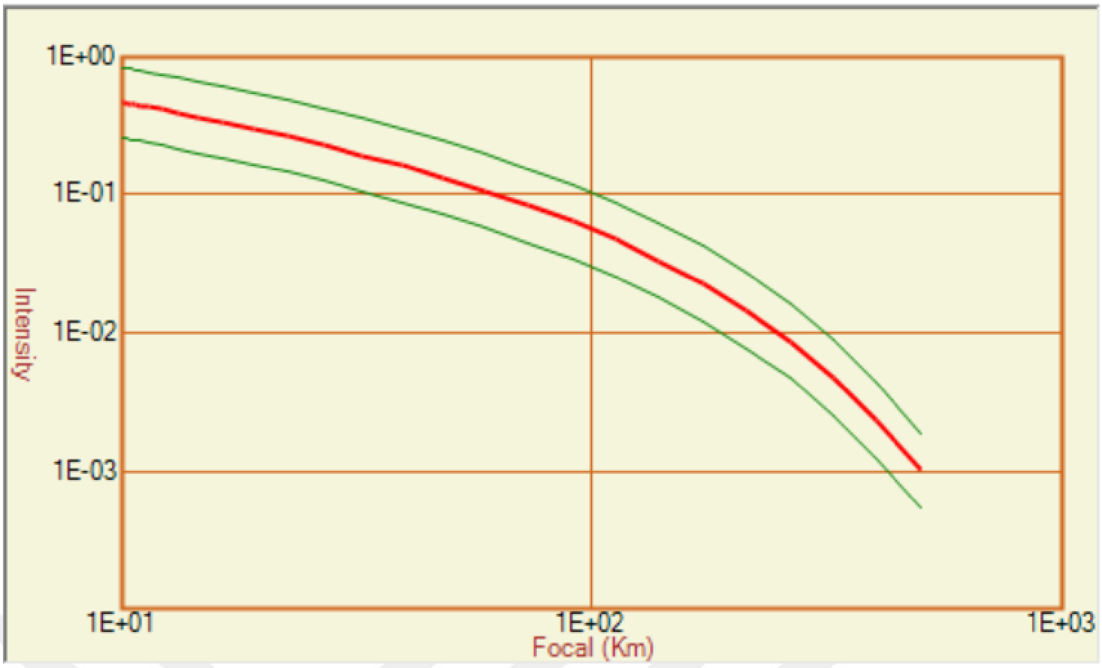

Figure 2.12: Scaling with V_{s30} = 450 m/s for a M 7.0 strike-slip event at a rupture distance of 20 km **(Abrahamson et al., 2014)**.

Abrahamson, Silva, Kamai (2014), **Figure 2.12**, Campbell & Bozorgnia (2014), **Figure 2.13** and Chiou & Youngs (2014), **Figure 2.13**, GMPEs have been tested for their regional applicability in Turkey's seismotectonic settings. Turkey is an active tectonic region where shallow crustal earthquakes frequently occur, making it comparable to other highly active seismic zones such as California, Japan, and New Zealand. Since these GMPEs were specifically developed for active crustal regions, they align well with Turkey's fault mechanisms and earthquake characteristics. The North Anatolian Fault Zone (NAFZ) and the East Anatolian Fault Zone (DAFZ) are major strike-slip fault systems similar to those present in the datasets used to develop these GMPEs.

These GMPEs are based on extensive global seismic datasets, particularly the NGA-West2 (Next Generation Attenuation-West2) database. NGA-West2 incorporates earthquake records not only North America but also from Europe, Asia, and the Middle East, representing diverse seismotectonic environments. Some of Turkey's major earthquakes have been included in this dataset, further enhancing the predictive capability of these models for Turkish earthquakes. Comparisons between Turkish ground motion records and these GMPEs indicate that their spectral acceleration predictions align well with observed data.

The accuracy of GMPEs also depends on how well they incorporate local site effects. Turkey has varying soil conditions, with softer sediments and deposits in the western regions and harder rock formations in the east. These GMPEs account for such variations by including parameters like the average shear-wave velocity at 30 meters (V_{s30}). Studies indicate that these models provide reliable spectral acceleration estimates for different site conditions in Turkey.

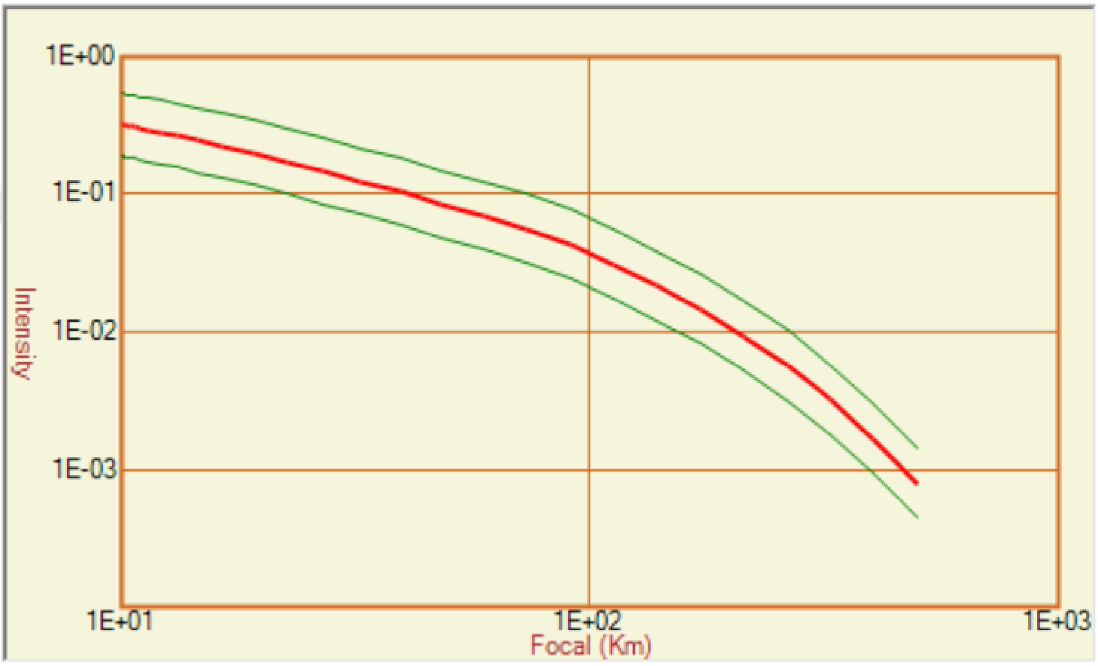

Figure 2.13: Scaling with V_{s30} = 450 m/s for a M 7.0 strike-slip event at a rupture distance of 20 km; Campbell and Bozorgnia (2014) NGA West 2.

Another reason for the applicability of these GMPEs in Turkey is their integration into national seismic design regulations. The Turkish Building Earthquake Code (TBEC-2018) relies on reliable GMPEs to define seismic hazard maps. The 2018 Turkey Seismic Hazard Map, prepared by AFAD (Disaster and Emergency Management Authority), was developed using predictions based on these GMPEs. The spectral amplification factors derived from these models form the basis for seismic design spectra used in engineering applications.

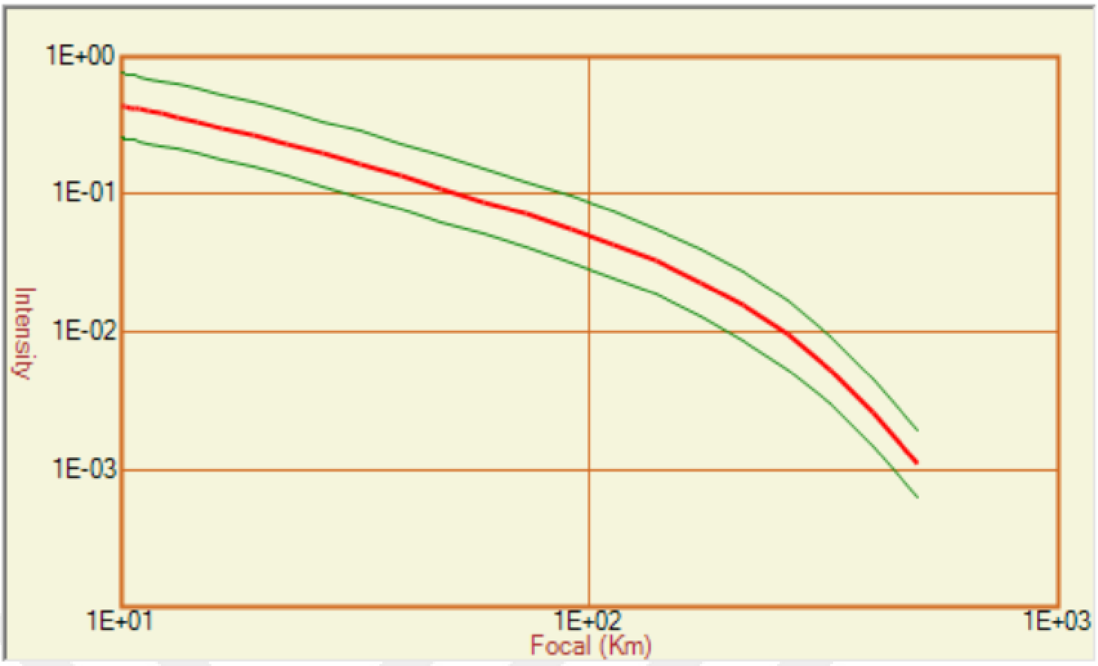

Figure 2.14: Scaling with V_{s30} = 450 m/s for a M 7.0 strike-slip event at a rupture distance of 20 km **(Chiou & Youngs, 2014).**

Regional validation studies confirm that these GMPEs provide accurate seismic hazard predictions for Turkey, supporting their widespread use in engineering design and risk assessment. Field data comparisons demonstrate that these models yield low prediction errors for spectral accelerations, making them reliable tools for seismic hazard assessment in Turkey. Consequently, the GMPEs developed by Abrahamson, Silva, Kamai (2014), Campbell & Bozorgnia (2014), and Chiou & Youngs (2014) are widely utilized in Turkey's seismic hazard studies and engineering applications. Additionally, in the Probabilistic Seismic Hazard Analyses (PSHA) conducted within the scope of this study, these GMPEs and their hybrid model have been utilized, **Figure 2.15**.

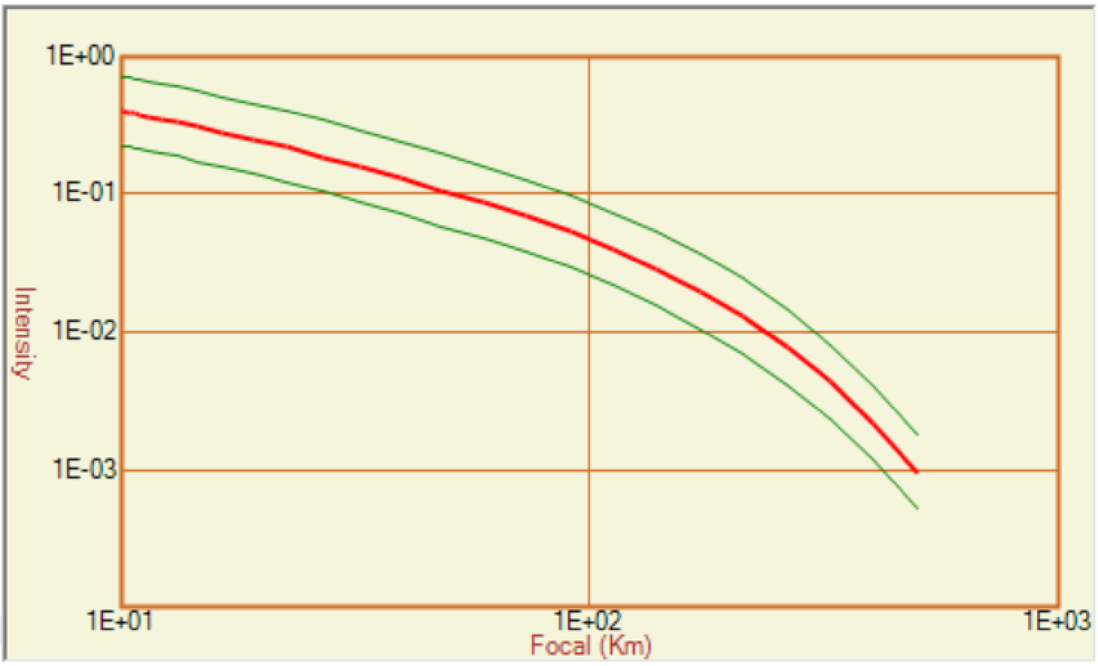

Figure 2.15: Scaling with V_{s30} = 450 m/s for a M 7.0 strike-slip event at a rupture distance of 20 km; Hybrid Models of 1 / 2 / 3.

2.2.6. Probabilistic Seismic Hazard Analyses Results

The Probabilistic Seismic Hazard Analysis (PSHA) has been examined in conjunction with faults obtained from the AFEAD 2022 study, newly conducted regression analysis, and the GMPEs used, as presented below.

As a result of the study, the horizontal elastic spectrum was plotted and compared with the Horizontal Elastic Design Spectrum prepared for DD-2 Earthquake Ground Motion according to TBEC-18. The results indicate that while the design spectrum of TBEC-18 is at a relatively similar level in terms of PGA with a 6% difference, it shows 28% higher values in short-period spectral acceleration ($S_{0.3}$) and 29% lower values in 1.0-second period spectral acceleration ($S_{1.0}$), **Figure 2.16**, **Figure 2.17**.

This demonstrates that the values obtained from the Probabilistic Seismic Hazard Analysis remain on the unfavorable side for long-period high-rise structures, whereas the TBEC-18 design spectrum is more unfavorable for short-period low- and mid-rise buildings. In the next stages, after the earthquake record selection, the TBEC-18 horizontal elastic design spectrum will be used for scaling process.

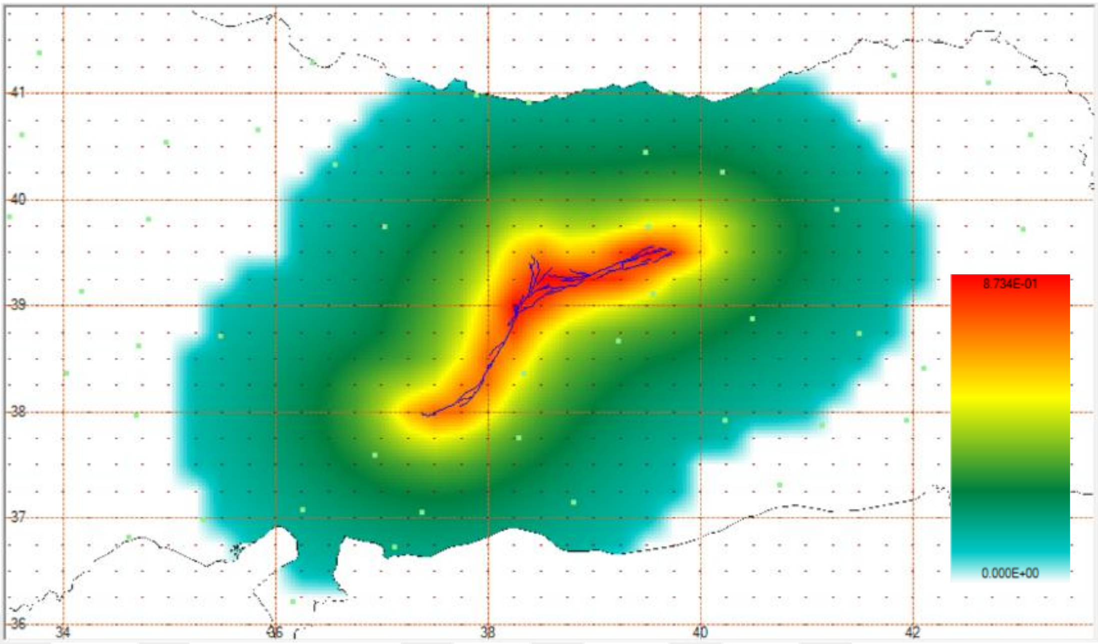

Figure 2.16: Peak Ground Acceleration (*PGA*) for the scenario earthquake with a 10% exceedance probability in 50 years and a return period of 475 years [g], T = 0.00 s.

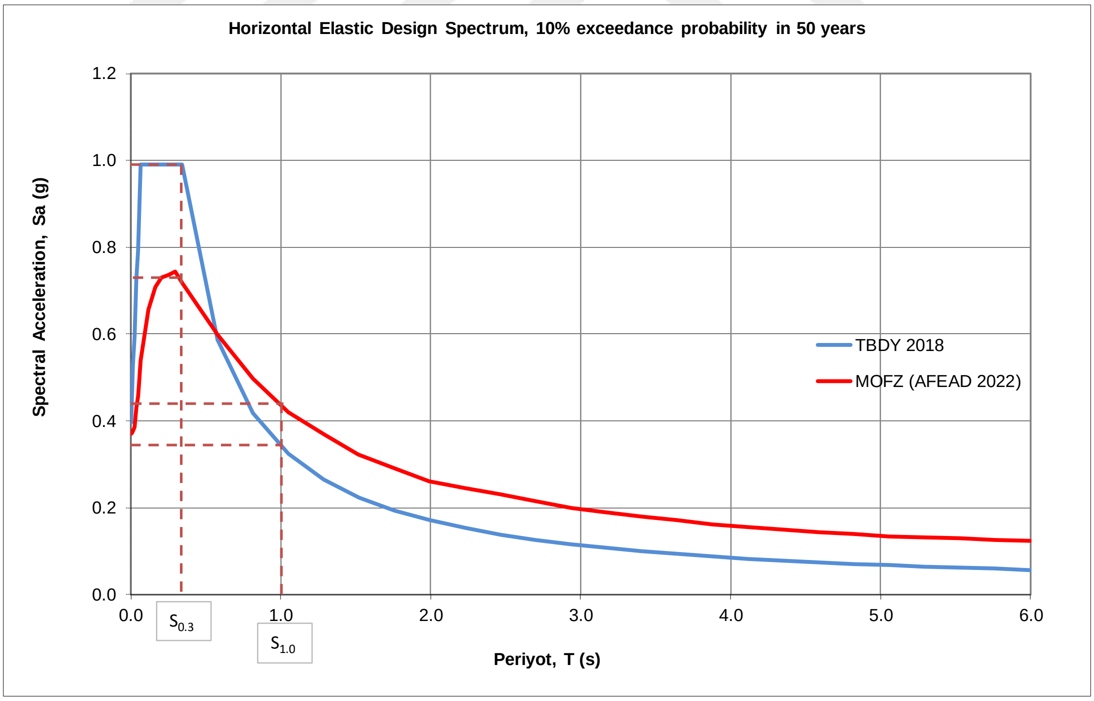

Figure 2.17: Comparison of the Probabilistic Seismic Hazard Analysis and the Horizontal Elastic Design Spectrum According to TBEC-18

3.SEISMIC EVALUATION PROCEDURES FOR REINFORCED CONCRETE STRUCUTURES [TBEC ‘18]

3.1. Seismic Parameters

3.1.1. Earthquake Ground Motion Levels

TBEC-2018, Section 2.2 outlines four levels of earthquake ground motions. These levels serve as critical parameters in evaluating and designing structures to base upon seismic forces. Each level is characterized by a specific exceedance probability and corresponding return period, forming the foundation for determining structural performance under earthquake effects.

Earthquake Ground Motion Level 1 (DD-1): DD-1 represents a "very rare" seismic event with a 2% probability of exceedance in 50 years, corresponding to a return period of 2,475 years. This level reflects the most severe earthquake ground motion and is generally used for designing critical infrastructure or structures requiring high resilience.

Earthquake Ground Motion Level 2 (DD-2): DD-2 represents a "rare" seismic event with a 10% probability of exceedance in 50 years, corresponding to a return period of 475 years. Commonly referred to as the standard design earthquake, it is the most widely used level in the design of ordinary buildings.

Earthquake Ground Motion Level 3 (DD-3): DD-3 represents a "frequent" seismic event with a 50% probability of exceedance in 50 years, equivalent to a return period of 72 years. This level accounts for moderate seismic impacts and is useful in evaluating the service performance of structures.

Earthquake Ground Motion Level 4 (DD-4): DD-4 represents a "very frequent" seismic event with a 68% probability of exceedance in 50 years (or 50% in 30 years), corresponding to a return period of 43 years. Known as the service earthquake, this level focuses on low-intensity seismic events.

3.1.2. Horizontal Earthquake Ground Motion Spectrum

The earthquake ground motion spectrum is established either in a standardized form or through site-specific seismic hazard analyses, incorporating a specified earthquake ground motion level, a 5% damping ratio, spectral acceleration coefficients from maps, and local soil effect coefficients, **Figure 3.1**. These spectra define horizontal ground motions acting on structures over distinct periods, enabling accurate seismic effect modeling in structural design **(Aochi & Madariaga, 2003)**.

The Spectrum Equations

The ordinates of the horizontal elastic design spectrum ($S_{ae}(T)$) are defined as follows:

$$S_a(T) = \begin{cases} (0.4 + 0.6\frac{T}{T_A})S_{DS}, & \text{if } T \leq T_A, \\ S_{DS}, & \text{if } T_A < T \leq T_B, \\ \frac{S_{D1}}{T}, & \text{if } T_B < T \leq T_L, \\ \frac{S_{D1}T_L}{T^2}, & \text{if } T > T_L. \end{cases} \tag{3.1}$$

In these expressions:

- S_{DS}: Short-period design spectral acceleration coefficient.
- S_{D1}: Design spectral acceleration coefficient at a 1.0-second period.

Corner periods:

- $T_A = 0.2 \cdot \frac{SD1}{SDS}$, (3.2)
- $T_B = \frac{SD1}{SDS}$, (3.3)
- T_L = 6 seconds.

These corner periods define the variation in acceleration across different period ranges in the spectrum.

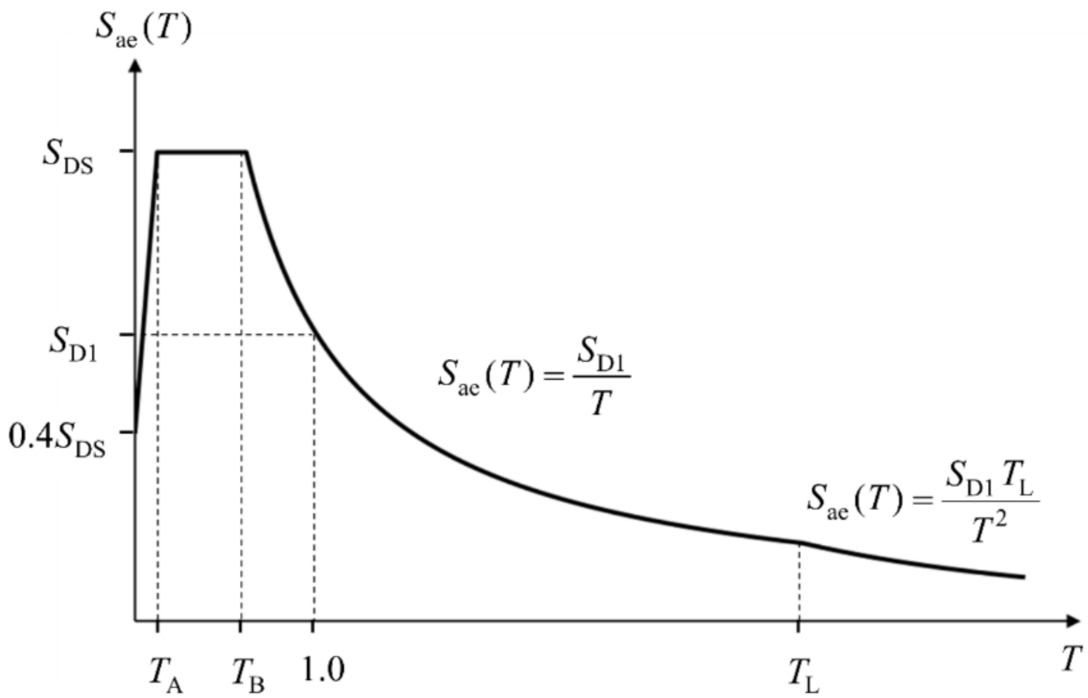

Figure 3.1: Definition of the Horizontal Elastic Design Spectrum.

Map Spectral Acceleration Coefficients

The TBEC-2018 defines map spectral acceleration coefficients based on the Turkish Earthquake Hazard Maps to establish the foundational parameters for seismic design at various hazard levels. These coefficients are categorized as follows:

- Short-period spectral acceleration coefficient (S_S),
- 1.0-second period spectral acceleration coefficient (S_1).

These coefficients are determined by considering ground conditions within the upper 30 meters, assuming a reference site condition with an average shear wave velocity of V_{S30} = 760 m/s and a damping ratio of 5%. Additionally, they are expressed in a dimensionless form by normalizing them with respect to the acceleration of gravity (*g*). These values reflect seismic hazards derived from the source and propagation characteristics, excluding local ground effects.

Design Spectral Acceleration Coefficients

Design spectral acceleration coefficients are derived from map spectral acceleration coefficients, adjusted to account for local ground conditions. They are defined as:

- Short-period design spectral acceleration coefficient (S_{DS}),

- 1.0-second period design spectral acceleration coefficient (S_{D1}).

These coefficients are calculated using the following equations:

$$SDS = SS \cdot FS;\ SD1 = S1 \cdot F1 \qquad (3.4)$$

Here, F_S and F_1 are local site effect coefficients representing amplification effects of the ground. These coefficients vary depending on the ground conditions and seismic hazard levels. For example, amplification effects are higher for weaker soils (ZD, ZE) and lower for stronger soils (ZA, ZB).

Local Site Effect Coefficients

Local site effect coefficients describe the amplification effects of different soil types during an earthquake and are directly used in calculating design spectral acceleration coefficients. Based on Section 16.4 of the TBEC-2018, the local site classes are categorized as follows, considering their geotechnical and dynamic properties:

- **Class ZA**: Very dense rock or igneous rock formations, characterized by high shear wave velocity and minimal amplification effects.
- **Class ZB**: Competent and dense soil layers or weathered rock with moderate amplification characteristics.
- **Class ZC**: Medium-dense granular soils or stiff cohesive soils with shear wave velocities indicative of average seismic amplification.
- **Class ZD**: Soft cohesive soils or loose granular soils, showing significant amplification effects under seismic loading.
- **Class ZE**: Very soft soil layers with low shear wave velocities, prone to high amplification and prolonged ground motion durations.
- **Class ZF**: Special soil conditions, including liquefiable soils, organic clays, or thick, soft clay layers, where site-specific analyses are required to assess seismic behavior accurately.

For these soil classes, the coefficients specified in **Table 3.1** and

Table 3.2 of the code provide different values for short- and long-period ground motions.

Table 3.1: Local Site Effect Coefficients for the Short-Period Region at the Spectrum.

Local Soil Category	Local soil effect coefficients for short period F_s					
	$S_s \leq 0.25$	$S_s = 0.50$	$S_s = 0.75$	$S_s = 1.00$	$S_s = 1.25$	$S_s \geq 1.50$
ZA	0.8	0.8	0.8	0.8	0.8	0.8
ZB	0.9	0.9	0.9	0.9	0.9	0.9
ZC	1.3	1.3	1.2	1.2	1.2	1.2
ZD	1.6	1.4	1.2	1.1	1	1
ZE	2.4	1.7	1.3	1.1	0.9	0.8
ZF	*Special soil behavior analysis will be done*					

Table 3.2: Local Site Effect Coefficients for the 1.0 Second Period at the Spectrum

Local Soil Category	Local soil effect coefficients for short period F_s					
	$S_s \leq 0.25$	$S_s = 0.50$	$S_s = 0.75$	$S_s = 1.00$	$S_s = 1.25$	$S_s \geq 1.50$
ZA	0.8	0.8	0.8	0.8	0.8	0.8
ZB	0.9	0.9	0.9	0.9	0.9	0.9
ZC	1.3	1.3	1.2	1.2	1.2	1.2
ZD	1.6	1.4	1.2	1.1	1	1
ZE	2.4	1.7	1.3	1.1	0.9	0.8
ZF	*Special soil behavior analysis will be done*					

3.1.3. Determination of Seismic Parameters

A single location from Malatya-Center was selected for the Seismic Evalution Analysis of the public buildings. The short-period spectral acceleration coefficient (S_S) and the 1.0-second spectral acceleration coefficient (S_1) were obtained from the Turkish Interactive Seismic Hazard Map. The coordinates of this location, based on the WGS84 system used in GIS software, are latitude 38°20'54.12"N and longitude 38°18'53.32"E, **Figure 3.2**.

Figure 3.2: Selected Location at Malatya-Center

The nearest recording station to Malatya-Center was scanned in the database for soil classification information, and Station TK-4401 was selected. This station is located at latitude 38°20'55.931"N, longitude 38°20'5.819"E, with an elevation of 998 meters and a shear wave velocity of V_{s30} = 481 m/s. Based on these values, the soil class was determined as ZC, and it was used in determining the seismic parameters for the analysis, **Figure 3.3**.

Using the soil class data, seismic parameters were determined for a specified coordinate in Malatya-Center using the Turkey Interactive Earthquake Hazard Maps. For the DD-2 design earthquake ground motion level, the following values were obtained: short-period map spectral acceleration coefficient (S_s) of 0.825, 1.0-second period map spectral acceleration coefficient (S_1) of 0.227, and Peak Ground Acceleration (PGA) of 0.345.

Figure 3.3: TK-4401 Earthquake Accelerometer Station

3.1.4. Earthquake Record Selection

The Turkish Building Earthquake Code (TBEC-2018) provides guidelines for the selection and application of earthquake ground motion records to be used in time history analyses. These criteria aim to ensure realistic and reliable analysis results. The following paragraphs elaborate on the fundamental principles regarding the selection process.

Earthquake ground motion records for time history analyses can either be obtained from naturally recorded ground motions or synthetically generated records. However, TBEC-2018 prioritizes the use of real earthquake records whenever possible. Synthetic records may be used only when suitable real records are unavailable.

The selected earthquake records must be compatible with the design spectrum specific to the region under analysis. This compatibility ensures that the chosen records reliably represent the design spectrum over a wide range of periods. The code mandates the scaling of the records to achieve this compatibility **(Kohrangi et al., 2019)**.

For one- or two-dimensional analyses, and for three-dimensional analyses requiring earthquake record sets, the minimum number of selected earthquake records or record sets shall be eleven. Nevertheless, no more than three records or record sets may be selected from the same earthquake.

Earthquake records must be selected in accordance with the local soil class of the construction site. TBEC-2018 classifies soils into categories ranging from ZA to ZE (without any special soil behavior analysis, and the selected records should represent the seismic amplification and frequency characteristics of these soil classes accurately.

For structures located in near-fault regions, the earthquake records must exhibit characteristics of forward directivity and long-period energy components. This ensures realistic results, particularly for critical structures. Considering these effects is essential for ensuring adequate structural performance against near-fault earthquakes **(Baker, 2007)**.

The code specifies that the magnitude range of the selected earthquake records should reflect the design earthquake magnitude of the region under analysis. Additionally, the tectonic and seismic hazard characteristics of the region should be consistent with the characteristics of the selected records **(Baker, 2011)**.

The PEER Ground Motion Database

The earthquake records utilized in this study were sourced from the PEER Ground Motion Database and subsequently scaled. Developed by the Pacific Earthquake Engineering Research Center (PEER), this database addresses the demand for reliable ground motion data in earthquake engineering and seismology. Since its establishment in 1996, PEER has focused on advancing performance-based design methodologies for earthquake-resistant structures and providing standardized datasets for engineering applications. The database was developed through collaborations with institutions such as the University of California, Berkeley, the United States Geological Survey (USGS), and other research organizations.

The database aggregates earthquake records from around the world, providing a comprehensive dataset for time history analyses, performance-based design approaches, and seismic hazard assessments. It encompasses both horizontal and vertical ground motion components from earthquakes of varying magnitudes and fault mechanisms, along with key parameters such as spectral acceleration (Sa), peak ground acceleration (PGA), peak ground velocity (PGV), and peak ground displacement (PGD). Each record is supplemented with detailed metadata, including earthquake magnitude, source-to-site distance, and site characteristics.

The PEER database allows engineers and researchers to select and scale ground motion records to match design spectra. It facilitates the analysis of critical parameters in earthquake engineering, such as near-fault effects, forward directivity, and site amplification, providing valuable tools for realistic and reliable seismic evaluations, **Table 3.3**.

Table 3.3: Selected Earthquake Records

#	PEER Record No	Earthquake Name	Date	M_w	Fault Type	V_s30 [m/sec]	R_{rup} [km]	Δt [s]	Scale Factor
1	1	"Helena_ Montana-01"	1935	6	Strike Slip	593.35	2.86	0.01	3.239
2	103	"Northern Calif-07"	1975	5.2	Strike Slip	368.72	34.67	0.005	3.218
3	150	"Coyote Lake"	1979	5.74	Strike Slip	663.31	3.11	0.005	0.952
4	212	"Livermore-01"	1980	5.8	Strike Slip	403.37	24.95	0.005	2.334
5	223	"Livermore-02"	1980	5.42	Strike Slip	377.51	18.28	0.005	2.146
6	239	"Mammoth Lakes-03"	1980	5.91	Strike Slip	537.16	18.13	0.005	1.960
7	240	"Mammoth Lakes-04"	1980	5.7	Strike Slip	382.12	5.32	0.005	1.771
8	569	"San Salvador"	1986	5.8	Strike Slip	455.93	6.99	0.005	0.650
9	585	"Baja California"	1987	5.5	Strike Slip	471.53	4.46	0.005	0.559
10	832	"Landers"	1992	7.28	Strike Slip	382.93	69.21	0.02	1.892
11	838	"Landers"	1992	7.28	Strike Slip	370.08	34.86	0.02	2.480

3.1.5. Selection and Scaling of Earthquake Records

As mentioned in the previous section, the scaling of earthquake records using the simple scaling method was performed using the modules of the PEER Ground Motion Database. During this scaling process, the building periods were considered, following the principles outlined below. The calculations for building periods are discussed in detail in subsequent sections, and the calculated periods are also illustrated in the corresponding **Figure 3.4** in this section.

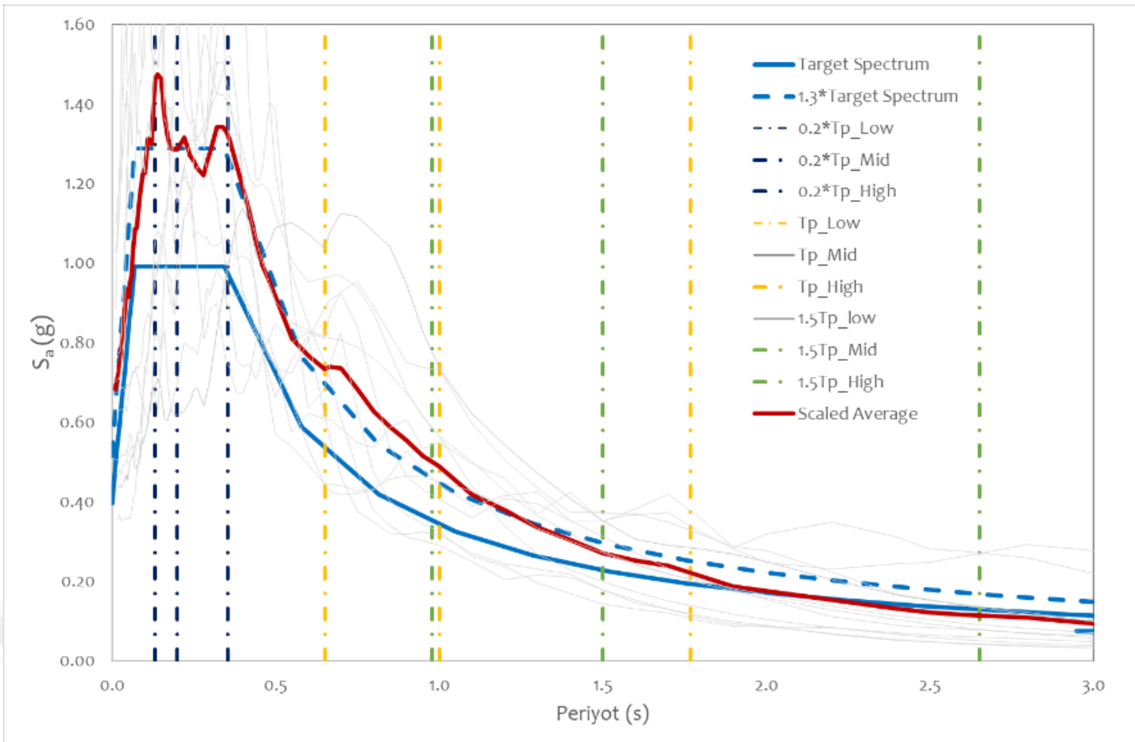

Figure 3.4: Comparison of the scaled average of earthquake records spectral accelerations with the DD-2 design spectrum and its 1.3 multiplier according to TBEC-2018 (Gray lines represent the spectra of each of the 11 earthquake records).

In time history analysis, earthquake records must be scaled to ensure compatibility with the target design spectrum. The simple scaling method is an effective technique designed to adjust the amplitude of ground motion records to align with the target spectrum. This method involves multiplying the acceleration time series of the earthquake record by a scaling factor. The scaling factor ensures that the spectral acceleration values of the record within a specified period range match the target design spectrum. According to TBEC-2018, this period range is typically defined as the interval around the structure's fundamental mode period, $0.2T_p$; $1.5T_p$, **Figure 3.5**, **Figure 3.6**.

The simple scaling method preserves the physical properties of the records by maintaining their energy content and frequency components, enabling realistic results in engineering analyses. Its key advantages include ease of application and the ability to produce results that are compatible with the target spectrum. However, this method only ensures compatibility within a specific period range, which may result in discrepancies outside this range. Additionally, using high scaling factors can limit the physical realism of the records. For near-fault records exhibiting special effects, such as forward directivity, more advanced scaling methods may be required, **Figure 3.7**.

An example of the scaled and directionality-affected earthquake records is provided below, making it possible to observe the differences.

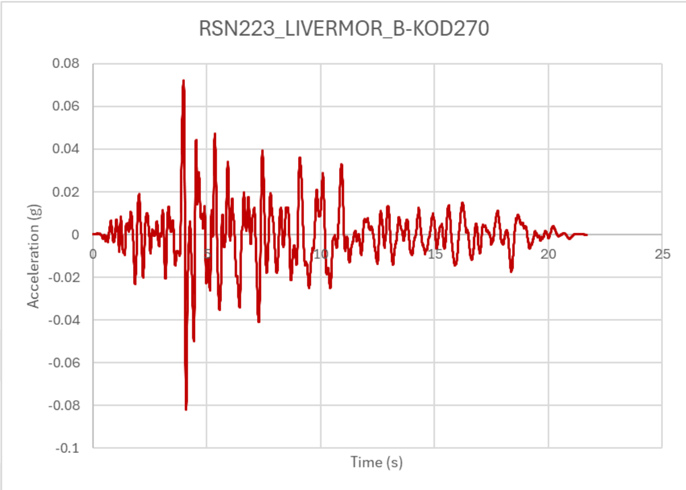

Figure 3.5: Original Earthquake Record

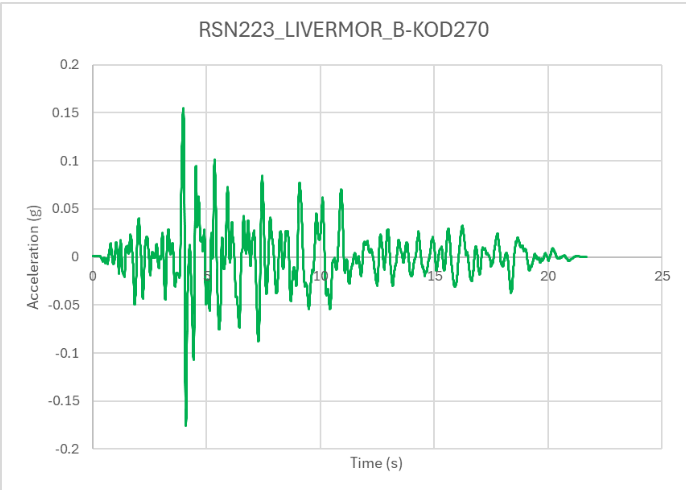

Figure 3.6: Scaled Earthquake Record

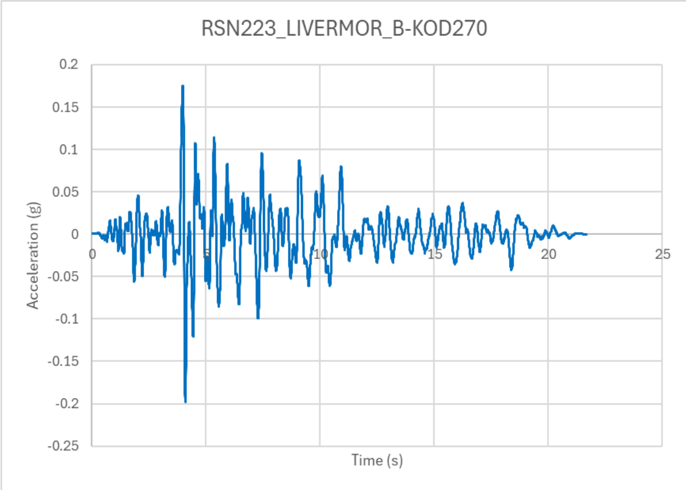

Figure 3.7: Earthquake Record Amplified by 13% Due to Directional Effect

3.2. Assessment Approaches and Performance Objectives

In the seismic resilience assessment of existing buildings in Malatya, TBEC-2018 has been taken as a reference, and all analyses have been conducted in accordance with the principles specified in this regulation. This section addresses linear and nonlinear analysis approaches for evaluating existing buildings. The assessment process begins with determining material properties at the micro-scale and integrating these properties into the mathematical model, followed by analyzing section behavior at the macro-scale. Finally, the evaluation criteria are detailed within the framework of structural performance objectives.

3.2.1. Linear Assessment Approaches

Linear assessment approaches are fundamental methods used to determine the seismic performance of structures. These approaches assume that structures exhibit linear (elastic) behavior under earthquake effects. Typically used in initial-stage analyses, these methods are preferred when more complex nonlinear analyses are not required. The determination of the structural load-carrying capacity is performed through calculations under specific load effects.

The primary objective of linear assessment methods is to analyze the elastic response of a structure under various loading conditions, particularly seismic loads. These approaches assume that structural elements and systems remain within elastic limits, and large deformations are not considered. If the structural capacity is not exceeded, this type of analysis can be sufficient.

Linear assessment can be conducted using two fundamental methods:

1. **Linear Static Procedure (LSP):** This method assumes that structural elements respond linearly to applied loads. Earthquake ground motion effects are directly modeled as static loads on the structure. Defined as the Equivalent Earthquake Load Method in TBEC-2018, this method requires separate calculations of seismic loads acting in the (X) and (Y) directions. It is generally suitable for small and symmetric structures where nonlinear ground motion effects can be neglected.
2. **Linear Dynamic Procedure (LDP):** This method is used to model the dynamic response of a structure under earthquake ground motion effects. Unlike static analysis, it considers time-dependent dynamic loading and accounts for resonance effects, providing a more precise evaluation.

According to TBEC-2018, this method can be applied using two different approaches:

- **Mode Combination Method (SRSS - Square Root of Sum of Squares):** In each earthquake direction, the design response spectrum is used to calculate the maximum modal response values in each vibration mode. These modal responses, which are not simultaneous, are then statistically combined to estimate the maximum structural response.
- **Mode Superposition Method:** This method is used when an earthquake is assumed to act simultaneously in two perpendicular horizontal directions. The modal response of each vibration mode is computed using time-domain analysis. The modal responses obtained for sufficient vibration modes are then directly summed in the time domain to determine the time-dependent response variations and the maximum response values for design purposes.

Although these linear assessment approaches are suitable for some structures within the scope of this thesis, performance analysis for all buildings was conducted using real earthquake records to ensure a more realistic evaluation.

3.2.2. Nonlinear Dynamic Assessment Approaches

Nonlinear Dynamic Procedure (NDP) is used for the seismic analysis of a structure by incorporating a mathematical model that directly includes the nonlinear load-deformation characteristics of structural components. In this method, the structure is subjected to ground motion acceleration histories, which are modeled based on discrete time intervals of ground motion acceleration. The resulting forces and displacements are then compared against predefined acceptance criteria.

The modeling and analysis requirements for NDP follow a similar framework to nonlinear static procedures. However, in NDP, nonlinear response history analysis is performed using ground motion acceleration histories to compute the structure’s dynamic response at each time step. The calculations are conducted by averaging the response values for each component depending on its direction of movement. If the response is direction-independent, the meaning of the maximum absolute response is used. If the response is direction-dependent, the average of positive and negative responses is considered.

Ground motion characterization in NDP is based on recorded or synthetic earthquake records, which serve as the foundation for accurately modeling the structure’s seismic response. During the analysis, the horizontal components of ground motion are used to conduct nonlinear response history analysis. If a Ritz vector-based solution is adopted, enough modes must be selected to ensure the local dynamic responses of the structure are accurately modeled.

Additionally, damping in NDP is modeled using Rayleigh damping or other rational methodologies. These damping ratios are carefully selected to accurately simulate the nonlinear structural response, ensuring that appropriate damping levels are applied to each mode of the structure.

This approach is defined in TBEC-2018 as nonlinear time history earthquake analysis. Nonlinear time history analysis involves the step-by-step direct integration of the differential equation system representing the motion of the structural system under earthquake ground motion effects. During this process, the time-dependent variation of the stiffness matrix is taken into account due to the nonlinear behavior of the system.

3.2.3. Material Identification and Nonlinear Models

For the assessment of reinforced concrete buildings, data collection on building geometry, element details, and material properties of concrete and reinforcing steel is essential. The structural system's project must be examined on-site, and if unavailable, a partial or complete survey should be conducted. The collected data must include the span, height, and dimensions of structural elements and be verified against available records. The foundation system of the building can be identified through exploration pits excavated inside or outside the structure. Additionally, the presence of short columns, horizontal and vertical irregularities must be identified and documented.

The material and geometric properties of all analyzed structures are detailed in the following sections. However, since on-site assessment was not feasible, material and geometric data were extracted from existing project documents, and analyses were performed based on these records.

Concrete Material Model

In the nonlinear concrete material model of the structural system, the confining and unconfined material models, shown in Figure 3.8, are used, which are known in the literature as the Mander Concrete Model.

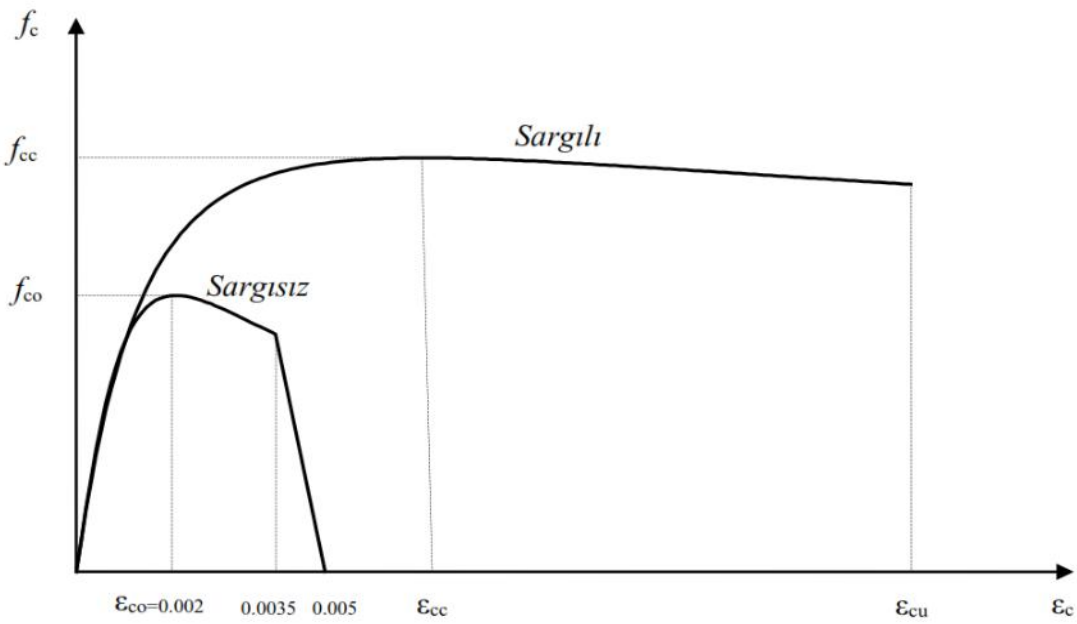

Figure 3.8: Confined and unconfined concrete material model

In confined concrete, the concrete compressive stress f_c, as a function of the strain ε_c, is given by the equation as follows, **Figure 3.8**:

$$f_c = \frac{f_{c*}\, r}{r-1+x} \qquad (3.5)$$

The relationship between confined concrete strength f_{cc} and unconfined concrete strength f_{co} is given as follows:

$$f_{cc} = \lambda_c\, f_{co} \quad \lambda_c = 2.254\left(1 + 7.94\frac{f_{co}}{f_{cc}} - 2\frac{f_{co}}{f_{cc}}\right) - 1.254 \qquad (3.6)$$

Here, f_e is the effective confining pressure is, which can be considered as the average of the two perpendicular directions in rectangular sections, as given as follows:

$$f_{ex} = k_e\, \rho_x\, f_{ex} \quad f_{ey} = k_e\, \rho_x\, f_{yw} \qquad (3.7)$$

In these equations, f_{yw} is the yield strength of transverse reinforcement, ρ_x and ρ_y are the volumetric ratios of transverse reinforcement in the relevant directions, and k_e is the confining effectiveness coefficient defined as follows:

$$k_e = \left(1 - \sum\frac{a_i^2}{6b_o h_o}\right)\left(1 - \frac{s}{2b_o}\right)\left(1 - \frac{A_s}{b_o h_o}\right)^{-1} \qquad (3.8)$$

Here, a_i represents the distance between the axes of longitudinal reinforcements around the section, b_o and h_o are the distances between the axes of transverse reinforcements surrounding the core concrete, and A_s is the longitudinal reinforcement area.

The normalized concrete strain ε_c with respect to the variables x and r is given as follows:

$$x = \frac{\varepsilon_c}{\varepsilon_{cc}}\ ;\ \varepsilon_{cc} = \varepsilon_{co}[1 + 5(\lambda_c - 1)]\ ;\ \varepsilon_{co} \approx 0.002 \qquad (3.9)$$

$$r = \frac{E_c}{E_c - E_{sec}}\ ;\ E_c \approx 5000\sqrt{f_{co}}\ [MPa]\ ;\ E_{sec} = \frac{f_{cc}}{\varepsilon_{cc}} \qquad (3.10)$$

Reinforcing Steel Properties

The stress and strain values for the nonlinear steel material model are obtained using the equations given below. The expressions used here are determined based on the material quality specified in

Table 3.4.

$$f_s = E_s \, \varepsilon_s \qquad (\varepsilon_s \leq \varepsilon_{sy}) \qquad (3.11)$$

$$f_s = f_{sy} \qquad (\varepsilon_{sy} < \varepsilon_s \leq \varepsilon_{sh}) \qquad (3.12)$$

$$f_s = f_{su} - \left(f_{su} - f_{sy}\right) \frac{(\varepsilon_{su} - \varepsilon_s)^2}{(\varepsilon_{su} - \varepsilon_{sh})^2} \quad (\varepsilon_{sh} < \varepsilon_s \leq \varepsilon_{su}) \qquad (3.13)$$

In the nonlinear material models created for reinforcing steel, the modulus of elasticity of steel is considered as E_s = 200 GPa. The stress and strain values, which vary depending on the steel quality, are provided in

Table 3.4.

Table 3.4: Reinforcing Steel Properties

Reinforcing Steel Class	f_{sy} (Mpa)	ε_{sy}	ε_{sh}	ε_{su}	f_{su} / f_{sy}
S220	220	0.0011	0.0011	0.12	1.2
S420	420	0.0021	0.008	0.08	1.15 -1.35
B420C	420	0.0021	0.008	0.08	1.15 -1.35
B500C	500	0.0025	0.008	0.08	1.15 -1.35

Based on the equations and material properties given above, the steel material model shown in **Figure 3.9** is obtained.

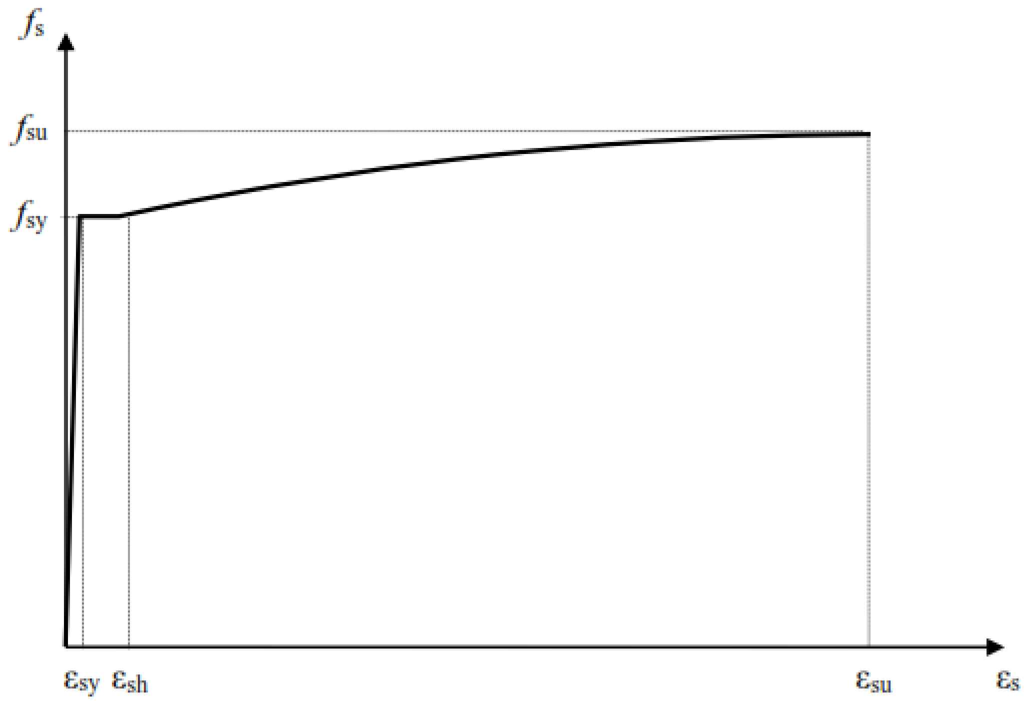

Figure 3.9: Reinforcing Steel Properties

3.2.4. Simple Bending and Nonlinear Behavior Model

Uncracked Section: As long as the tensile stress in the concrete remains below its tensile strength f_{ctk}, the strain and stress distribution behave as in an elastic, homogeneous beam. The only difference is the presence of reinforcing steel.

- In the elastic range, for any given strain value, the stress in the steel is "n" times that of the concrete, where n=E_c/E_s is the modular ratio.
- In calculations, the actual steel and concrete cross-section is replaced by a transformed section, which consists only of concrete. The actual steel area is replaced with an equivalent concrete area (nA_s), located at the level of the steel.
- Once the transformed section is determined, the beam is analyzed as an elastic homogeneous beam.

Cracked Section: When the tensile stress f_{ct} exceeds f_{ctk} , cracks develop in the tension zone of the section.

- If the compressive stress in concrete is below $0.5f_{ck}$ and the steel has not yet reached yield strength, both materials continue to behave elastically.

- At this stage, it is assumed that tension cracks extend to the neutral axis, and sections that were plane before bending remain plane after bending.

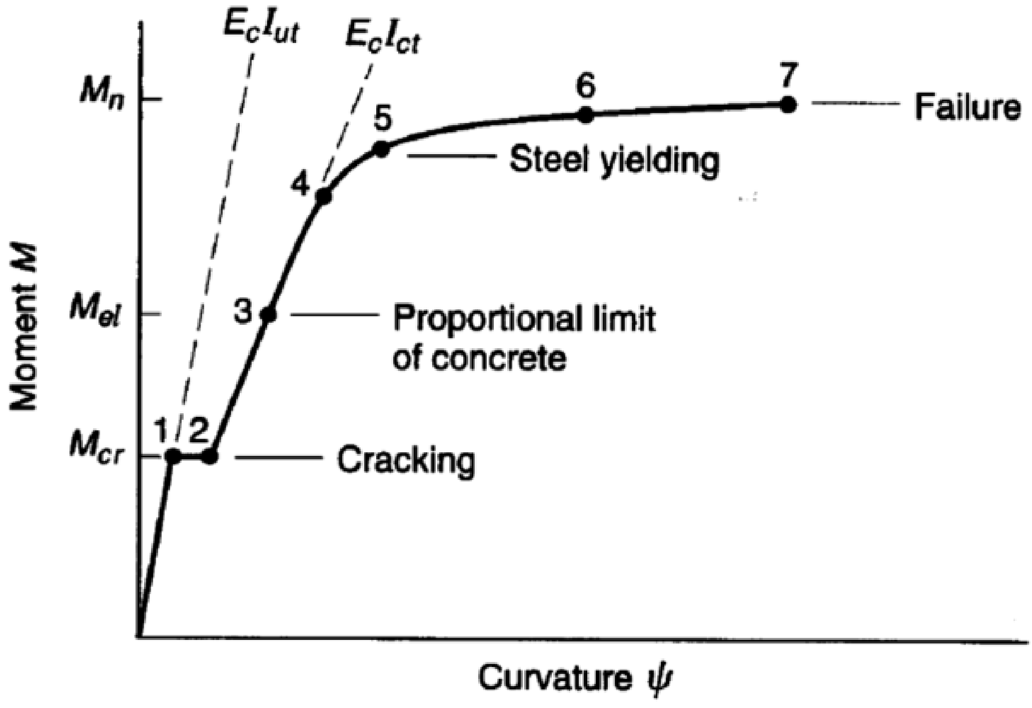

Figure 3.10: Distributed Plasticity Behavior Model

Moment-Curvature Relationship: By using idealized stress-strain relationships for steel and concrete, and assuming perfect bond and plane sections remain plane, the relationship between moment and curvature for a typical under-reinforced concrete beam section can be determined.

In TBEC-2018, two different behavioral models are defined for the nonlinear modeling of structural system elements. These behavioral models are referred to as the Concentrated Plasticity Behavior (Plastic Hinge) Model and the Distributed Plasticity Behavior Model. **Figure 3.9** presents the representative illustrations of these post-elastic behavior models.

Lumped Plastic (Plastic Hinge) Behavior Modeling

In earthquake engineering, assessing the nonlinear behavior of reinforced concrete structures plays a critical role in evaluating structural safety. The lumped plastic behavior model is an approach that assumes nonlinear deformations are concentrated at specific points within structural elements. The plastic hinge model is an essential method for evaluating the ductility capacity and performance of load-bearing elements. This model assumes that plastic deformations occur only at specific locations (e.g., beam-column joints), which are defined as plastic hinges.

- **Plastic Hinge Model and Fundamental Principles**

The plastic hinge model is widely used in nonlinear static pushover analysis and nonlinear time-history analysis. The fundamental principles of this model can be summarized as follows, **Figure 3.10**:

- **Separation of Elastic and Plastic Behavior:** While structural elements exhibit linear behavior in the elastic region, plastic deformations occur at specific points.
- **Determination of Hinge Locations:** Plastic hinges typically form at beam-column joints and at points where significant bending moments occur.
- **Plastic Hinge Length:** It is assumed that the plastic hinge extends over a certain length of the element. The plastic hinge length depends on material and section properties and is typically expressed using empirical formulas derived from experimental studies.

- **Mathematical Representation of the Plastic Hinge Model**

The plastic hinge model is based on the moment-curvature relationship, which determines the nonlinear deformations of load-bearing elements when their bending capacity is exceeded. This model is expressed as follows:

$$M = EI \cdot \kappa \qquad (3.14)$$

where:

- M is the moment,
- EI is the section stiffness,
- κ is the curvature.

When the curvature capacity is exceeded in the plastic hinge region, nonlinear deformations occur. The plastic hinge length L_p is calculated as follows:

$$L_p = \alpha L + \beta d_b \qquad (3.15)$$

where:

- L is the total length of the element,
- d_b is the reinforcement bar diameter,
- β are coefficients derived from experimental data.

Application of the Plastic Hinge Model in Structural Analyses

The plastic hinge model is used in various analysis methods within performance-based seismic design (PBEE):

- **Nonlinear Static Pushover Analysis:** The structure's response to increasing lateral loads in a specific direction is analyzed, and the locations of plastic hinges are determined.
- **Nonlinear Time-History Analysis:** Real or artificial earthquake acceleration records are applied to the structure to examine the formation and progression of plastic hinges over time.

The plastic hinge model is a simplified yet reliable approach for representing the nonlinear behavior of reinforced concrete elements in structural engineering. This model plays a crucial role in assessing the seismic performance of structures and is considered a fundamental component of nonlinear analyses. Modeling plastic hinges is essential for enhancing structural ductility and developing earthquake-resistant designs in compliance with seismic codes.

Distributed Plastic Behavior Modeling

Unlike the lumped plastic model, which assumes that plastic deformation is concentrated at specific points (plastic hinges), the distributed plastic model assumes that plastic deformation spreads over a certain length of the structural element (Scott & Fenves, 2006). This approach contributes to more realistic modeling of structural elements and allows for accurate calculation of ductility capacity and energy dissipation mechanisms.

Fundamental Principles of Distributed Plastic Behavior

The distributed plastic behavior model provides a more realistic approach in nonlinear structural analyses by assuming that plastic deformation is not confined to a single point but rather spreads over a specific region. The fundamental principles of this model are as follows:

- **Distribution of Plastic Deformation:** Unlike the plastic hinge model, plastic deformation is not concentrated at a single location but is distributed over a certain length of the element.
- **Plastic Zone Length:** The length over which plastic deformation spreads depend on material properties, reinforcement configuration, and section stiffness.
- **Realistic Stress-Strain Modeling:** The distributed plastic model allows for a more detailed examination of material damage mechanisms.
- **Seismic Performance Significance:** The distribution of energy dissipation over a larger region reduces the risk of collapse and promotes ductile behavior.
- **Mathematical Modeling and Calculation of the Distributed Plastic Zone**

One of the key parameters used in modeling distributed plastic behavior is the distributed plastic zone length (L_p), which is determined using empirical expressions derived from experimental studies:

$$Lp = c1 \times L + c_2 \times d_b \qquad (3.16)$$

where:

- L_p is the length of the distributed plastic zone,
- L is the total length of the element,
- d_b is the reinforcement bar diameter,
- c_1 are experimental coefficients.

By considering plastic curvature (ϕ_p) and the moment-curvature ($M - \kappa$) relationship, distributed plastic deformation can be modeled as:

$$\theta_p = \int_0 L_p \times \phi \times d_x \qquad (3.17)$$

where:

- θ_p represents plastic rotation,

- ϕ is the curvature in the element,
- d_x is the differential length.

These calculations are particularly crucial for nonlinear time-history analyses and pushover analyses.

- **Application of the Distributed Plastic Model in Structural Analyses**

The distributed plastic model is utilized in various structural analysis methods:

- **Nonlinear Static Pushover Analysis:** The distributed plastic model can be used to determine where and how plastic deformations concentrate within a structure.
- **Nonlinear Time-History Analysis:** The application of real earthquake records to structural models allows for the examination of plastic zone formation and progression over time.
- **Applicability to Reinforced Concrete and Steel Structures:** The distributed plastic behavior model can also be used for steel structural elements, aiding in the development of design principles that enhance ductility.
- **Conclusion**

The distributed plastic behavior model provides a more realistic structural analysis by assuming that plastic deformation is spread over a certain length of the element rather than being concentrated at a single point. This model plays a significant role in ductile structural design and performance-based seismic design approaches. The use of distributed plastic modeling in determining the plastic deformation capacities of structural elements is becoming increasingly widespread in engineering applications and seismic design codes.

4. SEISMIC PERFORMANCE EVALUATION OF PUBLIC AND RESIDENTIAL BUILDINGS IN THE MALATYA PROVINCE

Turkey, due to its location in an active seismic zone, has been subjected to numerous destructive earthquakes throughout its history. These earthquakes have demonstrated that a significant portion of the existing building stock is inadequate in resisting seismic effects. In structural engineering, assessing the seismic safety of existing buildings and determining appropriate strengthening strategies are of great importance for earthquake-resistant construction. In this context, evaluation approaches based on nonlinear time history analysis are among the fundamental methods used to assess how structures behave under different seismic levels.

In this study, the seismic performance analysis of three reinforced concrete buildings with different story heights and geometries located in Malatya-Center was conducted within the framework of the Turkish Building Earthquake Code (TBEC-2018). The selected buildings were classified into three categories: low-rise, mid-rise, and high-rise. The evaluation considered existing structural system characteristics, material strengths, and soil conditions. During the analysis process, nonlinear analysis methods were employed to determine the actual seismic performance of the structures, and the obtained results were compared with the performance levels defined in the code.

This section first explains the fundamental concepts and analytical methods used in performance evaluation, followed by a detailed discussion of the current conditions of the analyzed buildings and their behavior under seismic loads.

4.1. General Information About Structures

The structures located in Malatya-Center are assumed to be situated at the coordinates Latitude: 38° 20' 54.117"N, Longitude: 38° 18' 53.316"E, and their seismic parameters have been determined using the AFAD Turkey Earthquake Hazard Maps Interactive Web Application based on this location.

These are real structures located in Malatya City. In alignment with the objectives of this study, they have been selected to be analyzed under scaled earthquakes and their corresponding forces, allowing for an assessment of their actual seismic behavior. The findings will be presented to provide scientific insights for public benefit. In this context, a low-rise state library building, a mid-rise public office building, and a high-rise residential building have been chosen for this study. In the following section, these buildings will be referred to by their designated names and analyzed accordingly.

The first structure (Structure A) is a state library, classified as a low-rise structure with a ground floor and two normal stories (G+2F). A review of its static drawings indicates that the building was constructed using C10 concrete and S420 steel reinforcement. It has a strip foundation system with dimensions of 100x100 cm. The structural system consists of reinforced concrete moment-resisting frames, designed to withstand the full seismic loads, **Table 4.1**.

The ground floor slab and the first-floor slab have an area of 490 m², while the second-floor ceiling covers an area of 540 m². All floors are designed as ribbed or beam-supported slab diaphragms, with a slab thickness of 25 cm. The structural system includes columns with dimensions of 35x60 cm, 45x40 cm, 45x45 cm, 45x60 cm, and 60x60 cm, as well as beams measuring 30x30 cm and 30x70 cm in different reinforcement configurations. The ground floor has a height of 4.5 m, while the other two floors each have a height of 3.5 m, resulting in a total building height of 11.5 m.

Table 4.1: Summary of the State Library Building

Concrete Class	C10
Rebar Steel Class	S420
Snow Load Region	3. Region
Altitude	954 m
Building Total Height (H_N)	11.5 m
Building Height Class (BHC)	6
Total Footprint	515 m^2
Local Site Class	ZC
Total Column Quantity	94
Total Shell Element Quantity	0
Total Beam Quantity	289
Infill Wall Thickness	13.5 cm
Exterior Wall Thickness	20 cm
Floor Finishing	Marble + Screed
Slab Thickness	25 cm

The second structure (Structure B) is a public office building, classified as a mid-rise structure with a ground floor and seven normal stories (G+7F). A review of its static drawings indicates that the building was constructed using C10 concrete and S220 steel reinforcement. It has a raft foundation system with a slab thickness of 30 cm. The structural system consists of reinforced concrete moment-resisting frames and solid shear walls, designed to jointly withstand the seismic loads,

Table 4.2.

All floor slabs have an area of 479 m² each what are designed as beam-supported slab diaphragms, with a slab thickness of 17 cm. The structural system includes columns with dimensions of 30x40 cm, 30x50 cm, 30x60 cm, 30x80 cm, 60x30 cm, 70x30 cm, 80x30 cm, 90x30 cm, 100x30 cm and 130x30 cm as well as beams measuring 30x65 cm and 30x75 cm in different reinforcement configurations. The central part of the building contains a C-shaped reinforced concrete shear wall, with each leg having a thickness of 30 cm. All floors have a height of 2.9 m, resulting in a total building height of 23.2 m.

For this structure to fall under the category of mid-rise buildings, two additional stories were defined beyond its current configuration, and the analysis results were interpreted accordingly.

Table 4.2: Summary of the Public Office Building

Concrete Class	C10
Rebar Steel Class	S220
Snow Load Region	3. Region
Altitude	954 m
Building Total Height (H_N)	23.2 m
Building Height Class (BHC)	5 Upcaled Ver.
Total Footprint	548 m^2
Local Site Class	ZC
Total Column Quantity	336
Total Shell Element Quantity	24
Total Beam Quantity	664
Infill Wall Thickness	13.5 cm
Exterior Wall Thickness	20 cm
Floor Finishing	Marble + Screed
Slab Thickness	17 cm

The third structure (Structure C) is a residential building, classified as a high-rise structure with a ground floor and twelve normal stories (G+12F) A review of the structural drawings and the obtained laboratory data indicates that the building was constructed using C24.1 concrete strength and S420 steel reinforcement. It has a raft foundation system with a slab thickness of 65 cm. The structural system consists of reinforced concrete moment-resisting frames and solid shear walls, designed to jointly withstand the seismic loads, **Table 4.3**.

All floor slabs have an area of 479 m² each what are designed as beam-supported slab diaphragms, with a slab thickness of 15 cm. The structural system includes columns with dimensions of 30x30 cm, 30x90 cm, 30x95 cm, 30x100 cm, 40x40 cm, 50x50 cm, 90x30 cm, 125x30 cm, 135x30 cm and 145x30 cm as well as beams measuring 25x60 cm and 50x15 cm in different reinforcement configurations. The structure have four I-shaped and two U-shaped reinforced concrete shear walls with a thickness of 25 cm, as well as six I-shaped reinforced concrete shear walls with a thickness of 30 cm. The ground floor has a height of 4.05 m, while the other two floors each have a height of 3.05 m, resulting in a total building height of 40.65 m.

Table 4.3: Summary of the Public Office Building

Concrete Class	C24.1
Rebar Steel Class	S420
Snow Load Region	3. Region
Altitude	954 m
Building Total Height (H_N)	40.65 m
Building Height Class (BHC)	4
Total Footprint	1167 m^2
Local Site Class	ZC
Total Column Quantity	470
Total Shell Element Quantity	208
Total Beam Quantity	1095
Infill Wall Thickness	13.5 cm
Exterior Wall Thickness	20 cm
Floor Finishing	Marble + Screed
Slab Thickness	15 cm

4.1.1. Vertical Loads Acting on the Buildings

Vertical loads are forces acting vertically on the structural system of a building and are weight-related forces. These loads are divided into two main categories: dead loads (such as the building’s self-weight, finishing materials, weight of columns and beams) and live loads (such as furniture, people, vehicles, storage materials). Dead loads are typically fixed loads that do not change over time, usually established during construction. Live loads, on the other hand, vary according to user activities and are calculated according to specific standards to ensure maximum safety in building design.

In addition to the self-weight of the structural system, various loads are present on the floors. Dead loads, such as plaster, screed (leveling concrete), surface coverings (marble, granite, etc.), and wall loads are applied as distributed loads on the slabs.

In this study, it is assumed that all three buildings have floor coverings consisting of 2 cm plaster, 5 cm screed, and 3 cm marble, and this has been applied to the numerical model. The total slab load is 2.31 kN/m².

Plaster weight: 0.02 x 20 = 0.4 kN/m²
Screed: 0.05 x 22 = 1.10 kN/m²
Marble covering: 0.03 x 27 = 0.81 kN/m²
Total slab load: 0.4 + 1.1 + 0.81 = 2.31 kN/m²

For infill wall loads, an area load of 0.75 kN/m² was applied to the slabs.

On the roof slab, unlike the regular slabs, there is no marble covering. The slabs have 2 cm plaster and 5 cm screed, resulting in a weight of 1.5 kN/m². The snow load on the roof slab, as defined in TS 498 and TS EN 1991-1-3 standards, was determined to be 1.04 kN/m², given Malatya's altitude of 954 m, its classification in the third snow load region, roof slopes between 0 and 30 degrees, and normal topographical conditions.

Live loads are forces dynamically changing on the structural system due to external factors or user activities. These loads result from movable elements such as furniture, people, vehicles, and equipment, and are usually calculated with specific loading values according to standards and regulations. Since live loads can vary over time, it is necessary to perform both static and dynamic analyses. Accurate analysis of these loads is critical for the building’s safety, durability, and service life.

Based on TS 498, a live load of 2 kN/m² was used in the buildings for the analyses. In slabs with staircases, a load of 3.5 kN/m² was included in the calculations. 2 kN/m² load was also applied to the roof slabs.

4.2. Mathematical Models of Structures

In this section, mathematical models of all buildings have been developed, and the analysis steps have been approached by starting with building geometries. ETABS (Extended Three-dimensional Analysis of Building Systems) has been selected as the structural analysis software. ETABS is a structural analysis and design software specifically focused on building design and analysis. It was developed by Computers and Structures, Inc. (CSI) and is widely used by engineers, academics, and designers worldwide.

4.2.1. The State Library (Structure A)

When creating the mathematical model of the building, material properties are the first parameters defined in the model. It was previously mentioned that the building has C10 concrete and S420 steel class, and this information was obtained from the as-built survey of the existing project.

The acquired data has been defined in the analysis software, and additionally, the nonlinear behavior of the materials and the corresponding stress-strain relationships have been specified in accordance with TBDY-2018, as illustrated in **Figure 4.1** and **Figure 4.2**.

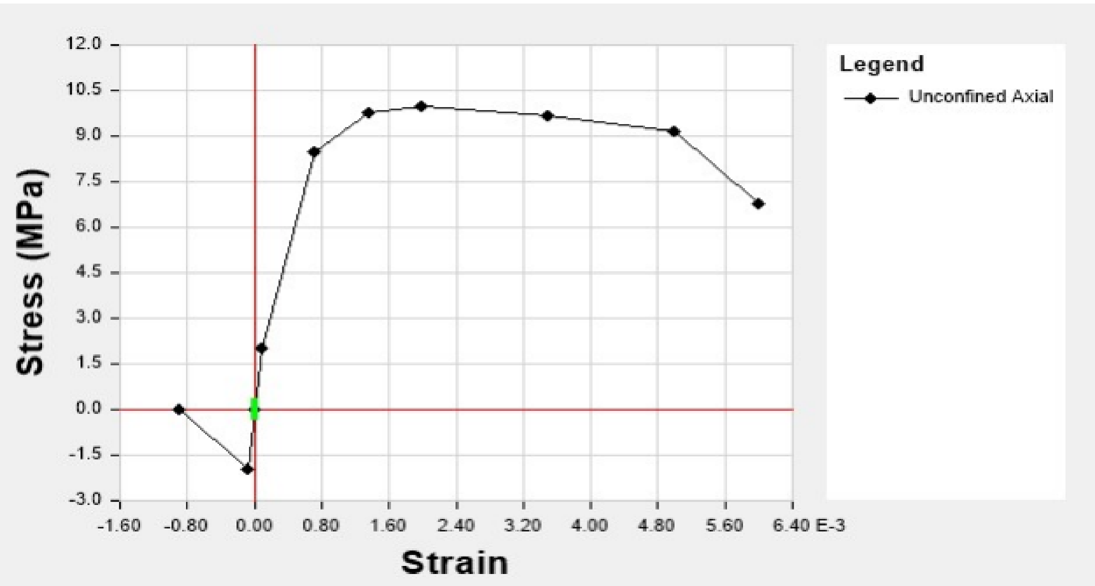

Figure 4.1: Stress-strain graph for unconfined C10 concrete class.

For the C10 concrete material, the following parameters have been defined; γ_c = 25 kN/m³ unit weight, E_c = 15,811 MPa modulus of elasticity, ε_{co} = 0.002 strain at unconfined compressive strength, and ε_{cu} = 0.005 ultimate unconfined strain capacity.

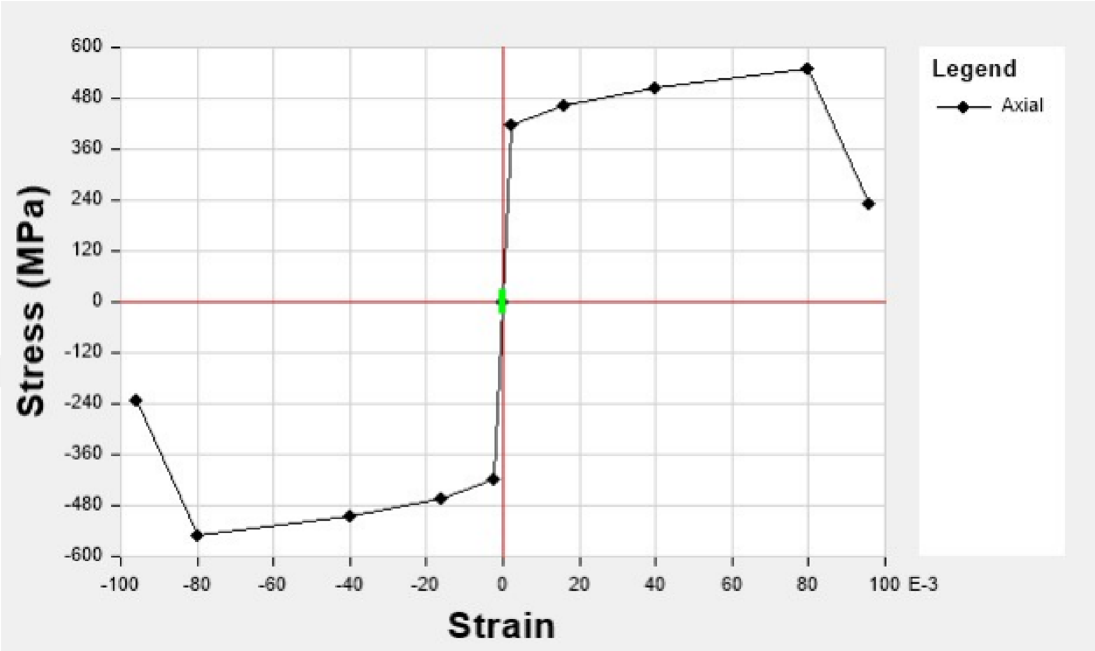

Figure 4.2: Stress-strain graph for S420 reinforcing steel class.

The Mander Model has been employed to more accurately represent the stress-strain behavior of concrete under axial compression, particularly the behavior of confined concrete.

For the S420 steel grade material, the following parameters have been defined: γ_c = 0 kN/m³ unit weight (considered in concrete weight), E_c = 200 GPa modulus of elasticity, ε_{so} = 0.008 strain at the onset of strain hardening, and ε_{su} = 0.08 ultimate strain capacity.

All sections defined in the mathematical model, **Figure 4.5**, are presented in this section. The beam and slab sections, along with the floor plans of the model, are shown in **Figure 4.3** and **Figure 4.4** below. The assigned column sections are provided in the general building information section.

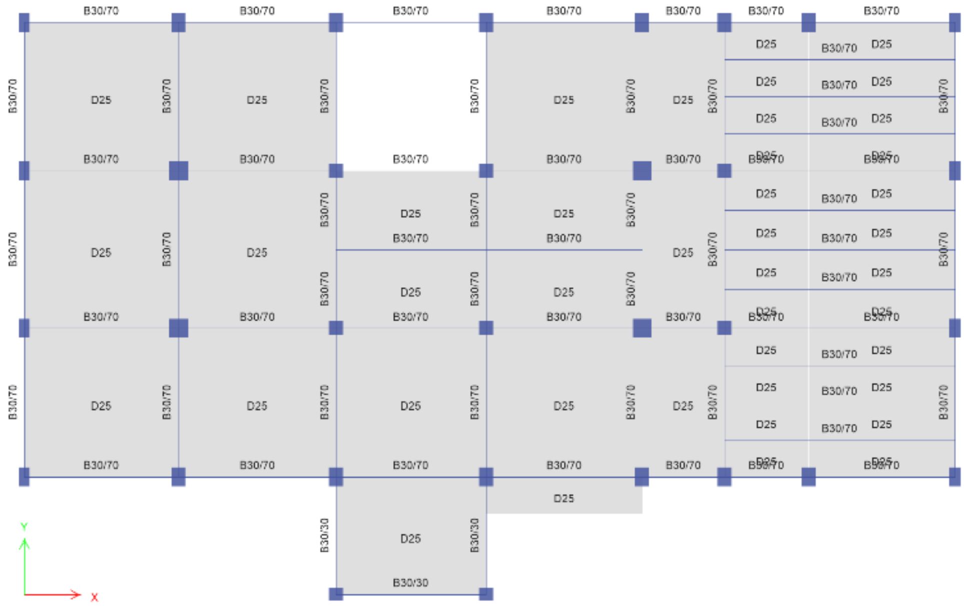

Figure 4.3: Formwork plan and element sections for the Ground and the 1st Floor.

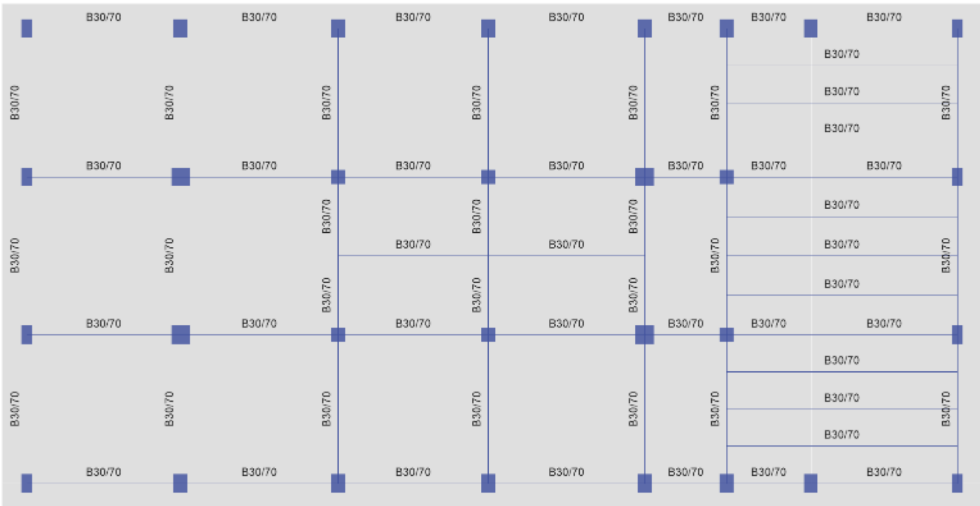

Figure 4.4: Formwork plan and element sections for the 2nd Floor.

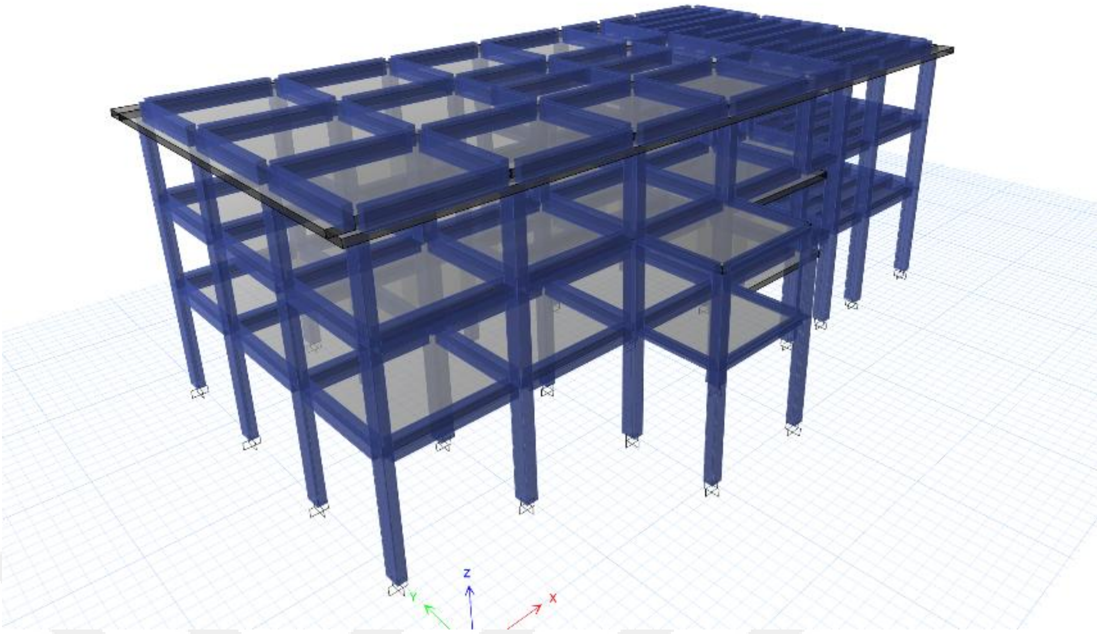

Figure 4.5: 3D Mathematical Model of the Library Building (Structure A).

4.2.2. Public Office Building (Structure B)

When creating the mathematical model of the building, material properties are the first parameters defined in the model. It was previously mentioned that the building has C10 concrete and S220 steel class, and this information was obtained from the as-built survey of the existing project.

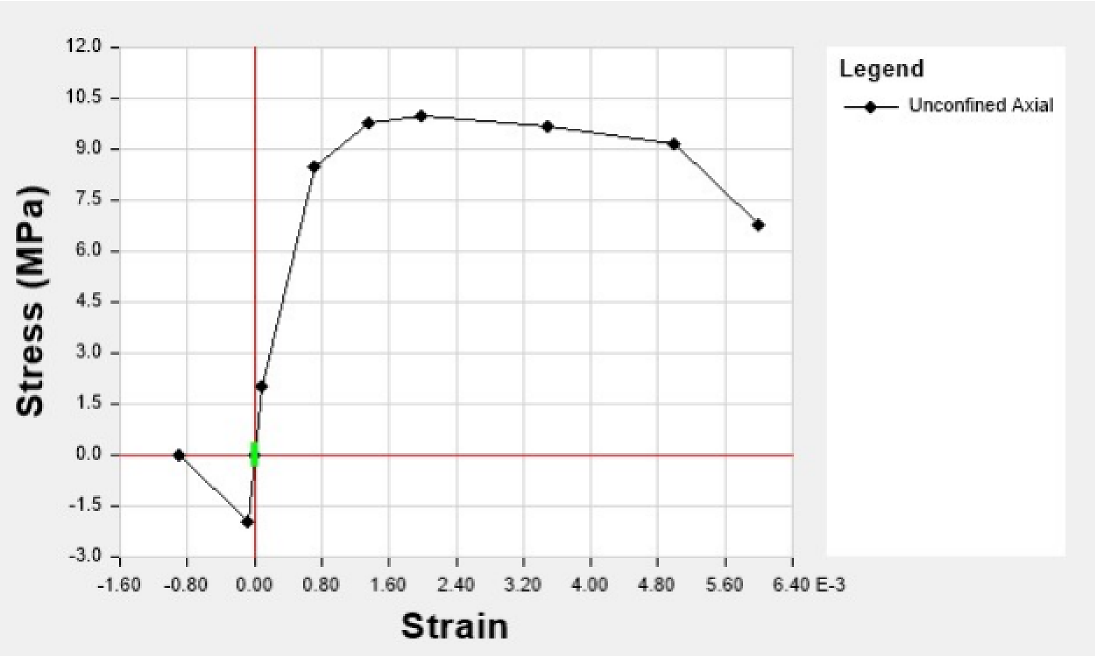

Figure 4.6: Stress-strain graph for unconfined C10 concrete class.

The acquired data has been defined in the analysis software, and additionally, the nonlinear behavior of the materials and the corresponding stress-strain relationships have been specified in accordance with TBDY-2018, as illustrated in **Figure 4.6** and **Figure 4.7**.

For the C10 concrete material, the following parameters have been defined; γ_c = 25 kN/m^3 unit weight, E_c = 15,811 MPa modulus of elasticity, ε_{co} = 0.002 strain at unconfined compressive strength, and ε_{cu} = 0.005 ultimate unconfined strain capacity.

The Mander Model has been employed to more accurately represent the stress-strain behavior of concrete under axial compression, particularly the behavior of confined concrete.

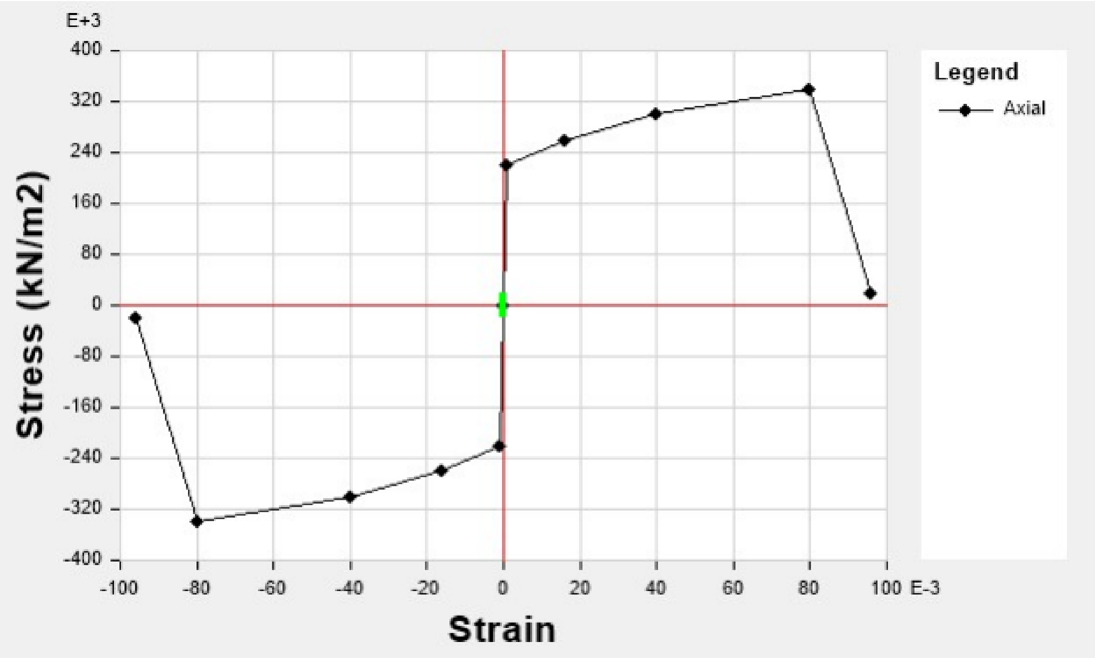

Figure 4.7: Stress-strain graph for S220 reinforcing steel class.

For the S220 steel grade material, the following parameters have been defined: γ_c = 0 kN/m³ unit weight (considered in concrete weight), E_c = 200 GPa modulus of elasticity, ε_{so} = 0.008 strain at the onset of strain hardening, and ε_{su} = 0.08 ultimate strain capacity.

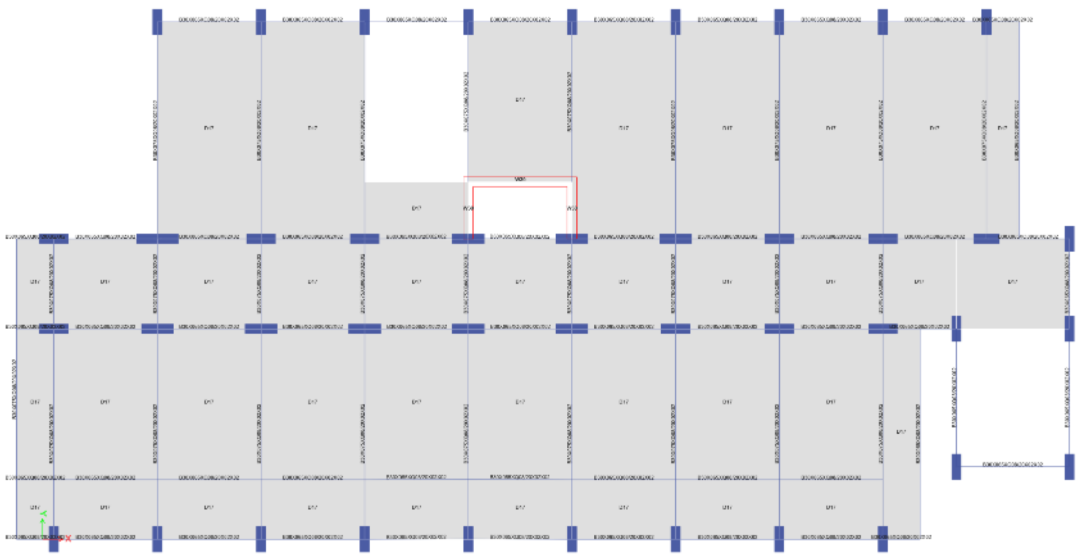

Figure 4.8: Formwork plan and element sections for the Ground and the 1st Floor.

All sections defined in the mathematical model, **Figure 4.11**, are presented in this section. The beam and slab sections, along with the floor plans of the model, are shown in **Figure 4.8**, **Figure 4.9** and **Figure 4.10** below. The assigned column sections are provided in the general building information section.

Figure 4.9: Formwork plan and element sections for the 2nd Floor.

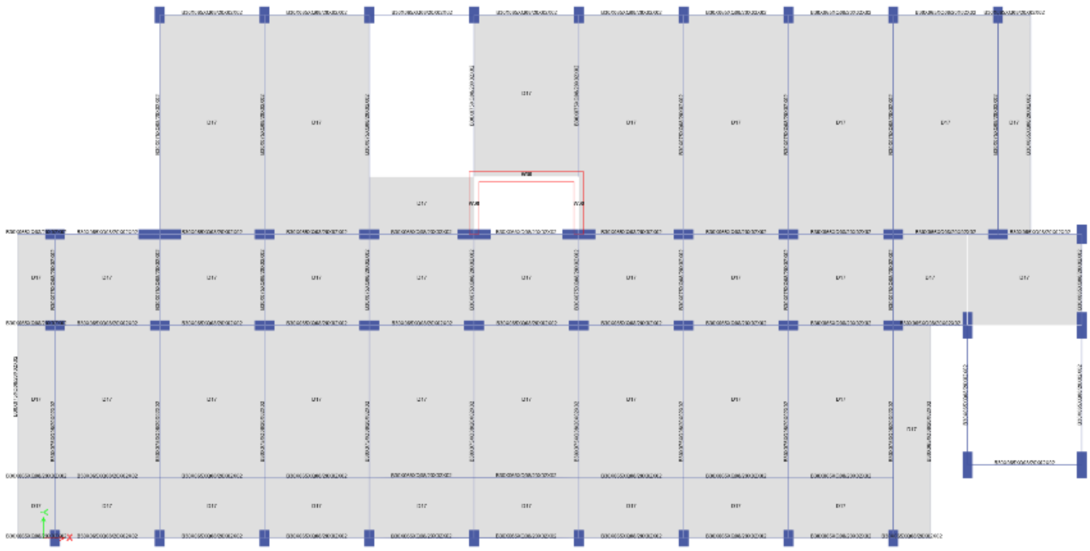

Figure 4.10: Formwork plan and element sections for the 3rd Floor and above.

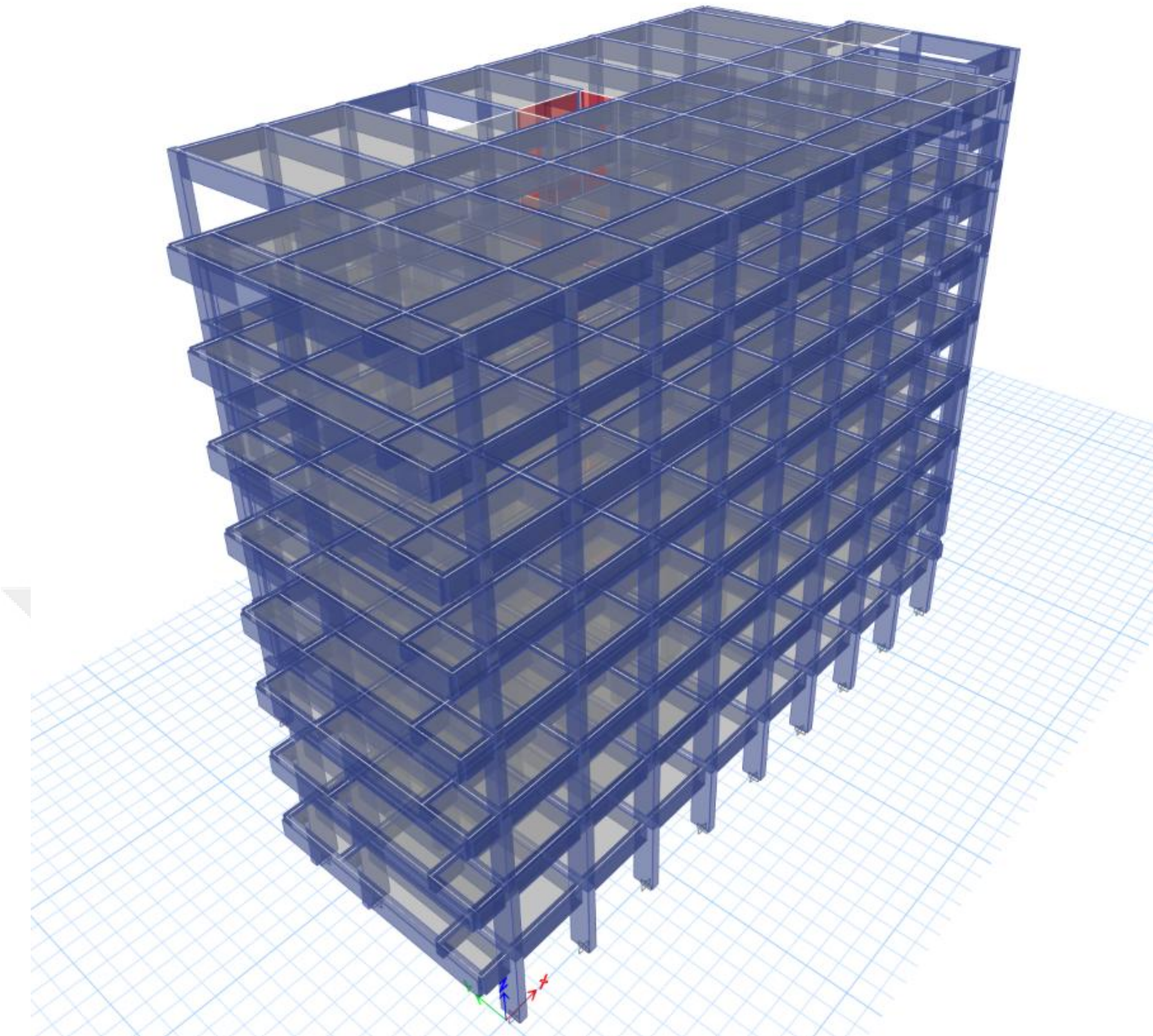

Figure 4.11: 3D Mathematical Model of the Public Building (Structure B).

4.2.3. Residential Building (Structure C)

When creating the mathematical model of the building, material properties are the first parameters defined in the model. It was previously mentioned that the building has C24.1 concrete and S420 steel class, and this information was obtained from the as-built survey of the existing project.

The acquired data has been defined in the analysis software, and additionally, the nonlinear behavior of the materials and the corresponding stress-strain relationships have been specified in accordance with TBDY-2018, as illustrated in **Figure 4.12** and **Figure 4.13**.

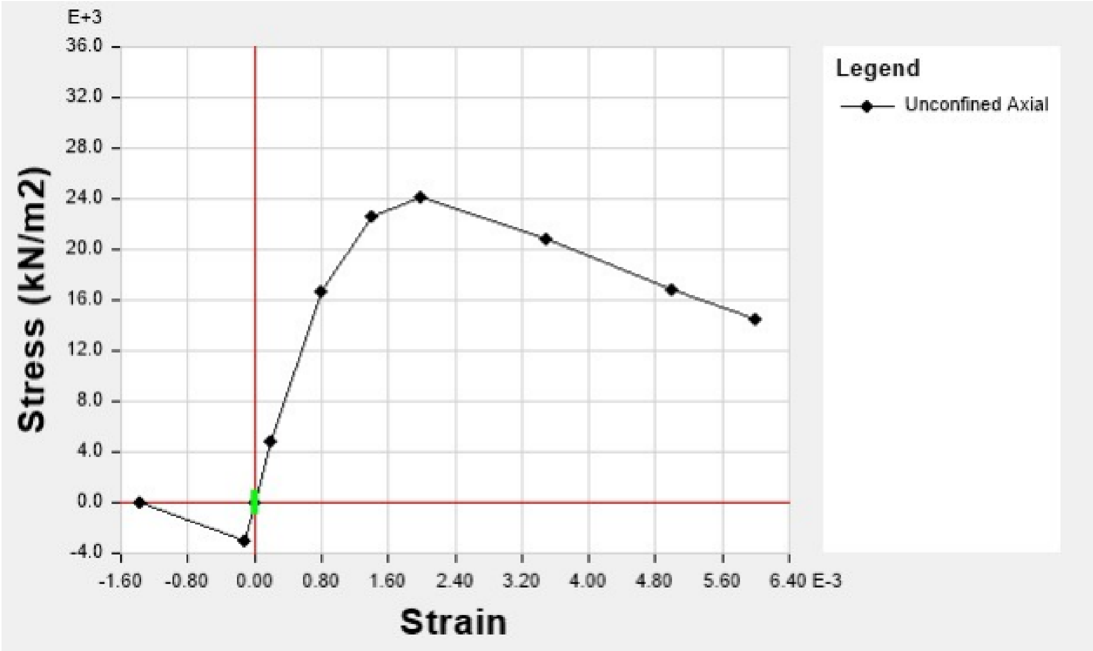

Figure 4.12: Stress-strain graph for unconfined C24.1 concrete class.

For the C24.1 concrete material, the following parameters have been defined; γ_c = 25 kN/m³ unit weight, E_c = 24,545 MPa modulus of elasticity, ε_{co} = 0.002 strain at unconfined compressive strength, and ε_{cu} = 0.005 ultimate unconfined strain capacity.

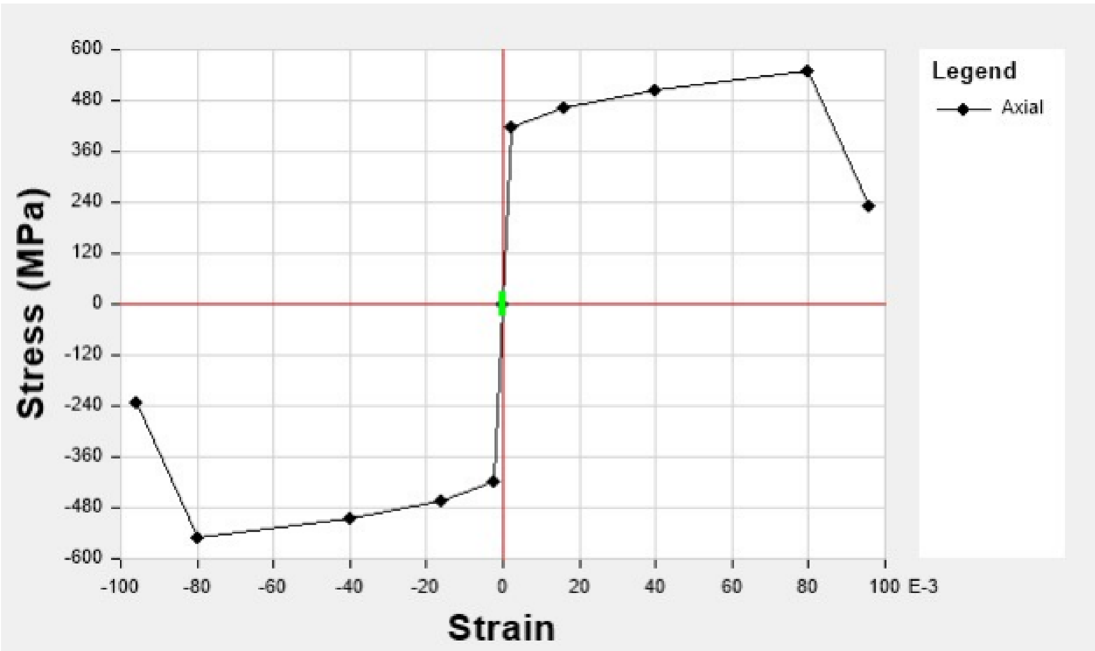

Figure 4.13: Stress-strain graph for S420 reinforcing steel class.

The Mander Model has been employed to more accurately represent the stress-strain behavior of concrete under axial compression, particularly the behavior of confined concrete.

For the S420 steel grade material, the following parameters have been defined: $\gamma_c = 0$ kN/m³ unit weight (considered in concrete weight), E_c = 200 GPa modulus of elasticity, $\varepsilon_{so} = 0.008$ strain at the onset of strain hardening, and $\varepsilon_{su} = 0.08$ ultimate strain capacity.

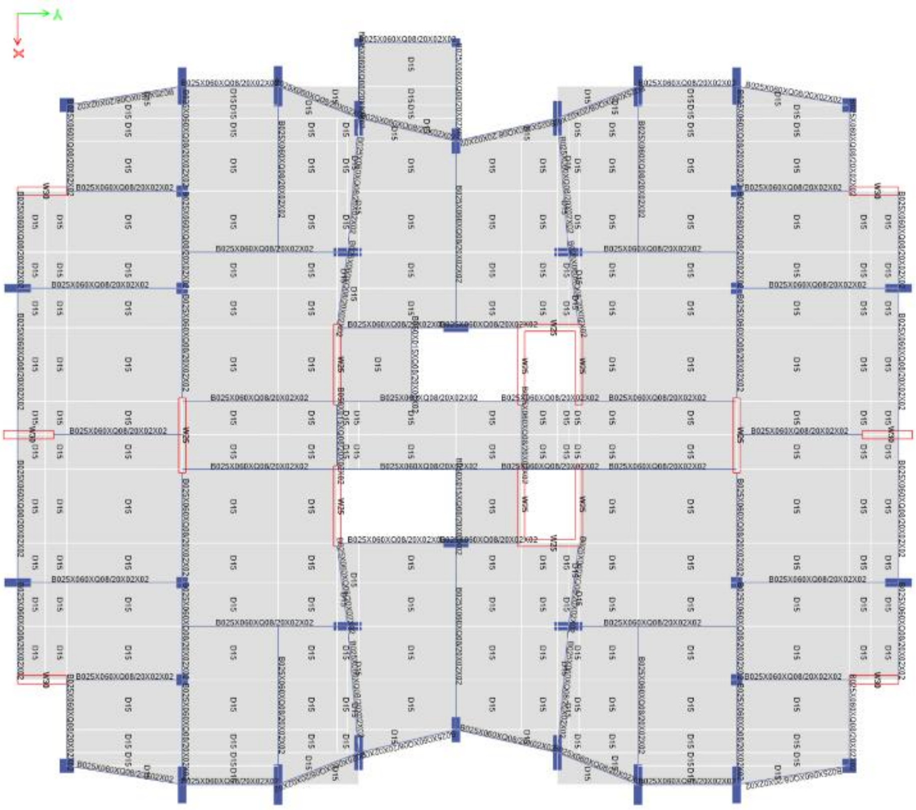

Figure 4.14: Formwork plan and element sections for the Ground Floor.

All sections defined in the mathematical model, **Figure 4.16**, are presented in this section. The beam and slab sections, along with the floor plans of the model, are shown in **Figure 4.14** and **Figure 4.15** below. The assigned column sections are provided in the general building information section.

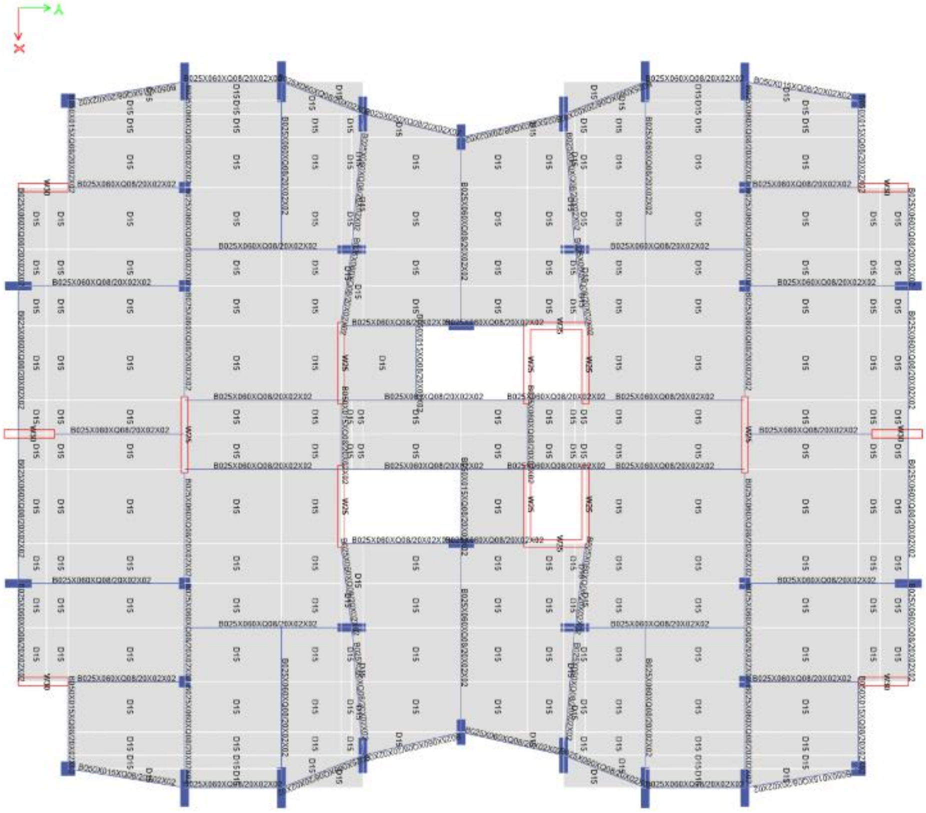

Figure 4.15: Formwork plan and element sections for the 1st Floor and above.

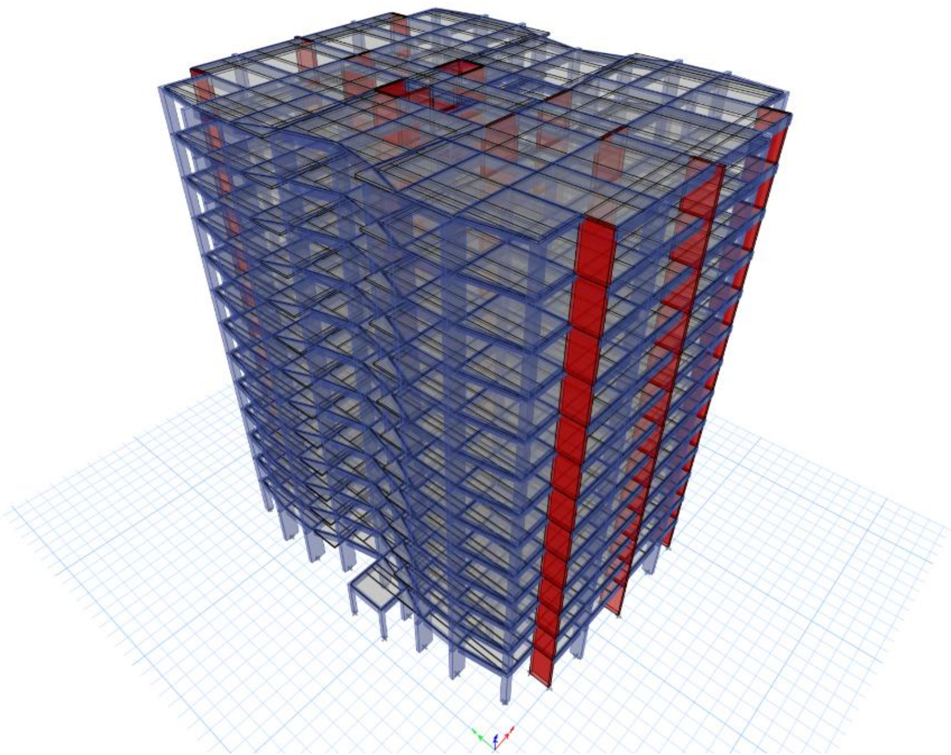

Figure 4.16: 3D Mathematical Model of the Public Building (Structure C).

4.2.4. Definition of Cracked Section (Effective Section Stiffness)

The effective section stiffness factors provided in the **Table 4.4** have been assigned to column, beam, shear wall, and slab section elements in accordance with TBEC-2018 for modeling the cross-sectional properties of reinforced concrete structural system elements.

Table 4.4: Effective Section Stiffness Assignments for Elements According to TBEC-2018

RC Stuctural System Member	Effective section stiffness factor	
Shear Wall - Slab (in-plane)	***Axial***	***Slide***
Shear Wall	0.50	0.50
Basement Shear Wall	0.80	0.50
Slab	0.25	0.25
Shear Wall - Slab (out of plane)	***Bearing***	***Shear***
Shear Wall	0.25	1.00
Basement Shear Wall	0.50	1.00
Slab	0.25	1.00
Frame Member	***Bearing***	***Shear***
Tie Beam	0.15	1.00
Frame Beam	0.35	1.00
Frame Column	0.70	1.00
Shear Wall (Equ. Frame Mem.)	0.50	0.50

4.2.5. Definition of Mass Source and Assumption of Rigid Diaphragm

In the structural models, dead loads (Element Self Weight, M-Wall, SDL, Roof) are directly considered, while live loads (Q) are reduced by 30 percent when defining the mass. Additionally, 30 percent of the snow load (S) is included in the roof mass calculation, **Figure 4.17**.

This approach is adopted to ensure a more realistic representation of the structure's dynamic behavior and response under seismic effects. The use of mass participation coefficients enhances the accuracy of modal analyses and seismic calculations, contributing to more reliable engineering assessments.

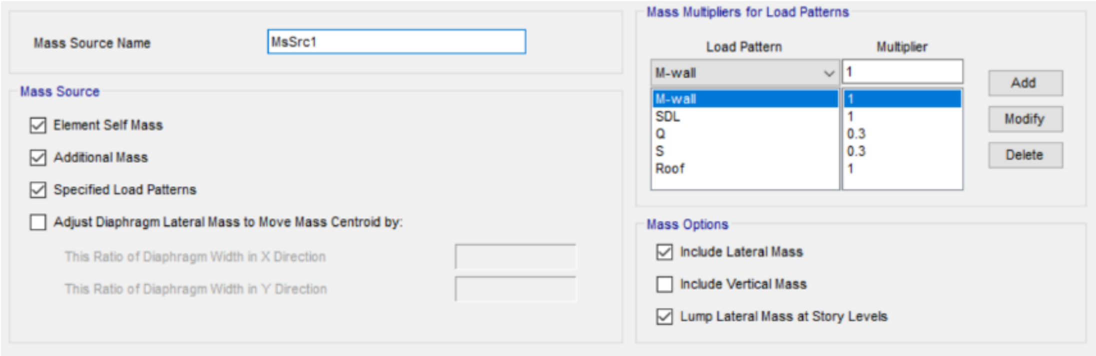

Figure 4.17: Definition of Mass Source

Reinforced concrete slabs can be modeled as a rigid diaphragm in regular buildings where A2 and A3 types of irregularities are not present and significant in-plane deformations are not expected. The rigid diaphragm model will also be used in the calculation of additional eccentricity effects, **Figure 4.18**.

According to the calculations based on the rigid diaphragm model, the force transferred from the slab to any vertical load-bearing system element, such as a column or shear wall, in any direction will be determined as the difference between the shear forces obtained for that element in the relevant direction on the floors above and below the slab.

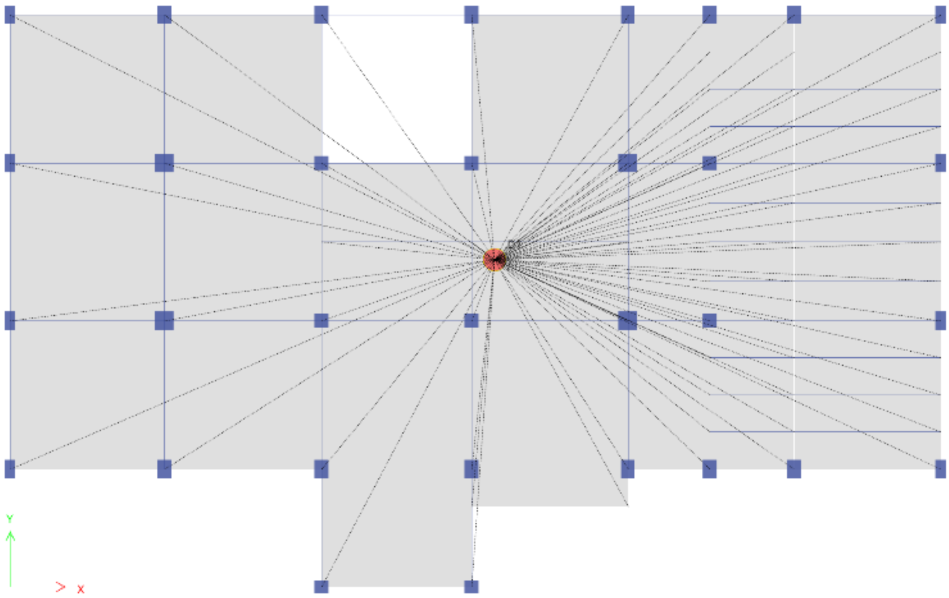

Figure 4.18: Rigid Diaphragm Assumption and Story Mass Center.

4.2.6. Lump Plastic Hinge Assignment

The definition of plastic hinges assumes that all plastic deformation is concentrated in these regions, while the other parts of the elements exhibit elastic behavior. In ETABS software, the definition of plastic hinges is carried out by assigning manually calculated properties to the elements.

In this study, section properties were manually calculated to obtain a more realistic solution. The characteristics of the defined plastic hinges are explained in the following sections.

Definition of Plastic Hinge in Columns

It is essential to perform Moment-Curvature analyses for all columns as a priority. In the nonlinear modeling of column elements, the moment-curvature relationship of the section is one of the most critical parameters. Through this relationship, information about the ductility and confinement condition of the section can be obtained.

For these analyses, all columns were modeled in SAP2000 using the Section Design option, where material properties, dimensions, and reinforcement details were defined. As an example, the cross-section of a 35×60 cm column is shown below, **Figure 4.19**.

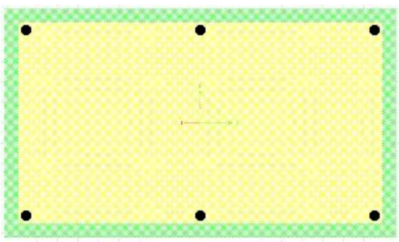

Figure 4.19: C035X060X06Q16XQ08/15X02X02 Section

The moment-curvature relationship varies depending on the material properties of the section, longitudinal and transverse reinforcement conditions, and the ratio of axial force acting on the section. According to TBEC-2018, the plastic hinge behavior model is considered appropriate for frame elements. Based on this approach, the moment-curvature relationships of column elements must be determined under different axial load levels and in different directions.

In this context, for column elements with five different cross-sections in the structure, analyses were conducted for axial load levels of 0%, 15%, 30%, and 45%, and for moment-curvature relationships in 0° and 90° directions, resulting in a total of 9 column section analyses, **Figure 4.20**, **Figure 4.21**, **Figure 4.22**, **Figure 4.23**.

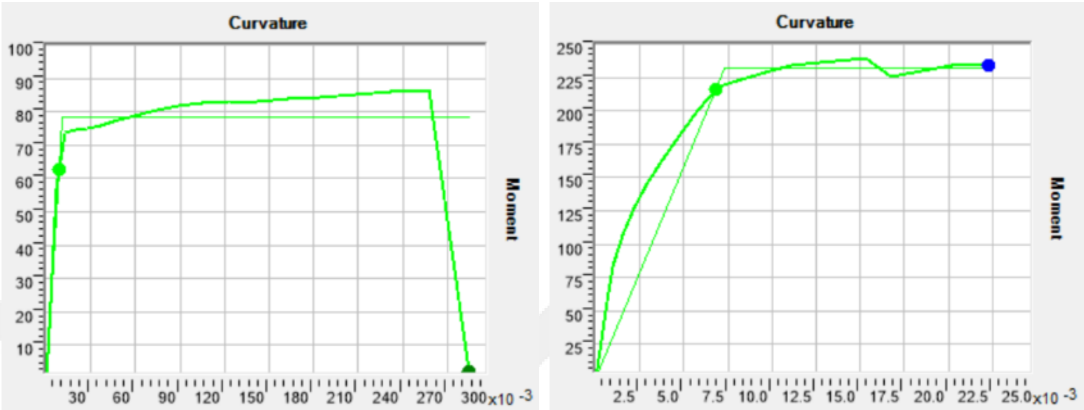

Figure 4.20: For P = 0% Axial Load; 0° for *M*-κ Graph (kNm-rad/m) and 90° for *M*-κ Graph (kNm-rad/m)

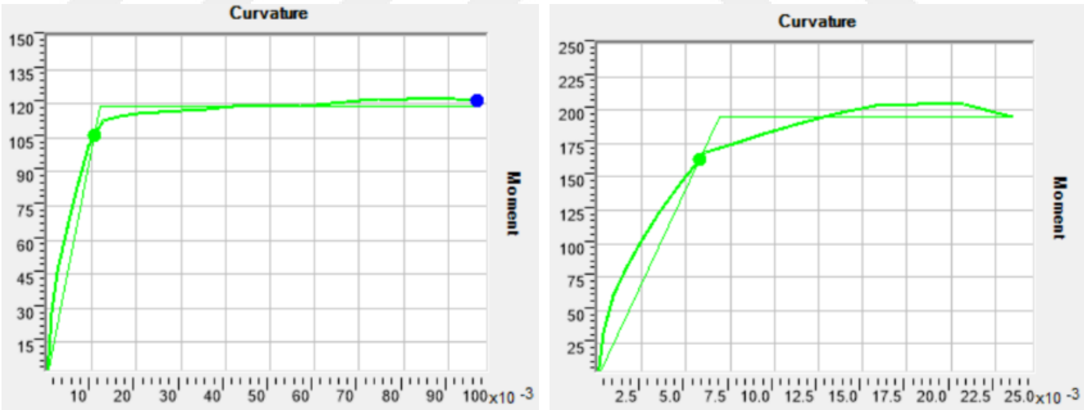

Figure 4.21: For P = 15% Axial Load; 0° for *M*-κ Graph (kNm-rad/m) and 90° for *M*-κ Graph (kNm-rad/m)

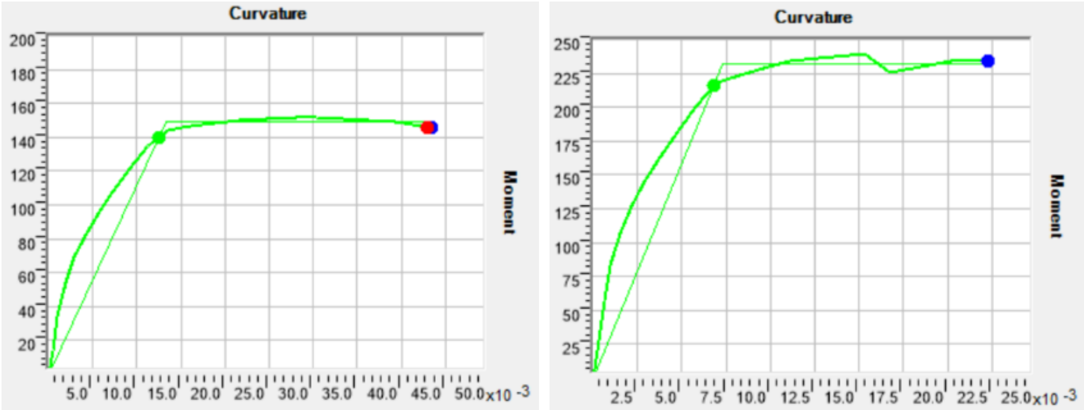

Figure 4.22: For P = 30% Axial Load; 0° for *M*-κ Graph (kNm-rad/m) and 90° for *M*-κ Graph (kNm-rad/m)

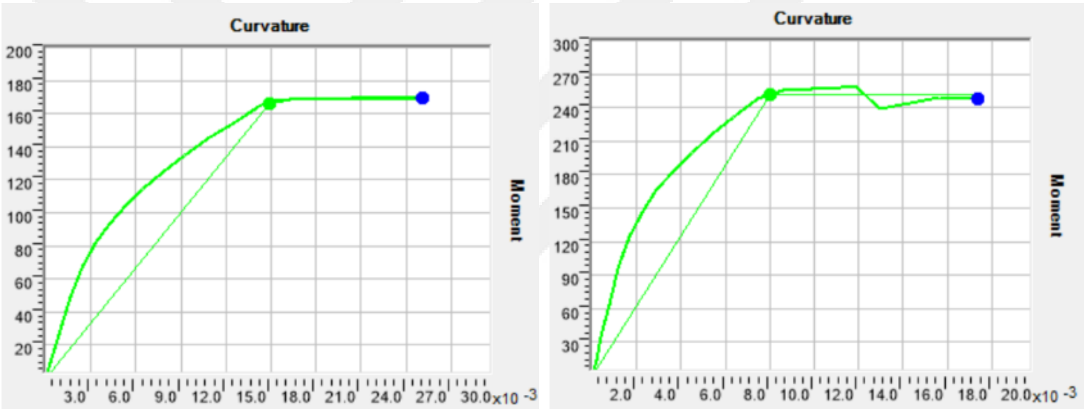

Figure 4.23: For P = 45% Axial Load; 0° for *M*-κ Graph (kNm-rad/m) and 90° for *M*-κ Graph (kNm-rad/m)

Moment–curvature analyses have been conducted for the columns of all structures, and the outputs have been utilized in determining the performance level of the structural elements.

Above, as an example, the moment-curvature relationships obtained from the analysis results of the "C035X060X06Q16XQ08/15X02X02" section are presented.

Considering the behavior of column elements, it is known that they are subjected to axial force and bending moments, leading to post-elastic behavior under these effects.

Below, the plastic hinge definition for the "C035X060X06Q16XQ08/15X02X02" section is explained step by step.

For column elements, the P-M2-M3 type hinge was selected in the analysis program to define the plastic hinge behavior. Here, a deformation-controlled hinge was used for ductile elements.

The interface used to define the plastic hinge properties of the column element in the program is shown below. Since the column element has a 35x60 cm cross-section, symmetry properties were not assigned, **Figure 4.24**.

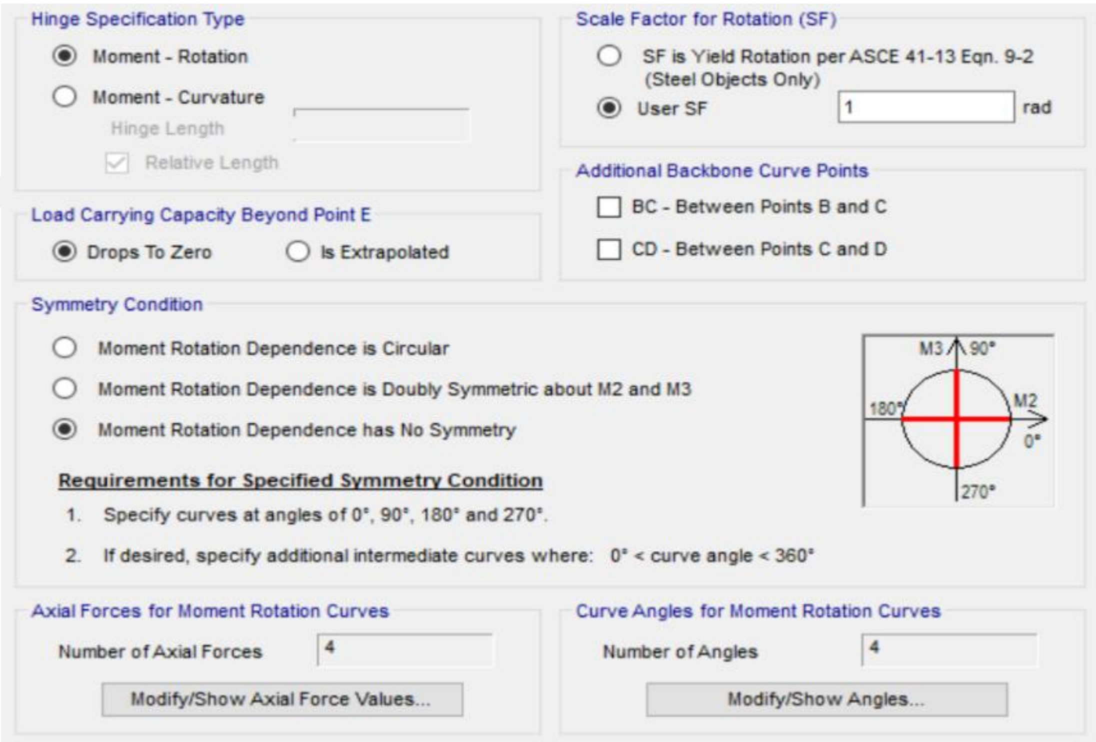

Figure 4.24: Main Panel for Plastic Hinge Assignment in the Analysis Software

The definitions for different axial load levels and moment-curvature relationships calculated for the columns have been entered below. Since the section exhibits symmetry in one direction, the same moment-curvature graph has been assigned in the program for 0° and 180°, as well as for 90° and 270°, **Figure 4.25**.

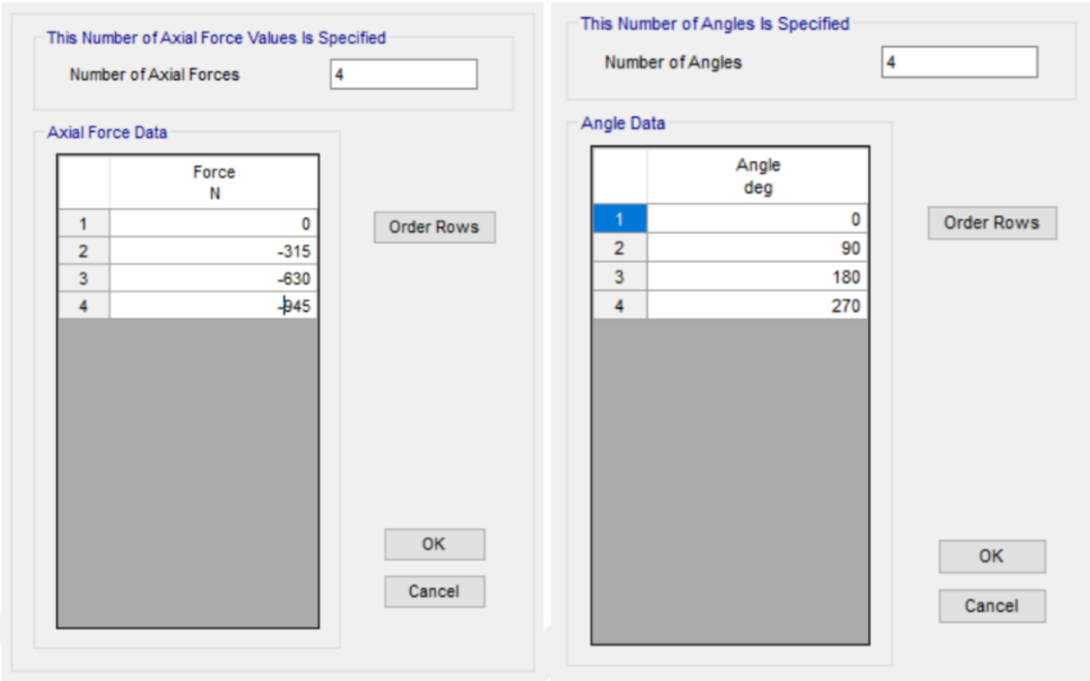

Figure 4.25: Axial Load Classes Resulting from the G + nQ Combination Symmetry Axes

In the following calculation, the Göçme Öncesi (GÖ) rotation value has been determined at 45% axial load level in the 90° direction.

For P = -945 kN, M_y = 166.05 kNm ve M_u = 168.92 kNm values,

$$\frac{Mu}{My} = \frac{168{,}92}{166{,}05} = 1.02$$

For ϕ_y = 0,0076 and ϕ_u = 0,021 rotation value,

$$\phi\mathrm{p} = \phi\mathrm{u} - \phi\mathrm{y} = 0{,}0134$$

The plastic location length L_p is assumed to be half of the section length,

$$Lp = \frac{60}{2} = 30\ cm$$

The plastic rotation θ_p is obtained by multiplying the plastic hinge length by the plastic curvature.

$$\theta\mathrm{p} = 0{,}3\ \times 0{,}0134 = 0{,}00402\ \mathrm{rad}$$

The calculated values have been entered into the program through the panel shown below, **Figure 4.26**.

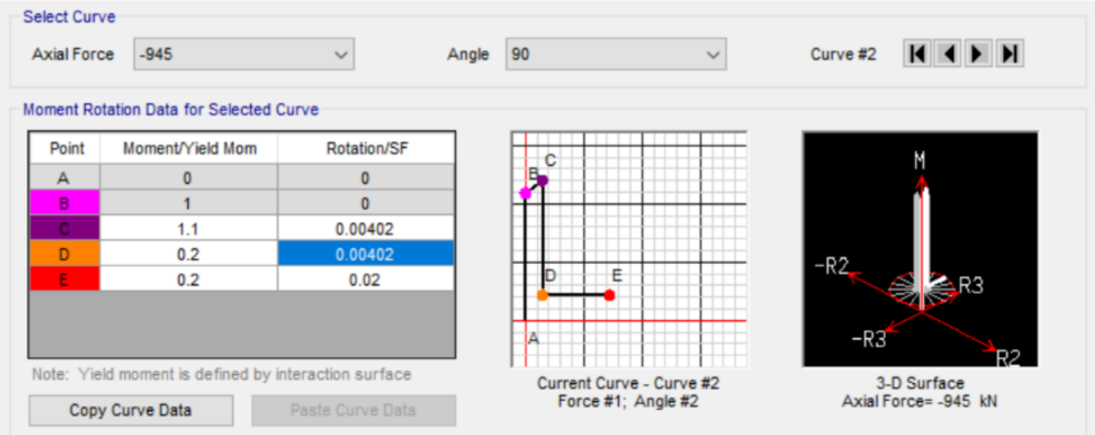

Figure 4.26: Plastic Hinge Definition

In post-elastic behavior, the column load-bearing capacity values to be considered are calculated by the program based on the element properties defined during the section assignment. The panel below illustrates this definition, **Figure 4.27**.

Figure 4.27: Material Properties Source Definition

Plastic Hinge Definition in Beams

SAP2000 software was also utilized for the section analysis of beam elements. In SAP2000, section geometry, material properties, vertical and horizontal reinforcement details were defined to perform the section analysis.

To conduct the section analysis, confined and unconfined concrete material models, as well as steel material models specified in TBEC-2018, were incorporated into the program.

As shown in the example **Figure 4.28**, moment-curvature relationships obtained from the section analysis in SAP2000 were also derived for beam elements. These data were assigned to beams in a similar manner to column sections, but exclusively as "M3 Bending Hinges."

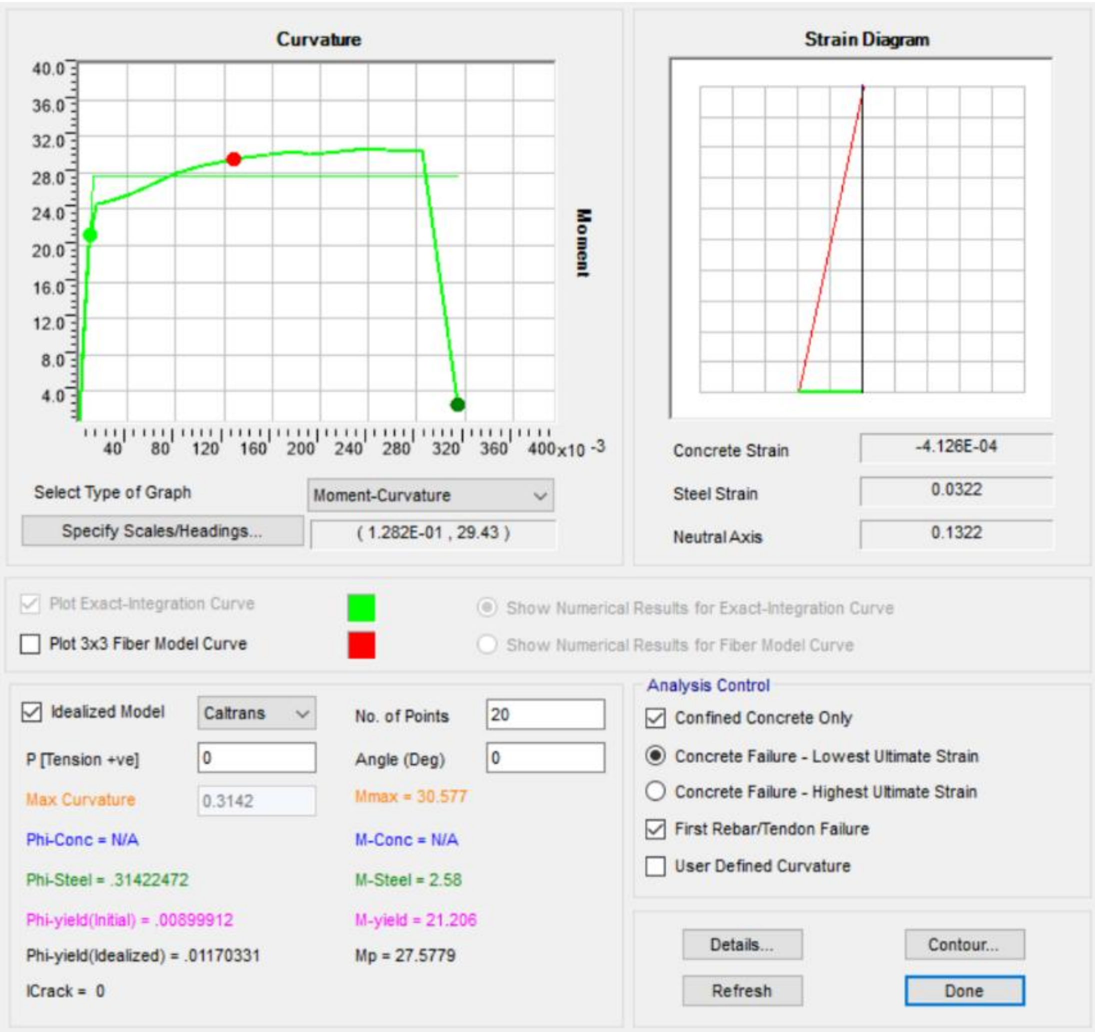

Figure 4.28: Moment – Curvature Analysis for Beams

Determination and Localization of Plastic Hinge Zone

It was previously explained that when structural elements reach their load-bearing capacity under seismic effects, they exhibit post-elastic behavior and undergo plastic deformation. In frame systems, the critical locations where plastic hinges form are the sections where the bending moment reaches its maximum. These locations are typically at beam ends, column-beam connections, and the base sections of shear walls.

The determination of plastic hinge regions should consider the moment distribution and the deformation capacity at the element ends. In frame elements subjected to lateral loads, maximum bending moments occur at the ends of the elements, meaning that plastic hinges should be modeled at these sections. In columns, plastic hinges generally form at story levels, while in beams, they occur at span ends.

According to TBDY-2018, the length of the plastic deformation region is considered to be half of the section height. Plastic hinges representing the lumped plastic behavior model should be placed at the center of this plastic region. The lengths of the plastic deformation regions for column and beam frame elements should be modeled as realistically as possible in nonlinear analyses, and the deformations occurring in these regions should be considered in the structural performance assessment.

For all sections, the calculation of the regions where plastic hinges will occur has been provided in the **Table 4.5** and defined in mathematical models as example below.

Table 4.5: Summary of the State Library Building (Example)

Section Name	h	L_{net} (m)	1st Hinge Relative Location	2nd Hinge Relative Location
	[cm]	[m]	[m]	[m]
B030X070XQ08/15X02X02	70	4.98	0.070	0.930
B030X070XQ08/15X02X02	70	5.08	0.069	0.931
B030X070XQ08/15X02X02	70	4.85	0.072	0.928
B030X070XQ08/15X02X02	70	5.05	0.069	0.931
B030X070XQ08/15X02X02	70	2.65	0.132	0.868
B030X070XQ08/15X02X02	70	2.72	0.129	0.871
B030X070XQ08/15X02X02	70	4.73	0.074	0.926
B030X070XQ08/15X02X02	70	4.8	0.073	0.927
B030X070XQ08/15X02X02	70	5.09	0.069	0.931
B030X070XQ08/15X02X02	70	7.45	0.047	0.953
B030X070XQ08/15X02X02	70	2.545	0.138	0.862
B030X030XQ08/15X02X02	30	3.8	0.039	0.961
C035X060X06Q14XQ08/20X02X02	60	3.5	0.086	0.914
C060X060X08Q14XQ08/15X02X02	60	3.5	0.086	0.914
C045X045X12Q16XQ08/15X02X02	45	3.5	0.064	0.936
C045X040X04Q14XQ08/20X02X02	40	3.5	0.057	0.943
C035X060X06Q16XQ08/15X02X02	60	4.5	0.067	0.933
C045X060X06Q16XQ08/15X02X02	60	4.5	0.067	0.933
C060X060X08Q16XQ08/10X02X02	60	4.5	0.067	0.933
C045X045X14Q16XQ08/10X02X02	45	4.5	0.050	0.950

4.3. Definition of Nonlinear Behavior

Within the scope of TBEC-2018, two fundamental analysis methods are proposed for evaluating structures based on deformation. The first of these is the Pushover Analysis Method, while the second is the Nonlinear Time-History Analysis Method. In this study, the earthquake performance of the designed structure was determined using the Nonlinear Time-History Analysis Method in the ETABS software. The adopted methods and calculation principles were determined in accordance with the relevant regulatory provisions, and all analyses were conducted following regulatory guidelines.

The Nonlinear Time-History Analysis Method is based on the step-by-step direct integration of the differential equation system that expresses the motion equations of the structural system under the influence of earthquake ground motion. In this method, the stiffness matrix of the system is considered to change over time due to nonlinear behavior. All calculations and analysis stages were performed in compliance with the regulatory requirements.

During the analysis process, the structure was examined under the effect of 11 pairs of earthquake ground motions, and time-history calculations were conducted for each earthquake record. The selection of earthquake records and their scaling to match the design spectrum were considered as one of the most critical stages of the analysis process. The earthquake records were determined based on the local soil conditions and seismicity parameters of the structure’s location. Additionally, to generate a damping matrix proportional to the mass and stiffness of the structure and compatible with its mode shapes, the Rayleigh Damping Model was utilized. This process was shaped in accordance with the regulatory requirements.

To enhance the reliability of analyses and obtain statistically meaningful results, the Nonlinear Time-History Analysis Method requires the use of at least eleven pairs of earthquake ground motions. Accordingly, two orthogonal horizontal components of acceleration records are applied simultaneously in the X and Y principal axes of the structural system. Subsequently, the acceleration record axes are rotated 90 degrees, and the calculations are repeated to thoroughly examine the structure’s behavior under different loading scenarios. These analysis steps were conducted to ensure compliance with the relevant regulatory provisions.

During the formation of earthquake loading cases, second-order effects were also considered in the analysis model, and rotational calculations were performed for 11 pairs of earthquake records. As a result, structural analyses were completed for a total of 22 different loading cases. All calculations conducted during the analysis process were performed in accordance with the regulatory provisions.

For ductile structural elements, deformation demands, and for non-ductile structural elements, internal force demands, are determined by taking the average of the absolute maximum values obtained from the (at least 2 × 11 = 22 analyses) conducted. This approach enhances the statistical reliability of the analyses and provides a more accurate representation of the structural elements' behavior under possible earthquake effects. All calculations and methodological choices were carried out in accordance with the principles set forth in the regulations.

4.3.1. Definition of Time History Functions

In the nonlinear time-history analysis method, acceleration records must be defined as functions within the software. Additionally, to incorporate the static vertical loads (G, G-Wall, Q, Roof, S, SDL) of the structure as initial conditions, it is appropriate to define them as a dynamic effect as a Ramp Function (RampTH), Figure 4.29. To ensure the dynamic application of vertical loads, a step function has been utilized. The step function is commonly accepted to have a sufficiently slow transition and an amplitude value of 1g.

The selected earthquakes, along with their assigned scale factors, have been defined as functions in the software, and an example definition for one of them is provided in the **Figure 4.29**.

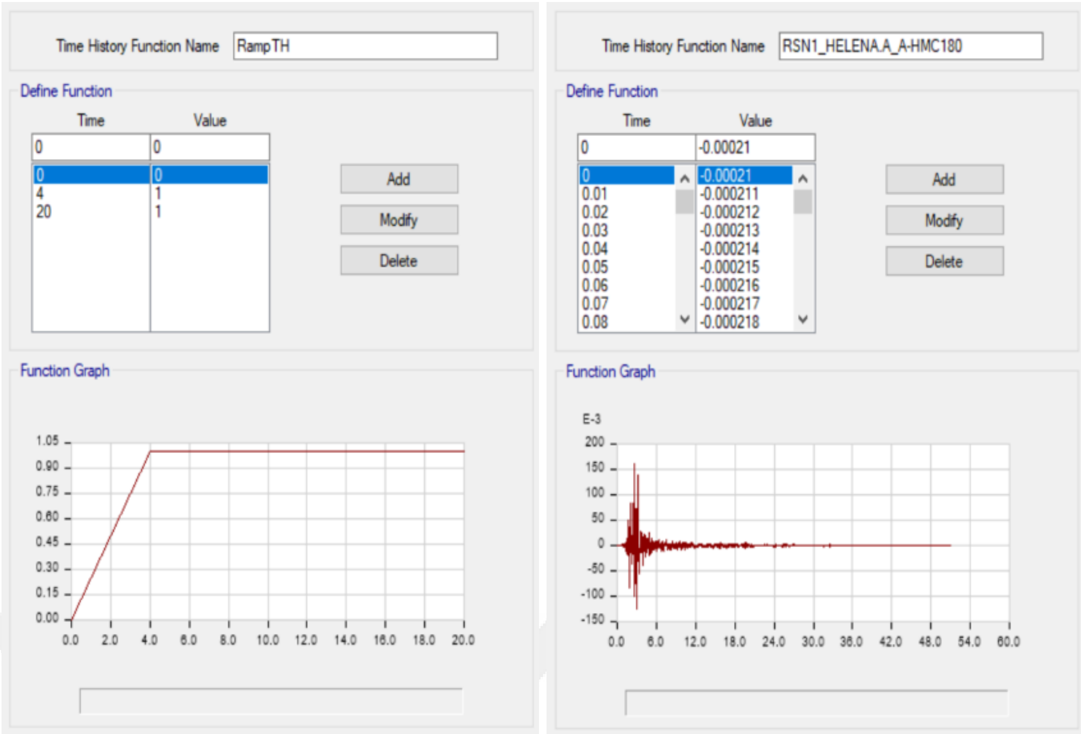

Figure 4.29: Function Definition for Vertical Load Application and Earthquake Record Assignment

4.3.2. Definition of Rayleigh Damping Matrix

Rayleigh damping is a linear damping model employed to characterize energy dissipation in mechanical systems. This approach defines damping as a combination of the system's mass (*M*) and stiffness (*K*) matrices. The primary objective of this model is to achieve a realistic estimation of energy loss across the system's natural frequency spectrum.

The damping matrix is defined as:

$$C = \alpha M + \beta K \qquad (4.1)$$

Where:

- *C*: Damping matrix,
- α: Mass-proportional damping coefficient,
- β: Stiffness-proportional damping coefficient,
- *M*: Mass matrix,

- K: Stiffness matrix.

The damping ratio for a mode (ξ_n) in Rayleigh damping is calculated as:

$$\xi n = \frac{1}{2}\left(\frac{\alpha}{\omega n} + \beta \cdot \omega n\right) \qquad (4.2)$$

Where:

- ω_n: Natural angular frequency of the system mode.

This formula represents the system's different damping behaviors at low and high frequencies:

- At low frequencies (ω_n is small): Mass-proportional damping (α/ω_n) dominates.
- At high frequencies (ω_n is large): Stiffness-proportional damping ($\beta \cdot \omega_n$) dominates.

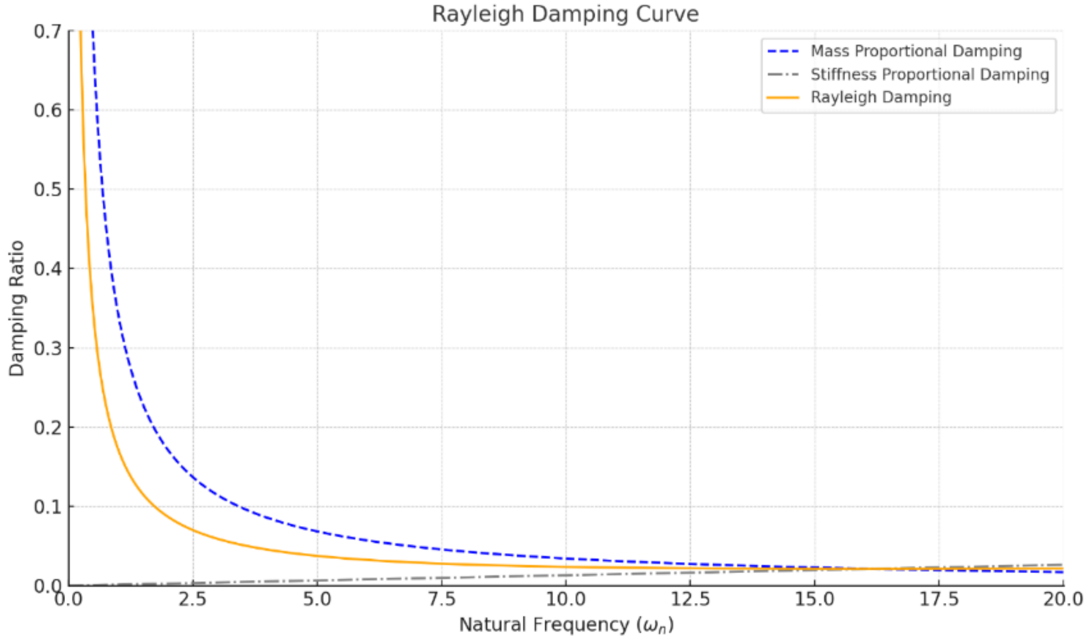

Figure 4.30: Rayleigh Damping Curve for Library Building

- The calculation of the mass-proportional damping coefficient (α) is expressed as follows:

$$\alpha = 2 \cdot \xi 1 \left(\frac{\omega i \cdot \omega j}{\omega i + \omega j}\right) \qquad (4.3)$$

- The calculation of the stiffness-proportional damping coefficient (β) is expressed as follows:

$$\beta = 2 \cdot \xi 1 \left(\frac{1}{\omega i + \omega j}\right) \qquad (4.4)$$

Where:

- ω_i: The angular frequency corresponding to the building's natural fundamental vibration period,
- ω_j: The angular frequency corresponding to the period at which the structure reaches 95% of its modal mass participation,
- ξ_1: default damping ratio.

As a result, the mass-proportional damping coefficient is calculated as 0.686, and the stiffness-proportional damping coefficient is calculated as 0.00262 for the library building.

4.3.3. Definition of Load Cases for Nonlinear Time History

In nonlinear time-history analysis, the definition of loading cases is a critical step to accurately simulate the structural response under seismic effects. Previously introduced into the analysis software as time-dependent functions, earthquake records ensure the correct application of both horizontal and vertical ground motions. The loading cases are then assigned to the model within the analysis program, ensuring that seismic loads and static effects are applied in accordance with the selected ground motion records and scaling factors, allowing for a comprehensive assessment of the structural response.

Primarily, the load case associated with the function created for vertical loads has been defined and is provided below, **Figure 4.31**.

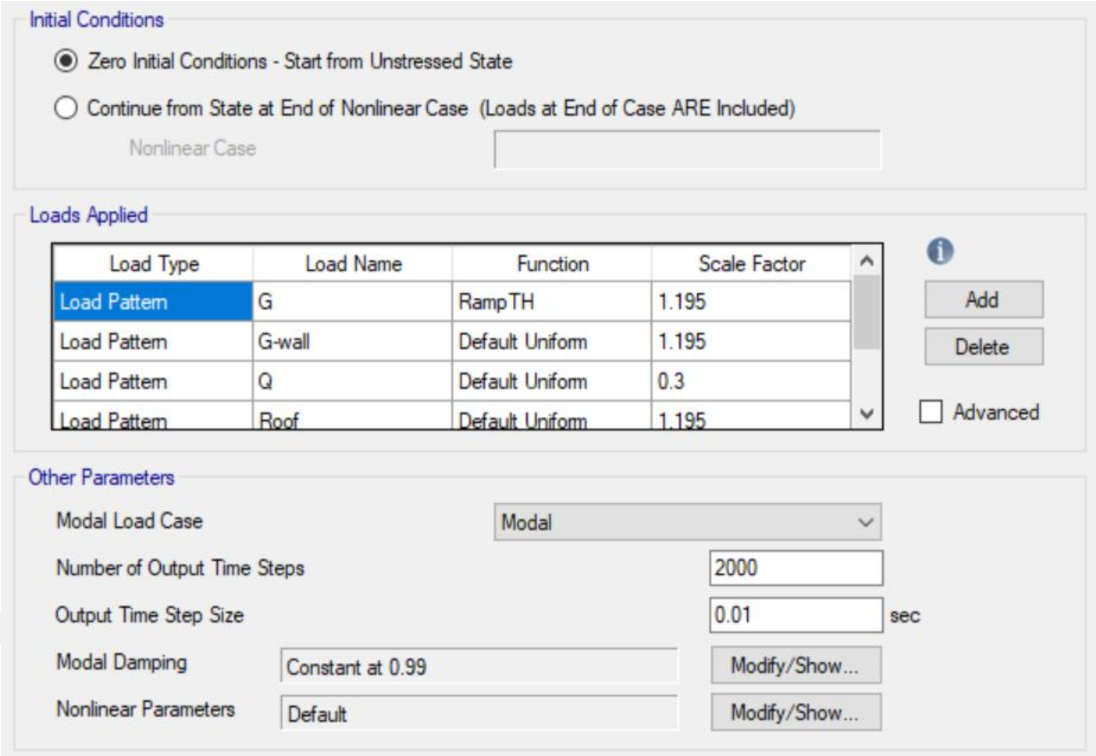

Figure 4.31: Initial Load Case for Time – History Load Cases

Here, damping is generally not expected in structural behavior; therefore, an approximate value of 1 (0.99) has been defined to avoid creating a vertical damping model.

According to TBEC-2018, the calculated 0.585G vertical load effect has been reduced by 0.3, resulting in 0.195, which has been added to all dead loads.

Subsequently, 11 earthquake records, including horizontal and vertical components, have been applied separately to the structural model.

For this, the load case defined for the vertical load function was set as the initial load case, and then these earthquake records were applied as seismic loads to the structural model. The calculated damping value was assigned to each load case.

The load case prepared for the horizontal components of the "Helena-Montana 01" earthquake is provided below, **Figure 4.32**.

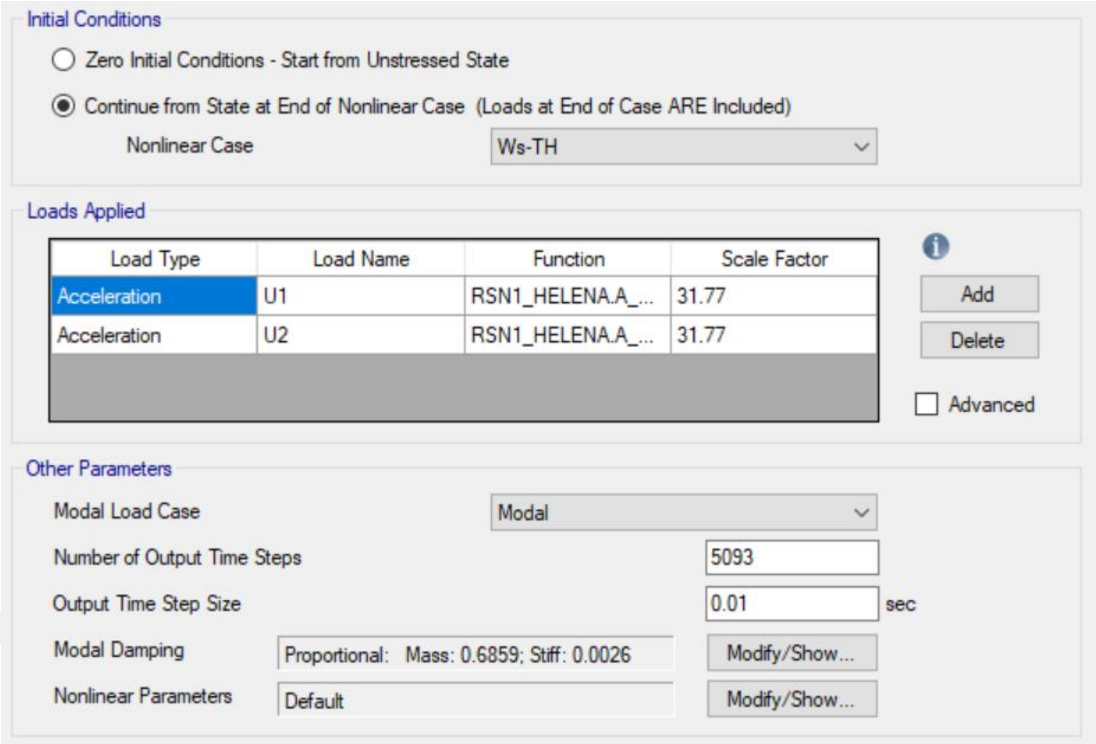

Figure 4.32: An example of Time – History Load Case

4.3.4. Building Assessment Outputs

The analysis results for Structure A – Library Building are presented in this section. The natural vibration periods and mode shapes of the structure are provided below, **Table 4.6**.

Table 4.6: Building Natural Vibration Periods and Modal Analysis Results

Mode	Period	UX	UY	SumRZ
	sec			
1	0.7	93.6%	0.0%	0.0%
2	0.68	0.1%	76.5%	14.8%
3	0.604	0.0%	14.7%	91.9%
4	0.216	5.6%	0.0%	91.9%
5	0.203	0.0%	6.4%	93.1%
6	0.182	0.0%	1.2%	99.0%
7	0.123	0.7%	0.0%	99.0%
8	0.107	0.0%	1.0%	99.2%
9	0.098	0.0%	0.2%	100.0%
10	0.005	0.0%	0.0%	100.0%
11	0.001	0.0%	0.0%	100.0%
12	0.001	0.0%	0.0%	100.0%

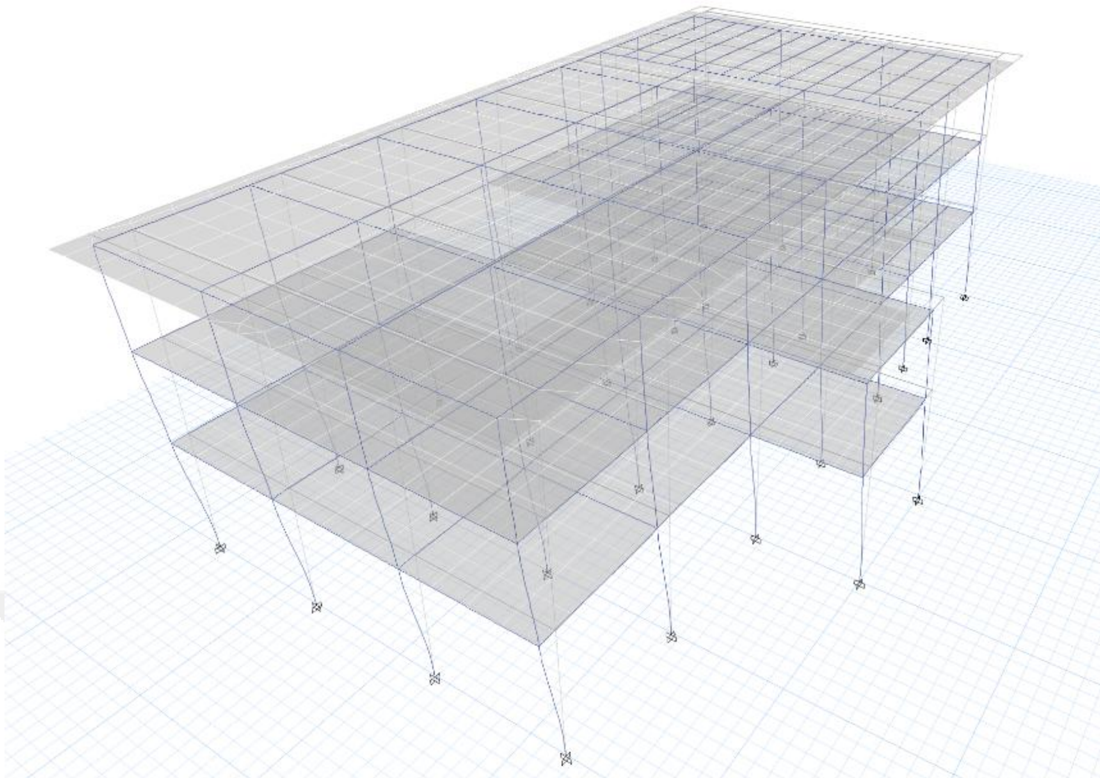

Figure 4.33: The first mode in the X-direction of the building at T = 0.7

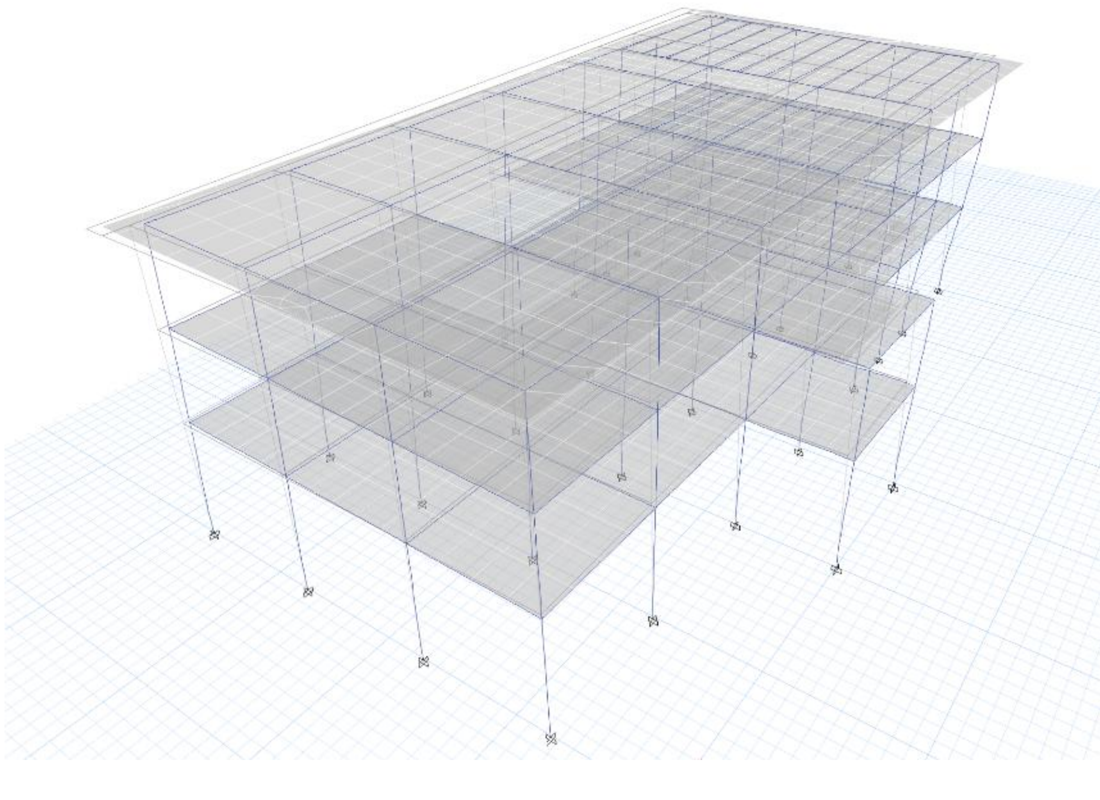

Figure 4.34: The second mode in the Y-direction of the building at T= 0.679

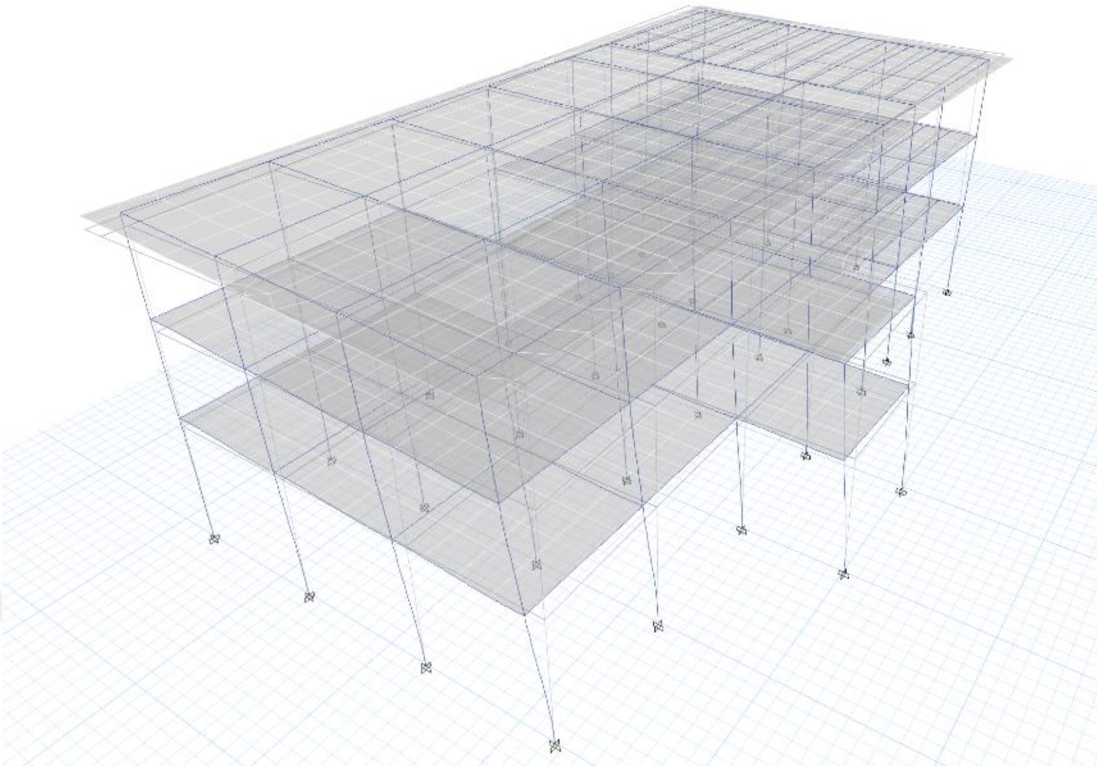

Figure 4.35: The third mode in the Z-rotation direction of the building at T= 0.609

The displacement, inter story drifts, and base shear force values occurring in Structure A were obtained through 22 nonlinear time-history analyses performed using the analysis software. The values obtained from all earthquake records were evaluated considering the analysis outputs, and the average of the absolute maximum values from the 22 analyses were calculated.

As a result of the analysis of 11 pairs of earthquake records, the story displacement graphs obtained in the X and Y directions and their average values are presented in **Figure 4.36**Hata! Başvuru kaynağı bulunamadı..

As the average result, the peak displacement was calculated as:

0.07/11.5 m = 0.6% in the X direction,

0.06/11.5 m = 0.52% in the Y direction.

This result remains below the 2% limit value specified in internationally recognized codes such as FEMA 356 and ASCE 41-17.

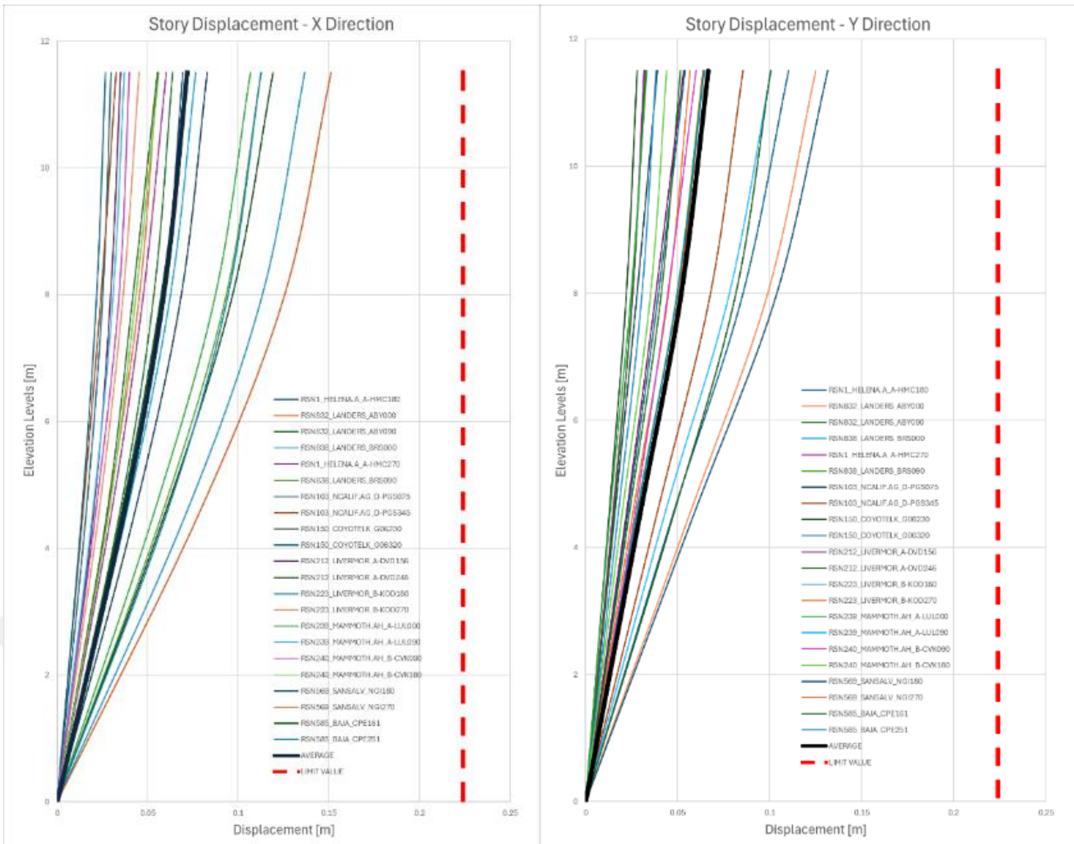

Figure 4.36: Displacement Outputs for X and Y Directions

The Inter story Drift Check for the Library Building was performed according to TBEC-2018, based on the values calculated using the following formula.

$$\frac{\delta_{i,max}^{(X)}}{h_i} \leq 0.008\,\kappa \quad (4.5)$$

As can be seen from the graphs:

- In the X direction, the calculated average value exceeds the limit, and similarly, the maximum value also exceeds the limit, **Figure 4.37**.
- In the Y direction, the average value remains below the limit, but the maximum value exceeds the limit in this direction as well, **Figure 4.38**.

Another observation from the graph is that the first story height is 4.5 meters, while the upper stories have a height of 3.5 meters. This indicates that the building exhibits B2 – Stiffness Irregularity Between Adjacent Stories (Soft Story) as defined in TBEC-2018.

From this perspective, we can once again mathematically and visually observe the effects of this common irregularity encountered in Turkey.

The base shear forces are provided in **Table 4.7**, and upon examining these results, it is observed that the highest base shear force values occurred under the influence of the "RSN 569 – San Salvador" earthquake.

When analyzing the acceleration records of the 11 pairs of earthquakes, it was determined that the highest peak ground acceleration (PGA) values among all ground motions were 0.74g and 0.96g, recorded during the "RSN 240 – Mammoth Lakes – 04" earthquake.

The inconsistency between the base shear forces results and the earthquake acceleration records may indicate that the structure experienced a resonance condition under the "RSN 569 – San Salvador" earthquake. This phenomenon can be validated by applying the Fast Fourier Transform (FFT) method to decompose the acceleration record in the time domain into its frequency components and comparing them with the structure's natural frequency.

The plastic hinge rotation values in frame elements were compared with the limit values specified in TBEC-2018 to assess the damage levels.

For columns and beams, the plastic hinge rotation limits corresponding to Göçmenin Önlenmesi (GÖ) and Kontrollü Hasar (KH) were determined using the equations provided below.

$$\theta_P^{(GÖ)} = \frac{2}{3}\left[(\phi_u - \phi_y)L_p\left(1 - 0.5\frac{L_p}{L_s}\right) + 4.5\,\phi_u\,d_b\right] \quad (4.6)$$

$$\theta_P^{(KH)} = 0.75\,\theta_P^{(GÖ)} \quad (4.7)$$

The plastic rotation values of all frame elements in the structure were compared with the limit values specified in the code, as defined by the equations provided above.

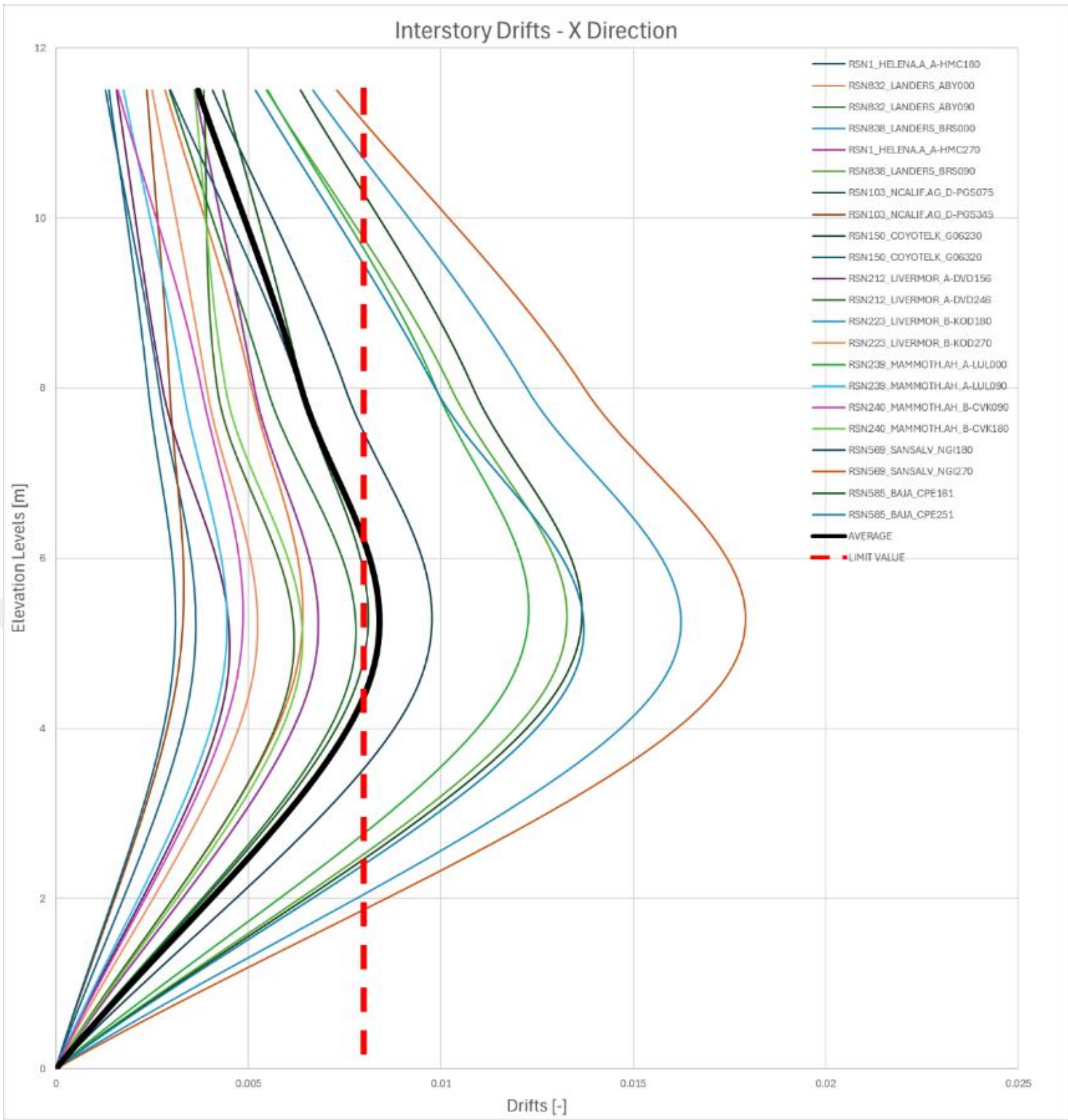

Figure 4.37: Inter story Drift Check for the X Direction

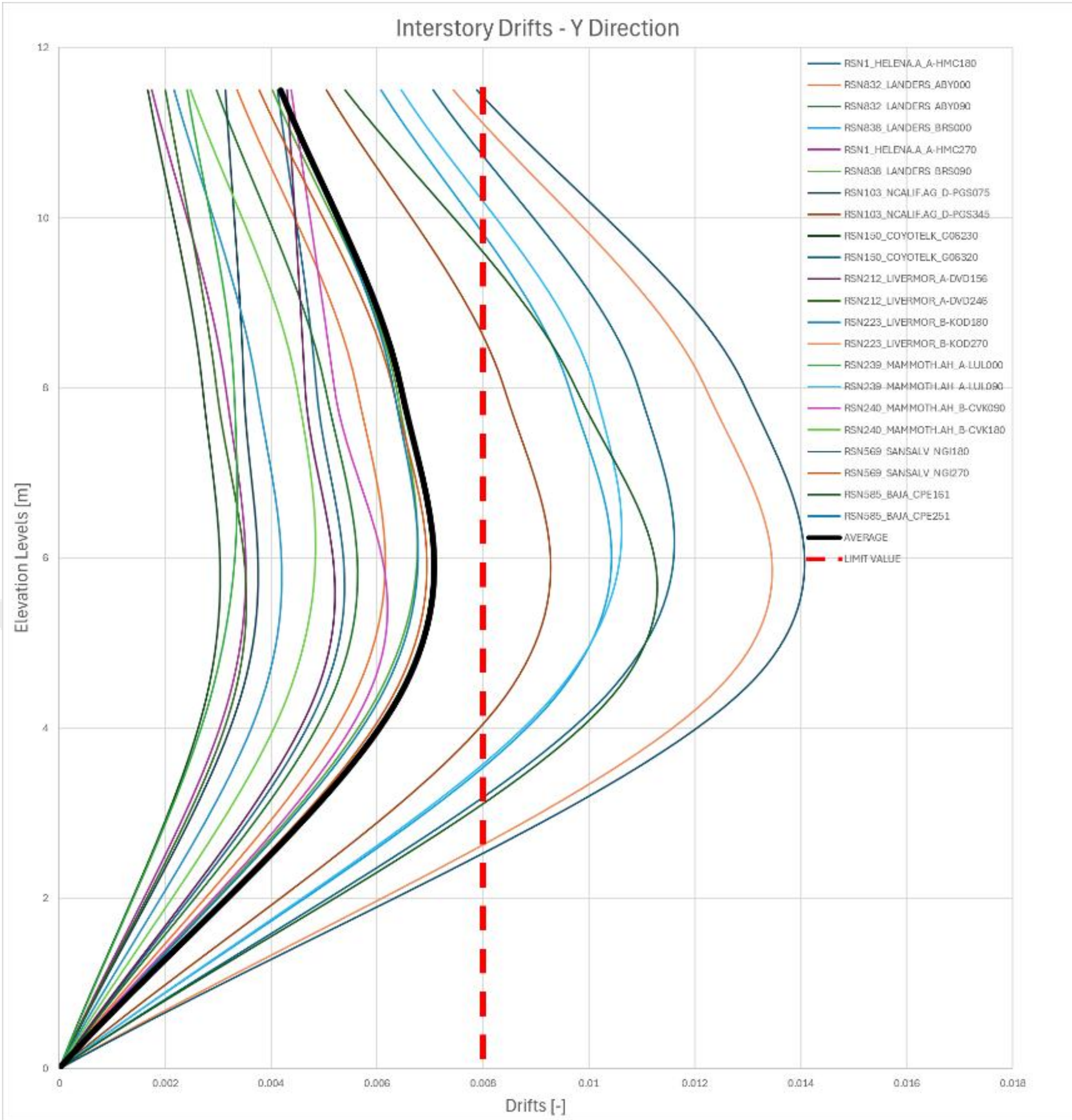

Figure 4.38: Inter story Drift Check for the Y Direction

Table 4.7: Base Shear Forces in X and Y Directions from All Time History Analyses

Earthquake Name		X - Direction [kN]	Y - Direction [kN]
RSN1_HELENA.A_A-HMC180	Max	4133.52	5901.95
RSN1_HELENA.A_A-HMC180	Min	-3179.54	-7846.53
RSN103_NCALIF.AG_D-PGS075	Max	11466.54	5100.50
RSN103_NCALIF.AG_D-PGS075	Min	-8215.19	-4461.65
RSN150_COYOTELK_G06230	Max	12217.55	3370.88
RSN150_COYOTELK_G06230	Min	-16561.95	-3608.62
RSN212_LIVERMOR_A-DVD156	Max	4771.73	7095.96
RSN212_LIVERMOR_A-DVD156	Min	-5883.42	-7835.99
RSN223_LIVERMOR_B-KOD180	Max	18399.45	5245.17
RSN223_LIVERMOR_B-KOD180	Min	-19809.68	-5055.86
RSN239_MAMMOTH.AH_A-LUL000	Max	13603.86	3971.25
RSN239_MAMMOTH.AH_A-LUL000	Min	-12783.66	-3631.13
RSN240_MAMMOTH.AH_B-CVK090	Max	5191.85	9219.80
RSN240_MAMMOTH.AH_B-CVK090	Min	-5596.03	-7823.02
RSN569_SANSALV_NGI180	Max	9655.51	17988.51
RSN569_SANSALV_NGI180	Min	-10116.21	-17340.26
RSN585_BAJA_CPE161	Max	9333.96	13531.35
RSN585_BAJA_CPE161	Min	-10367.31	-15639.59
RSN832_LANDERS_ABY000	Max	6362.56	7243.77
RSN832_LANDERS_ABY000	Min	-7164.97	-6367.71
RSN838_LANDERS_BRS000	Max	10357.57	12939.18
RSN838_LANDERS_BRS000	Min	-10476.89	-11706.10
RSN1_HELENA.A_A-HMC270	Max	7097.03	4875.42
RSN1_HELENA.A_A-HMC270	Min	-8843.63	-3064.68
RSN103_NCALIF.AG_D-PGS345	Max	3536.04	12407.01
RSN103_NCALIF.AG_D-PGS345	Min	-3122.29	-7764.36
RSN150_COYOTELK_G06320	Max	2627.30	11090.03
RSN150_COYOTELK_G06320	Min	-3711.83	-14778.51
RSN212_LIVERMOR_A-DVD246	Max	6702.83	4680.55
RSN212_LIVERMOR_A-DVD246	Min	-8312.25	-5016.10
RSN223_LIVERMOR_B-KOD270	Max	5381.47	16824.63
RSN223_LIVERMOR_B-KOD270	Min	-6034.58	-18112.84
RSN239_MAMMOTH.AH_A-LUL090	Max	4031.31	12379.54
RSN239_MAMMOTH.AH_A-LUL090	Min	-4839.29	-10660.62
RSN240_MAMMOTH.AH_B-CVK180	Max	8029.14	5778.19
RSN240_MAMMOTH.AH_B-CVK180	Min	-7128.99	-6657.26
RSN569_SANSALV_NGI270	Max	20860.36	9220.19
RSN569_SANSALV_NGI270	Min	-20330.85	-8867.44
RSN585_BAJA_CPE251	Max	14161.74	8824.62
RSN585_BAJA_CPE251	Min	-17108.63	-9026.48
RSN832_LANDERS_ABY090	Max	8659.96	6477.90
RSN832_LANDERS_ABY090	Min	-8032.24	-7108.18
RSN838_LANDERS_BRS090	Max	15607.98	8965.87
RSN838_LANDERS_BRS090	Min	-14757.55	-8327.02

As a result of the calculations:

- Out of 195 beams, 99 beams (50.77%) were classified as Brittle Element, indicating that, even if the structure meets its performance target according to TBEC-2018, the shear capacities of these elements must be increased.
- 132 beams (68.04%) were found to be at the Belirgin Hasar level (BH).
- 63 beams (31.95%) remained at the Sınırlı Hasar level (SH).

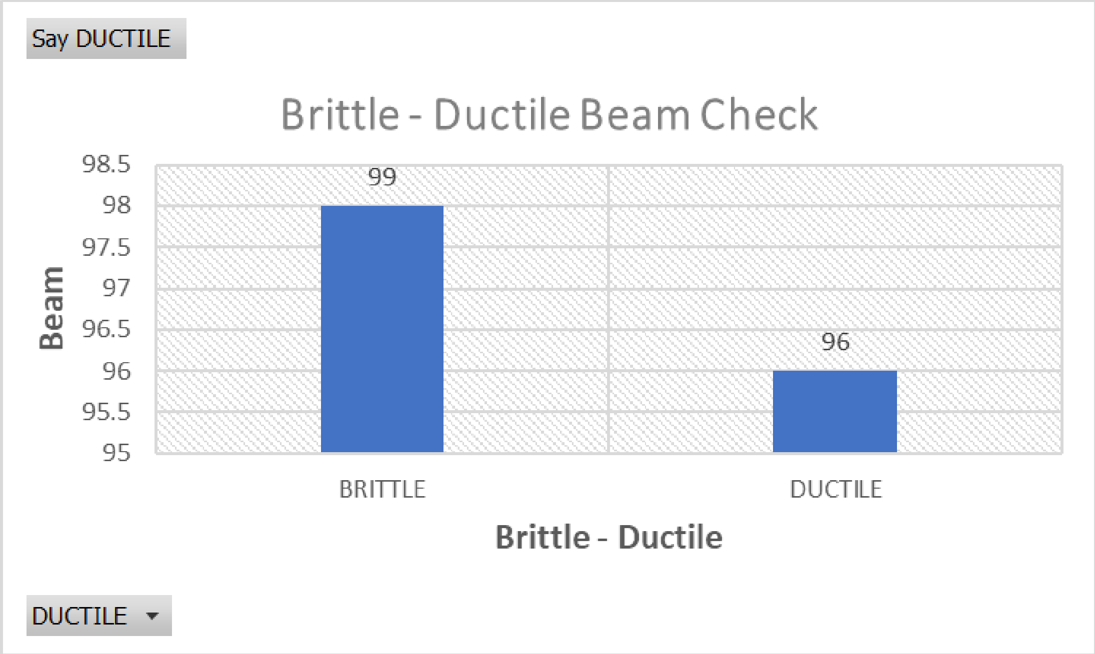

Figure 4.39: Brittle-Ductile Element Verification for Beams

As a result of the calculations performed for column elements, out of a total of 94 columns:

- 83 columns (88.29%) were classified as Brittle Element, indicating that even if the structure meets its performance target according to TBEC-2018, the shear capacities of these elements must be increased.
- 13 columns (13.93%) were classified in the Göçme Hasar level.
- 3 columns (3.2%) were classified in the İleri Hasar level (İH).
- 78 columns (82.97%) were classified in the Belirgin Hasar level (BH).

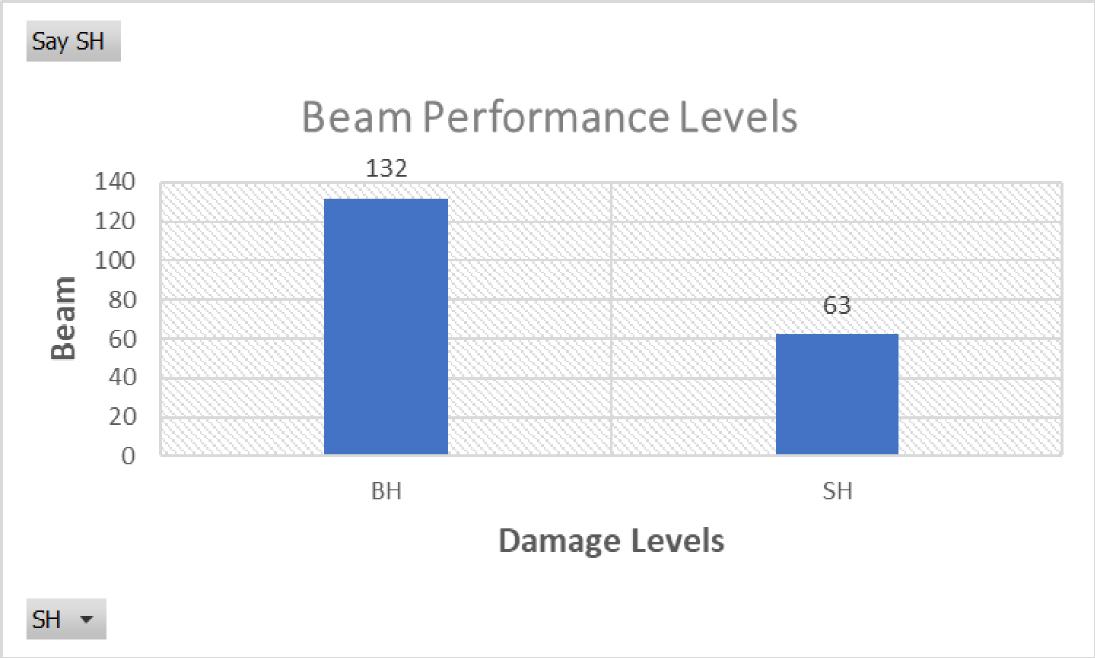

Figure 4.40: Final Performance Levels of Beam Elements

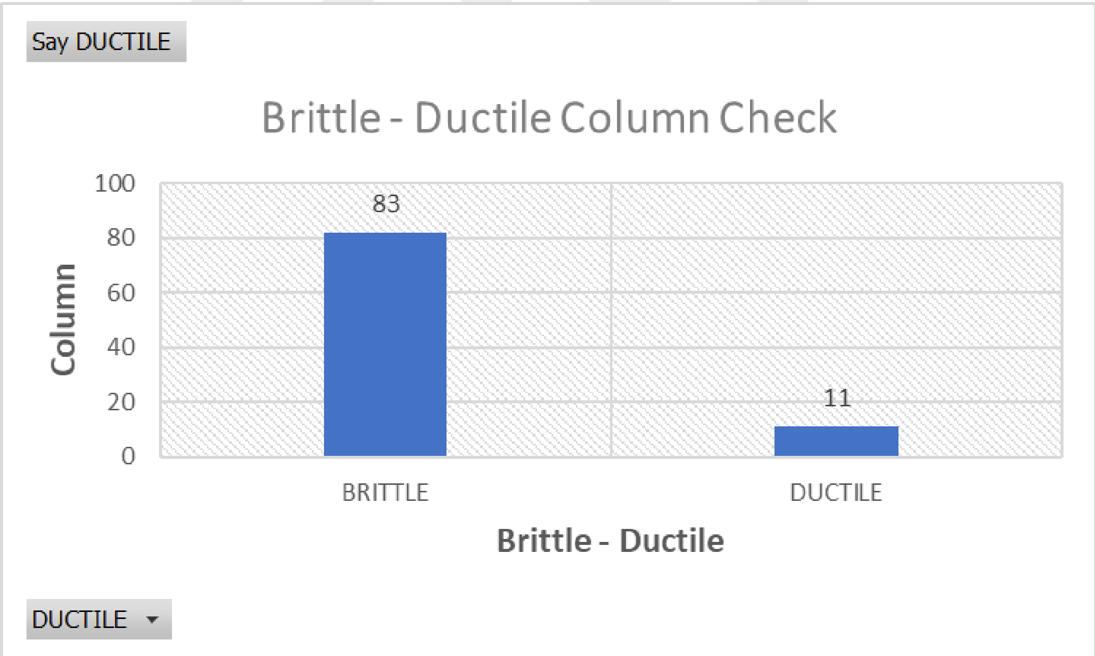

Figure 4.41: Brittle-Ductile Element Verification for Columns

Based on these damage level results, according to TBEC-2018, the performance level of the structure is in the "Göçme" condition. Depending on the feasibility study, the appropriate course of action would be:

- Increasing the flexural capacity of the columns and strengthening the building by adding shear walls to improve rigidity.
- Considering demolition if strengthening is deemed unfeasible.

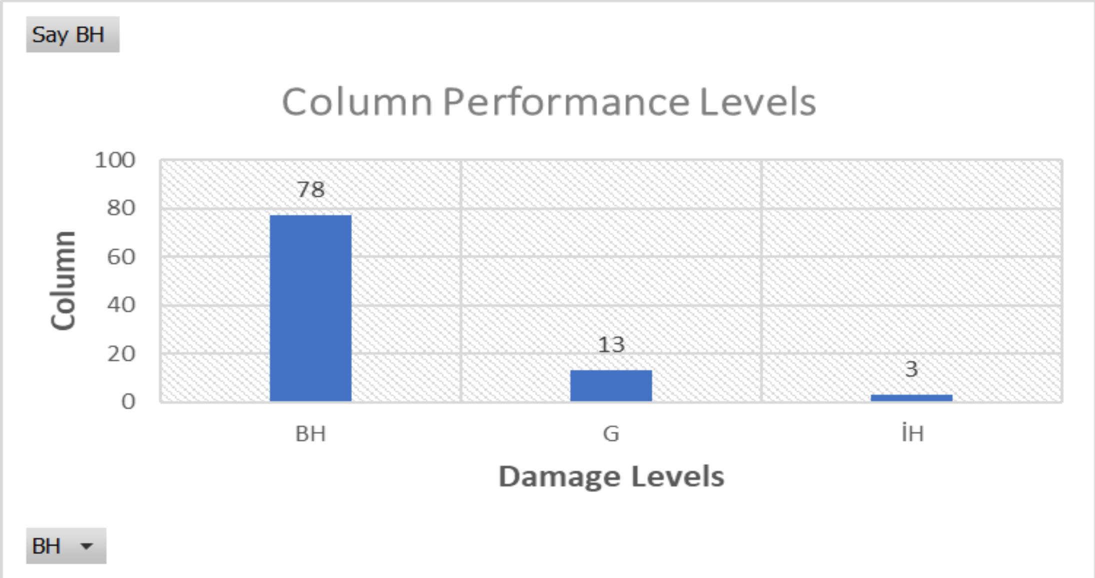

Figure 4.42: Final Performance Levels of Column Elements

In the previous sections, the "Directivity Effect" and its mathematical influence on the inputs of nonlinear analysis were explained, and its impact on buildings was observed through a scenario within the scope of this study. The newly calculated input parameters were introduced into the analysis software for all structures, and the analyses were repeated accordingly.

Below, the brittle element outputs and the final performance level of Structure A, analyzed considering the directivity effect, are presented along with their respective comparisons as the results.

As a result of the calculations:

- Out of 195 beams, 102 beams (52.5%) were classified as Brittle Element, indicating that, even if the structure meets its performance target according to TBEC-2018, the shear capacities of these elements must be increased.
- 145 beams (74.22%) were found to be at the Belirgin Hasar level (BH).
- 50 beams (25.77%) remained at the Sınırlı Hasar level (SH).

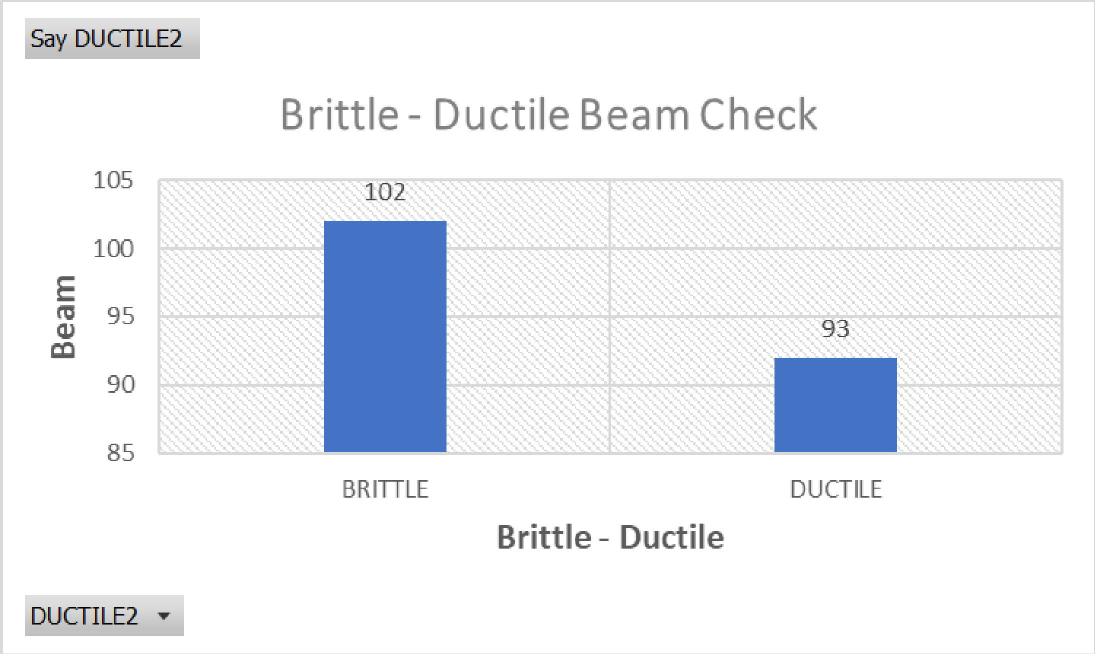

Figure 4.43: Analysis Results with Directivity Effect: Brittle-Ductile Element Verification for Beams

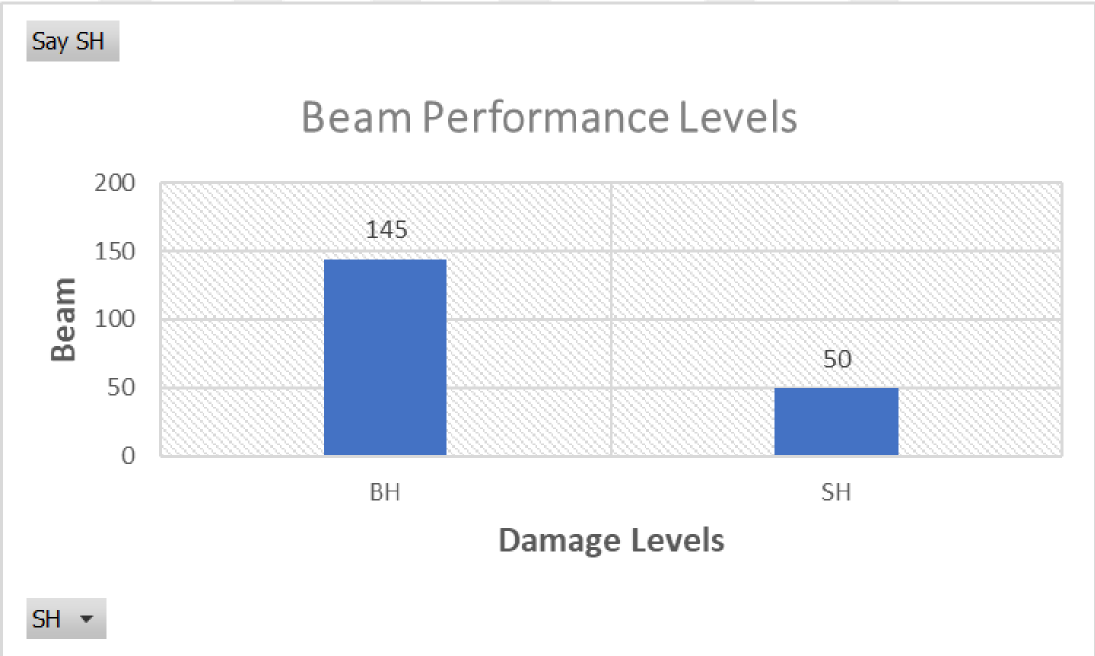

Figure 4.44: Analysis Results with Directivity Effect: Final Performance Levels of Beam Elements

As a result of the calculations performed for column elements, out of a total of 94 columns:

- 86 columns (92.47%) were classified as Brittle Element, indicating that even if the structure meets its performance target according to TBEC-2018, the shear capacities of these elements must be increased.
- 14 columns (15.05%) were classified in the Göçme Hasar level.
- 6 columns (6.45%) were classified in the İleri Hasar level (İH).
- 73 columns (78.49%) were classified in the Belirgin Hasar level (BH).

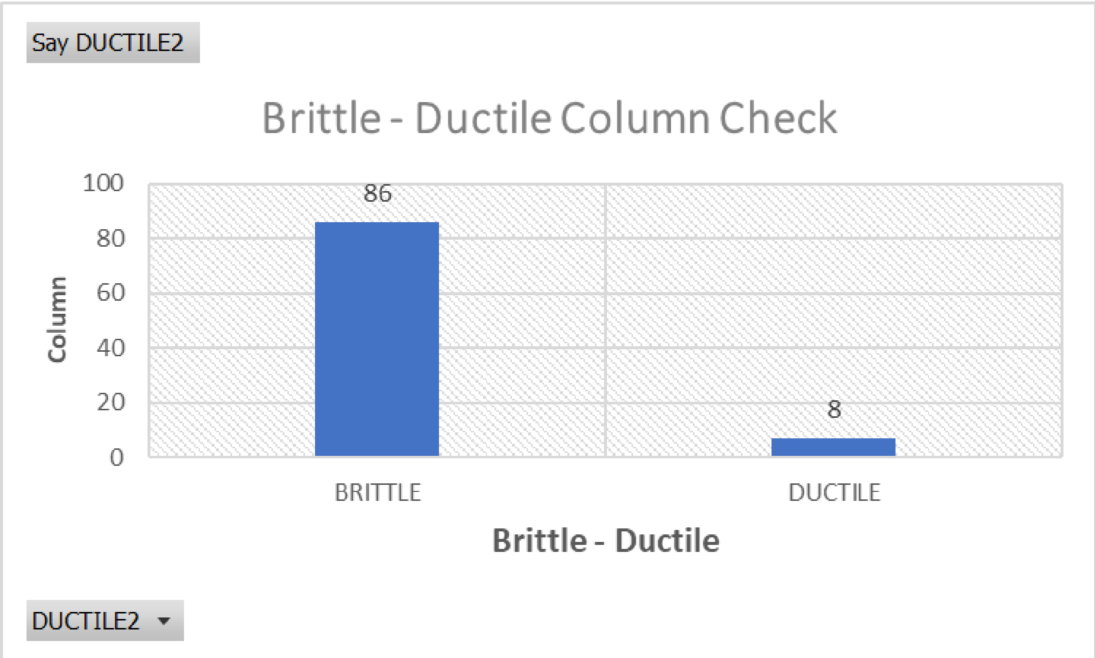

Figure 4.45: Analysis Results with Directivity Effect: Brittle-Ductile Element Verification for Columns

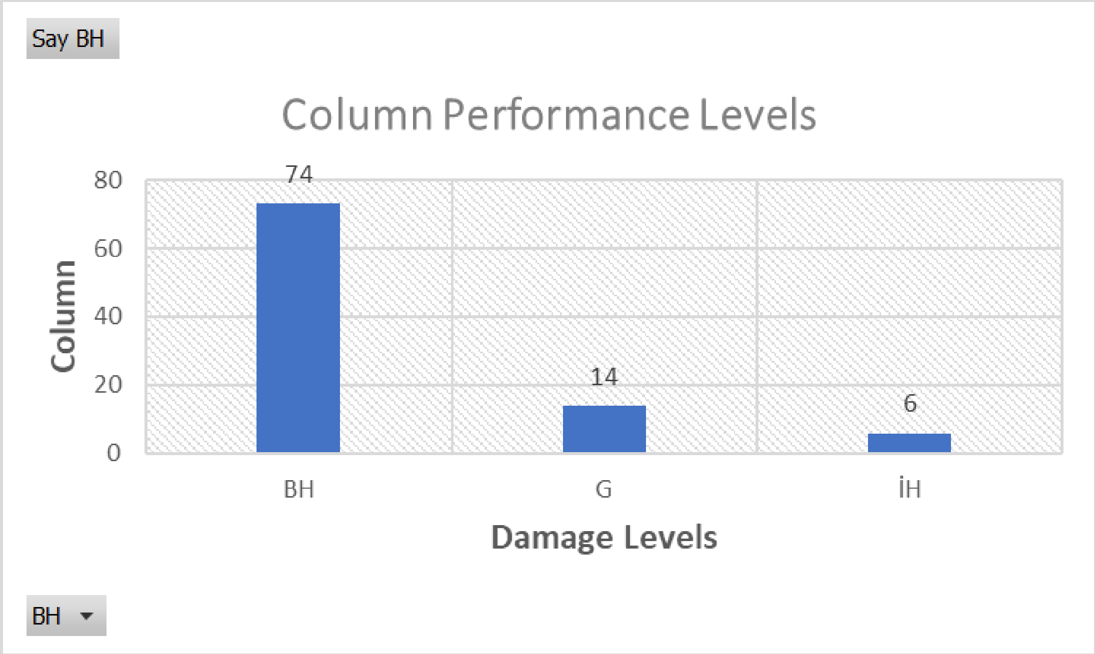

Figure 4.46: Analysis Results with Directivity Effect: Final Performance Levels of Column Elements

When the analysis results including the directivity effect are compared with the standard performance analysis outputs:

For Beams:

- An additional 4 beams (2%) were classified as brittle elements due to increased shear forces.
- 12 beams (6.18%) transitioned to the Belirgin Hasar (BH) performance level.

For Columns:

- An additional 4 columns (5.24%) were classified as brittle elements due to increased shear forces.
- 1 column (1.12%) transitioned to the Göçme damage level, and 3 columns (3.25%) transitioned to the İleri Hasar level.

The analysis results for Structure B – Public Office Building are presented in this section. The natural vibration periods and mode shapes of the structure are provided below, **Table 4.8**.

Table 4.8: Building Natural Vibration Periods and Modal Analysis Results

Mode	Period	UX	UY	SumRZ
	sec			
1	1.049	10.2%	5.6%	61.7%
2	0.913	1.9%	68.3%	66.0%
3	0.728	62.5%	0.2%	77.7%
4	0.342	1.7%	0.4%	87.1%
5	0.273	0.0%	0.1%	87.1%
6	0.271	0.2%	13.6%	87.3%
7	0.217	13.1%	0.0%	89.4%
8	0.179	0.9%	0.3%	92.8%
9	0.136	0.3%	5.7%	92.9%
10	0.113	4.1%	0.5%	92.9%
11	0.075	2.9%	2.1%	93.2%
12	0.065	1.5%	2.6%	93.3%

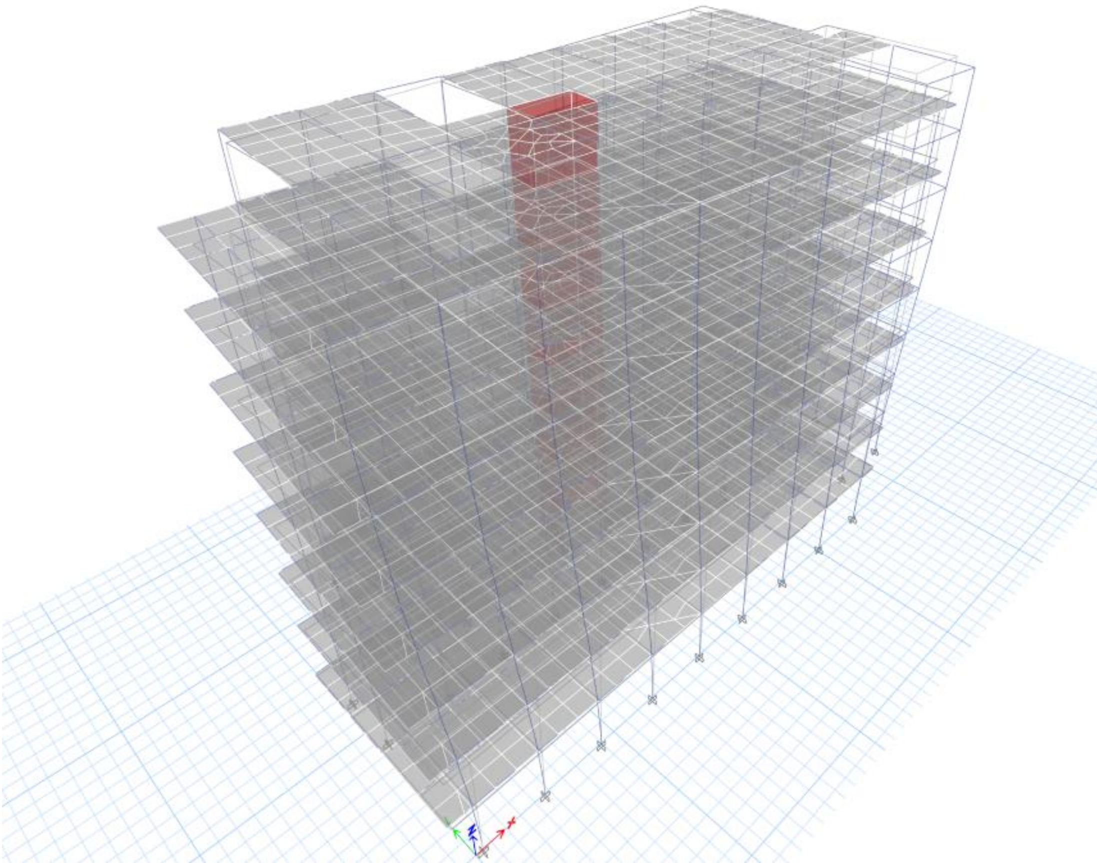

Figure 4.47: The first mode in the Z-rotation direction of the building at T = 1.05

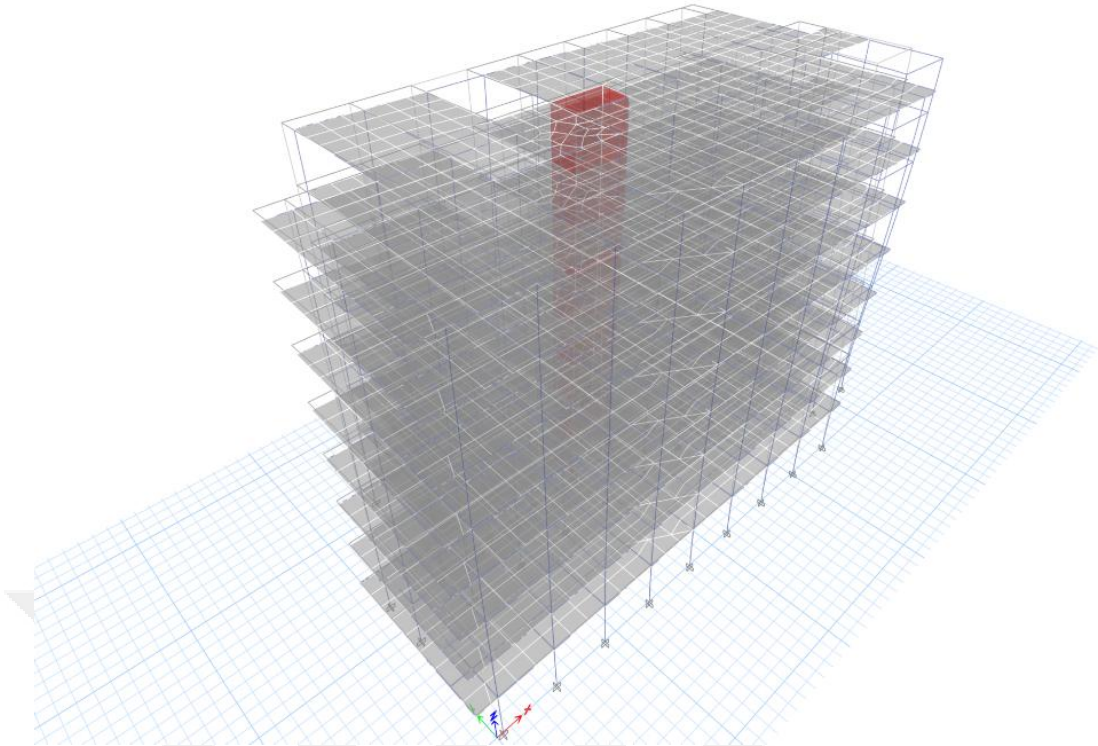

Figure 4.48: The second mode in the Y-direction of the building at T= 0.91

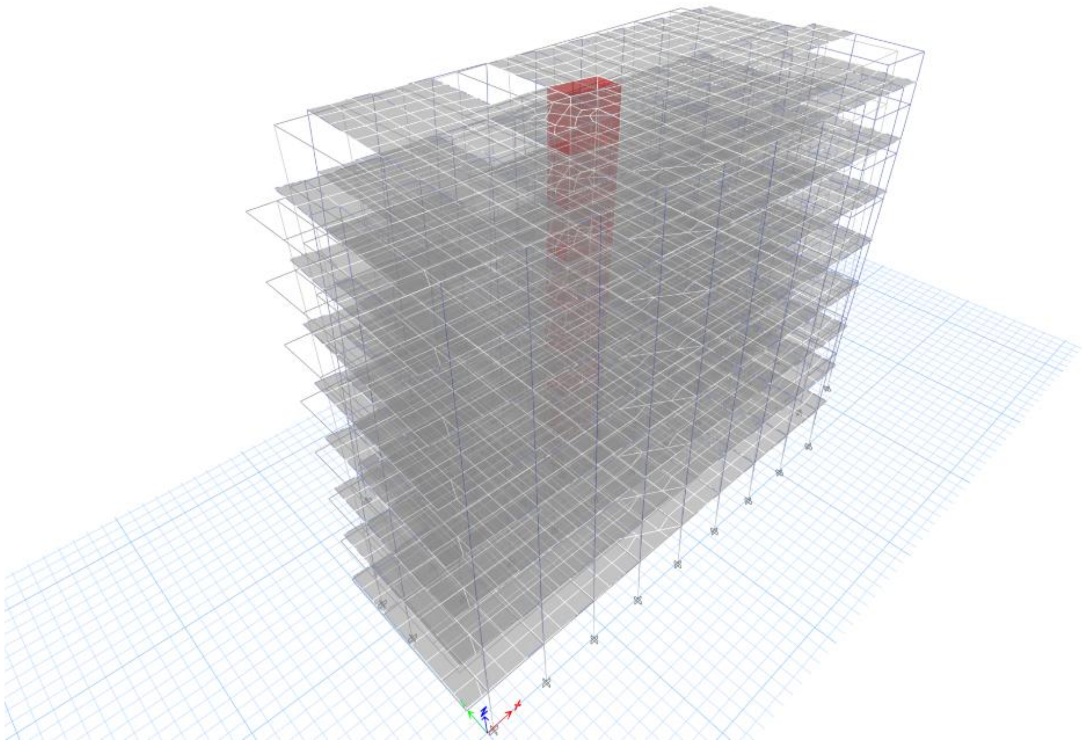

Figure 4.49: The third mode in the X-direction of the building at T= 0.609

The displacement, inter story drifts, and base shear force values occurring in Structure A were obtained through 22 nonlinear time-history analyses performed using the analysis software. The values obtained from all earthquake records were evaluated considering the analysis outputs, and the average of the absolute maximum values from the 22 analyses were calculated.

As a result of the analysis of 11 pairs of earthquake records, the story displacement graphs obtained in the X and Y directions and their average values are presented in **Figure 4.50**.

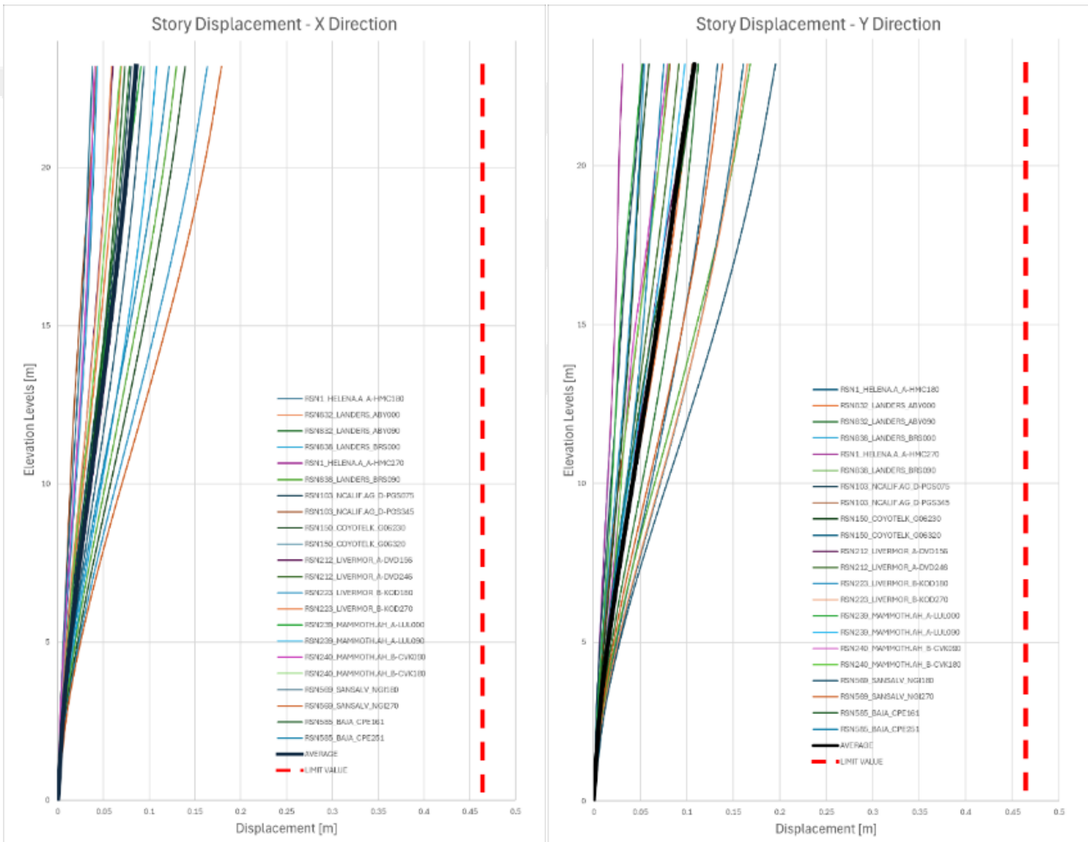

Figure 4.50: Displacement Outputs for X and Y Directions

As the average result, the peak displacement was calculated as:

0.085/23.2 m = 0.37% in the X direction,

0.107/23.2 m = 0.46% in the Y direction.

This result remains below the 2% limit value specified in internationally recognized codes such as FEMA 356 and ASCE 41-17.

The Inter story Drift Check for the Library Building was performed according to TBEC-2018, based on the values calculated using the following formula.

$$\frac{\delta_{i,max}^{(X)}}{h_i} \leq 0.008\,\kappa \quad (4.5)$$

As can be seen from the graphs:

- In the X direction, the average value remains below the limit, but the maximum value almost exceeds the limit in this direction, **Figure 4.51**.
- In the Y direction, the average value remains below the limit, but the maximum value exceeds the limit in this direction as well, **Figure 4.52**.

Each story of this building has the same height of 2.9 meters. As can be observed from the displacement and interstory drift graphs, the irregularity observed in Building A was not present in this type of structure with uniform story heights.

The base shear forces are provided in Table 4.9, and upon examining these results, it is observed that the highest base shear force values occurred under the influence of the "RSN 569 – San Salvador" earthquake.

When analyzing the acceleration records of the 11 pairs of earthquakes, it was determined that the highest peak ground acceleration (PGA) values among all scaled ground motions were 0.74g and 0.96g, recorded during the "RSN 240 – Mammoth Lakes – 04" earthquake.

The inconsistency between the base shear forces results and the earthquake acceleration records may indicate that the structure experienced a resonance condition under the "RSN 569 – San -Salvador" earthquake. This phenomenon can be validated by applying the Fast Fourier Transform (FFT) method to decompose the acceleration record in the time domain into its frequency components and comparing them with the structure's natural frequency.

The plastic hinge rotation values in frame elements were compared with the limit values specified in TBEC-2018 to assess the damage levels.

For columns and beams, the plastic hinge rotation limits corresponding to Göçmenin Önlenmesi (GÖ) were determined using the equations provided below. The limits for other performance levels are obtained by multiplying these values by specific factors relative to this performance level.

$$\theta_P^{(GÖ)} = \frac{2}{3}\left[(\phi_u - \phi_y)L_p\left(1 - 0.5\frac{L_p}{L_s}\right) + 4.5\,\phi_u\,d_b\right] \quad (4.6)$$

$$\theta_P^{(KH)} = 0.75\,\theta_P^{(GÖ)} \quad (4.7)$$

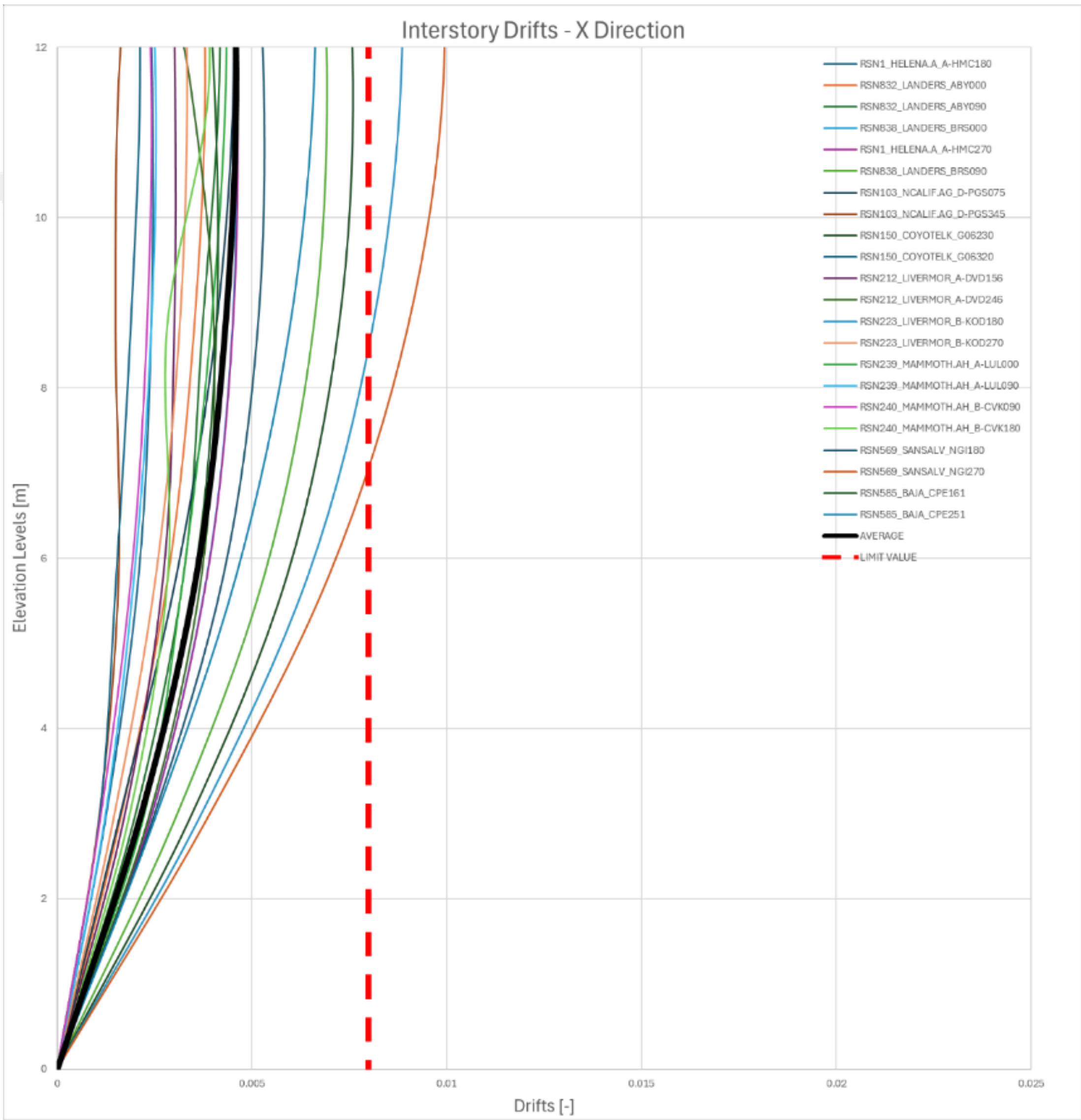

Figure 4.51: Inter story Drift Check for the X Direction

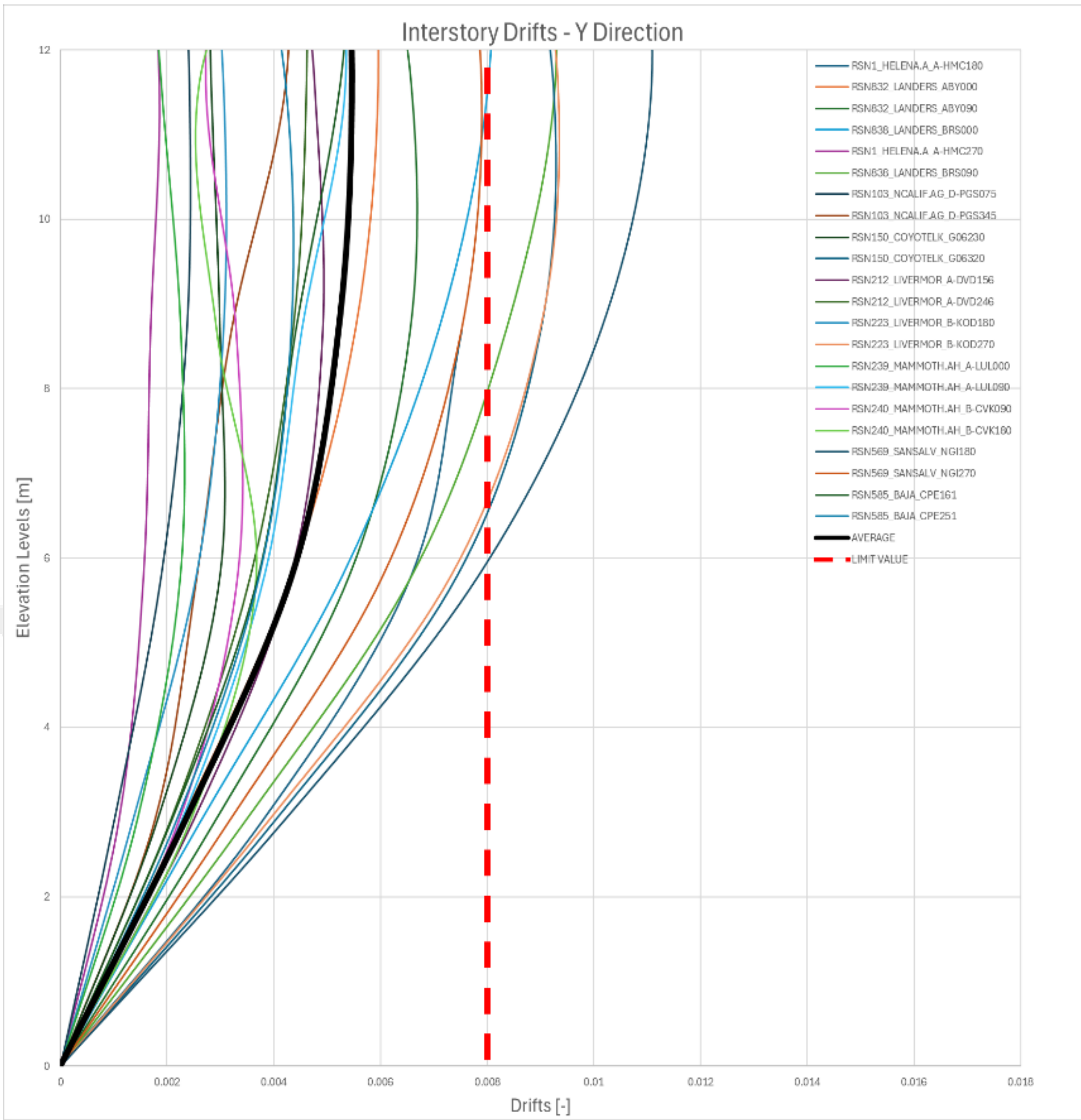

Figure 4.52: Inter story Drift Check for the Y Direction

Table 4.9: Base Shear Forces in X and Y Directions from All Time History Analyses

Earthquake Name		X - Direction	Y - Direction
		[kN]	[kN]
RSN1_HELENA.A_A-HMC180	Max	7298.7519	18602.3583
RSN1_HELENA.A_A-HMC180	Min	-7553.345	-19869.2921
RSN103_NCALIF.AG_D-PGS075	Max	10221.1616	5245.4423
RSN103_NCALIF.AG_D-PGS075	Min	-10067.9672	-6035.0043
RSN150_COYOTELK_G06230	Max	17937.4167	10045.4283
RSN150_COYOTELK_G06230	Min	-22097.5244	-6948.7205
RSN212_LIVERMOR_A-DVD156	Max	9463.0865	13988.2168
RSN212_LIVERMOR_A-DVD156	Min	-12174.8815	-10008.1525
RSN223_LIVERMOR_B-KOD180	Max	23233.45	6643.9355
RSN223_LIVERMOR_B-KOD180	Min	-23834.1384	-6549.5159
RSN239_MAMMOTH.AH_A-LUL000	Max	17315.6094	6755.5804
RSN239_MAMMOTH.AH_A-LUL000	Min	-15458.4068	-8374.8088
RSN240_MAMMOTH.AH_B-CVK090	Max	7835.7557	13306.722
RSN240_MAMMOTH.AH_B-CVK090	Min	-8642.7864	-13254.033
RSN569_SANSALV_NGI180	Max	14717.6298	20587.4785
RSN569_SANSALV_NGI180	Min	-12087.8577	-18808.9058
RSN585_BAJA_CPE161	Max	12165.6099	8867.1468
RSN585_BAJA_CPE161	Min	-15876.8343	-12204.3179
RSN832_LANDERS_ABY000	Max	10239.8904	10910.7019
RSN832_LANDERS_ABY000	Min	-10997.3469	-10818.9847
RSN838_LANDERS_BRS000	Max	18495.964	12895.04
RSN838_LANDERS_BRS000	Min	-18172.318	-12680.7841
RSN1_HELENA.A_A-HMC270	Max	14107.59	5645.9414
RSN1_HELENA.A_A-HMC270	Min	-16691.2726	-6583.9846
RSN103_NCALIF.AG_D-PGS345	Max	5035.4012	10767.7037
RSN103_NCALIF.AG_D-PGS345	Min	-7674.6148	-8039.7778
RSN150_COYOTELK_G06320	Max	8540.7799	17013.3792
RSN150_COYOTELK_G06320	Min	-5805.2694	-20003.6355
RSN212_LIVERMOR_A-DVD246	Max	15221.6133	9973.2499
RSN212_LIVERMOR_A-DVD246	Min	-16863.7078	-10113.1802
RSN223_LIVERMOR_B-KOD270	Max	9095.3843	18132.9498
RSN223_LIVERMOR_B-KOD270	Min	-8643.1232	-18795.3084
RSN239_MAMMOTH.AH_A-LUL090	Max	8324.654	12251.9542
RSN239_MAMMOTH.AH_A-LUL090	Min	-6278.6936	-8666.6525
RSN240_MAMMOTH.AH_B-CVK180	Max	11857.0919	10504.1917
RSN240_MAMMOTH.AH_B-CVK180	Min	-13884.4393	-14523.9183
RSN569_SANSALV_NGI270	Max	24537.7287	14607.5397
RSN569_SANSALV_NGI270	Min	-25026.8333	-14411.5713
RSN585_BAJA_CPE251	Max	13426.095	7953.1931
RSN585_BAJA_CPE251	Min	-15861.1784	-11398.0834
RSN832_LANDERS_ABY090	Max	13737.262	14070.7326
RSN832_LANDERS_ABY090	Min	-13413.4693	-12761.5874
RSN838_LANDERS_BRS090	Max	20280.3549	15036.2378
RSN838_LANDERS_BRS090	Min	-17278.8418	-16316.8219

The plastic rotation values of all frame elements in the structure were compared with the limit values specified in the code, as defined by the equations provided above.

As a result of the calculations:

- Out of 664 beams, 256 beams (38.55%) were classified as Brittle Element, indicating that, even if the structure meets its performance target according to TBEC-2018, the shear capacities of these elements must be increased.

- 544 beams (81.92%) were found to be at the Belirgin Hasar level (BH).
- 120 beams (18.08%) remained at the Sınırlı Hasar level (SH).

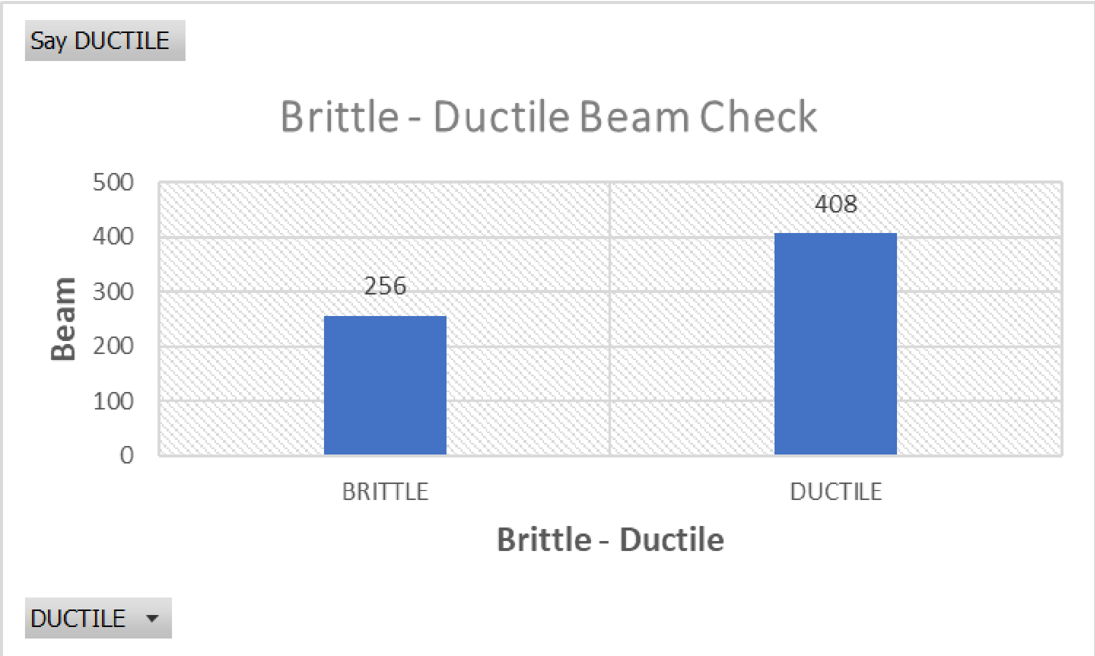

Figure 4.53: Brittle-Ductile Element Verification for Beams

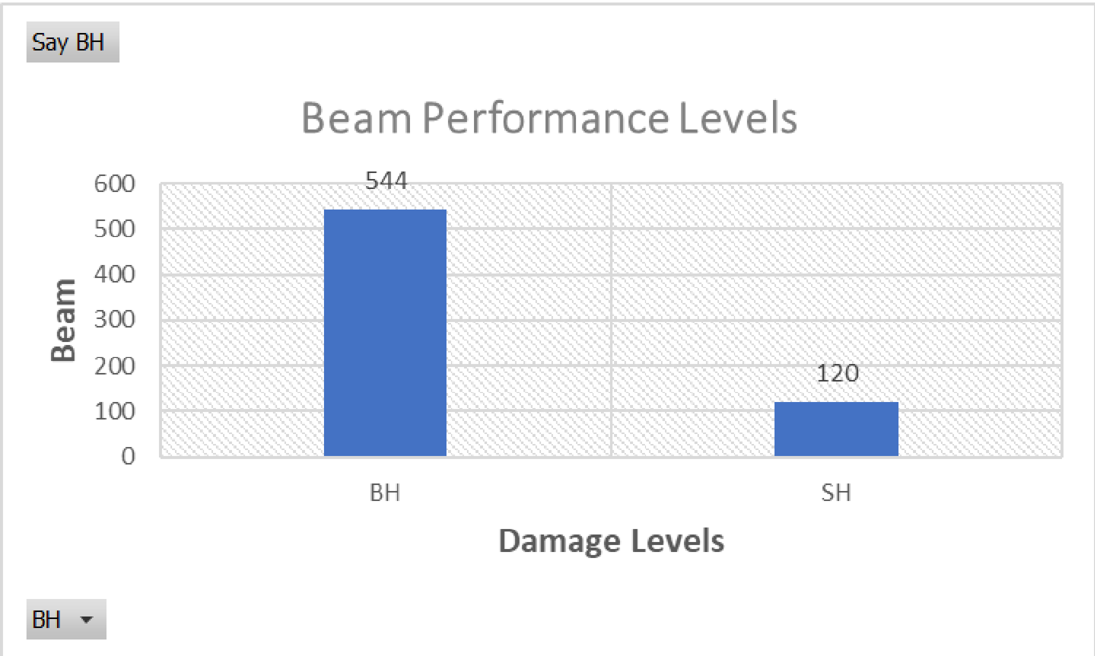

Figure 4.54: Final Performance Levels of Beam Elements

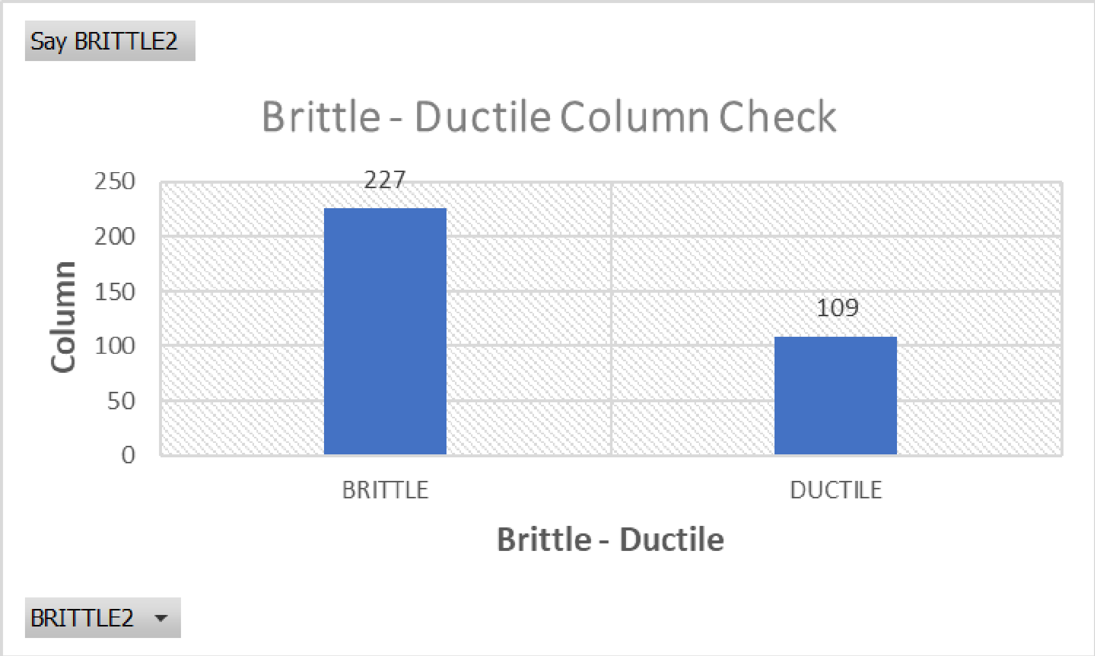

Figure 4.55: Brittle-Ductile Element Verification for Columns

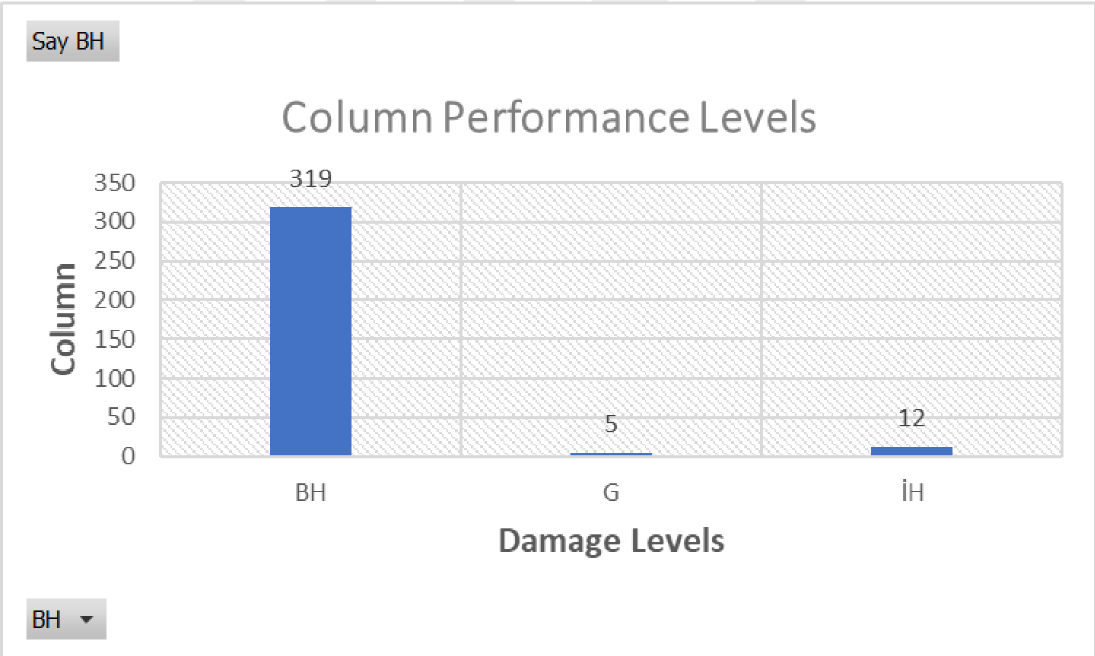

Figure 4.56: Final Performance Levels of Column Elements

As a result of the calculations performed for column elements, out of a total of 336 columns:

- 227 columns (67.55%) were classified as Brittle Element, indicating that even if the structure meets its performance target according to TBEC-2018, the shear capacities of these elements must be increased.
- 5 columns (1.48%) were classified in the Göçme Hasar level.
- 12 columns (3.57%) were classified in the İleri Hasar level (İH).
- 318 columns (94.64%) were classified in the Belirgin Hasar level (BH).

For shear walls, the strain limits corresponding to the Göçmenin Önlenmesi (GÖ) performance level were determined using the equations provided below. In shear wall elements, the strains for concrete and steel were calculated separately and compared with the relevant limit values. The strain limits for other performance levels were obtained by multiplying the values corresponding to this performance level by specific factors.

$$\varepsilon_c^{(GÖ)} = 0.0035 + 0.04\sqrt{\omega_{we}} \leq 0.018 \qquad (4.8)$$

$$\varepsilon_s^{(GÖ)} = 0.4\ \varepsilon_{su} \qquad (4.9)$$

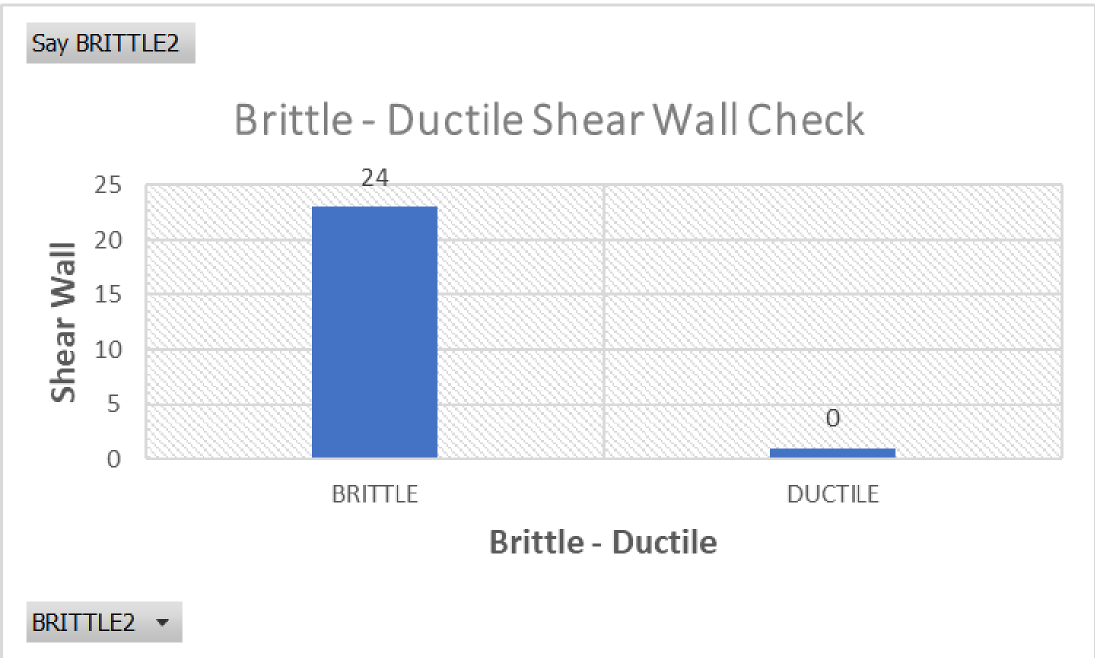

Figure 4.57: Brittle-Ductile Element Verification for Shear Walls

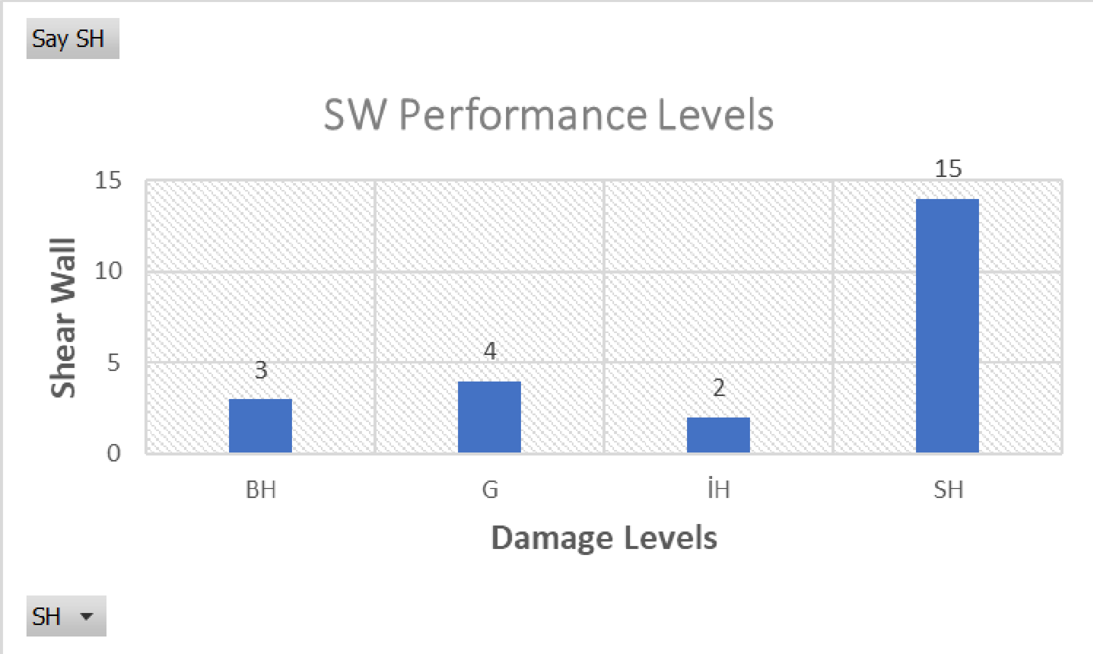

Figure 4.58: Final Performance Levels of Shear Wall Elements

As a result of the calculations performed for shear wall elements, out of a total of 24 shear walls:

- All of the shear walls (100%) were classified as Brittle Element, indicating that even if the structure meets its performance target according to TBEC-2018, the shear capacities of these elements must be increased. The main reason for this outcome is that 80.8% of the total base shear force caused by the earthquake in the X-direction, calculated as 25026 kN, is attempted to be resisted by the shear walls.
- 4 shear walls (16.6%) were classified in the Göçme Hasar level.
- 2 shear walls (8.33%) were classified in the İleri Hasar level (İH).
- 3 shear walls (12.5%) were classified in the Belirgin Hasar level (BH).

Based on these damage level results, according to TBEC-2018, the performance level of the structure is in the "Göçme" condition. Depending on the feasibility study, the appropriate course of action would be:

- Increasing the flexural capacity of the columns and strengthening the building by adding shear walls to improve rigidity.
- Considering demolition if strengthening is deemed unfeasible.

Below, the brittle element outputs and the final performance level of Structure B, analyzed considering the directivity effect, are presented along with their respective comparisons as the results.

As a result of the calculations:

- Out of 664 beams, 312 beams (46.98%) were classified as Brittle Element, indicating that, even if the structure meets its performance target according to TBEC-2018, the shear capacities of these elements must be increased.
- 549 beams (82.68%) were found to be at the Belirgin Hasar level (BH).
- 115 beams (17.31%) remained at the Sınırlı Hasar level (SH).

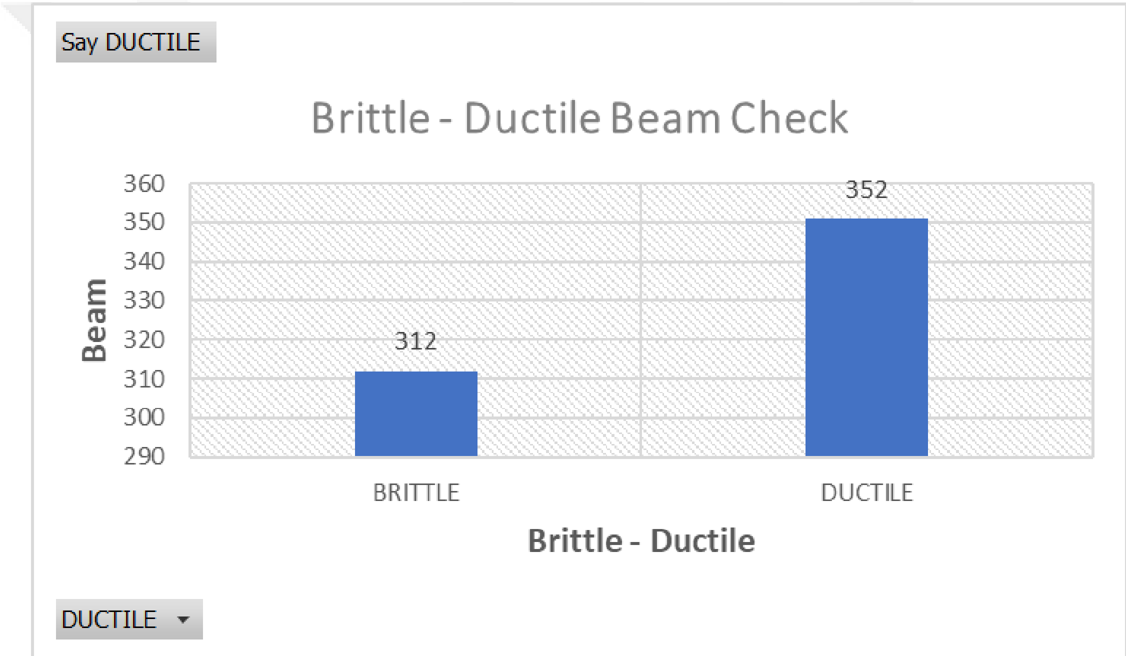

Figure 4.59: Analysis Results with Directivity Effect: Brittle-Ductile Element Verification for Beams

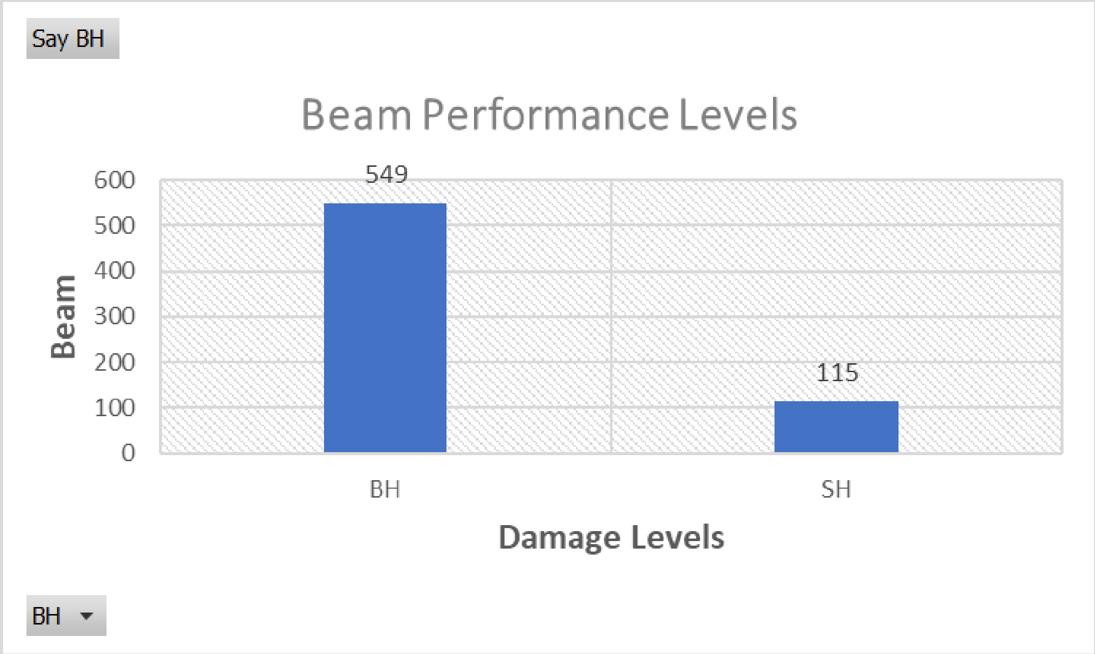

Figure 4.60: Analysis Results with Directivity Effect: Final Performance Levels of Beam Elements

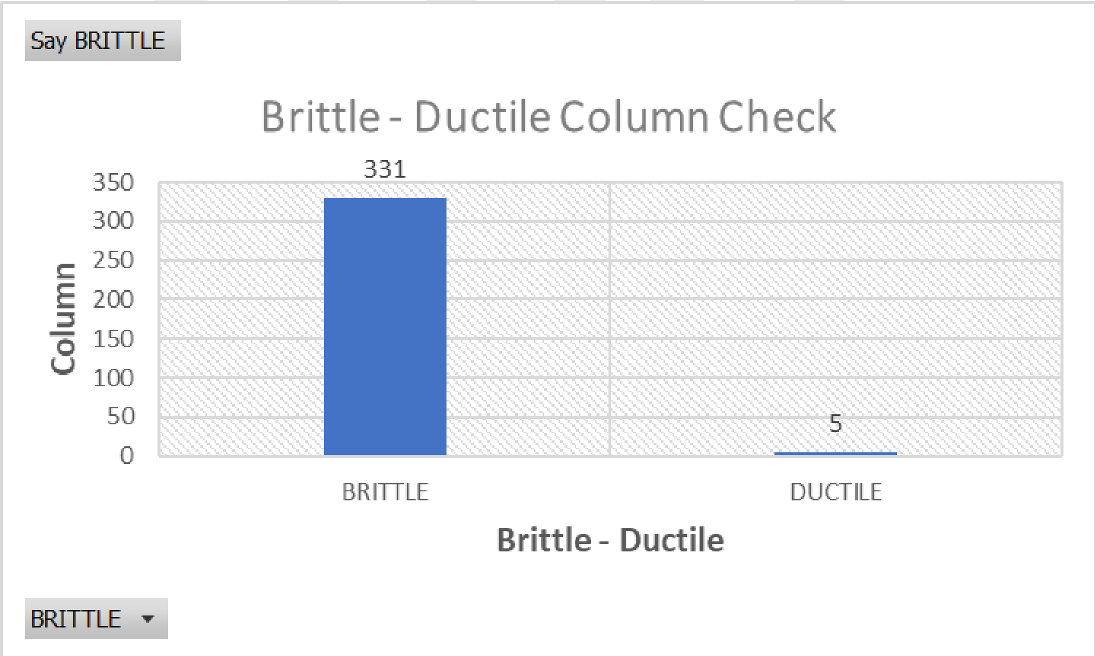

Figure 4.61: Analysis Results with Directivity Effect: Brittle-Ductile Element Verification for Columns

As a result of the calculations performed for column elements, out of a total of 336 columns:

- 331 columns (98.51%) were classified as Brittle Element, indicating that even if the structure meets its performance target according to TBEC-2018, the shear capacities of these elements must be increased.
- 25 columns (7.55%) were classified in the Göçme Hasar level.
- 32 columns (9.52%) were classified in the İleri Hasar level (İH).
- 279 columns (83.03%) were classified in the Belirgin Hasar level (BH).

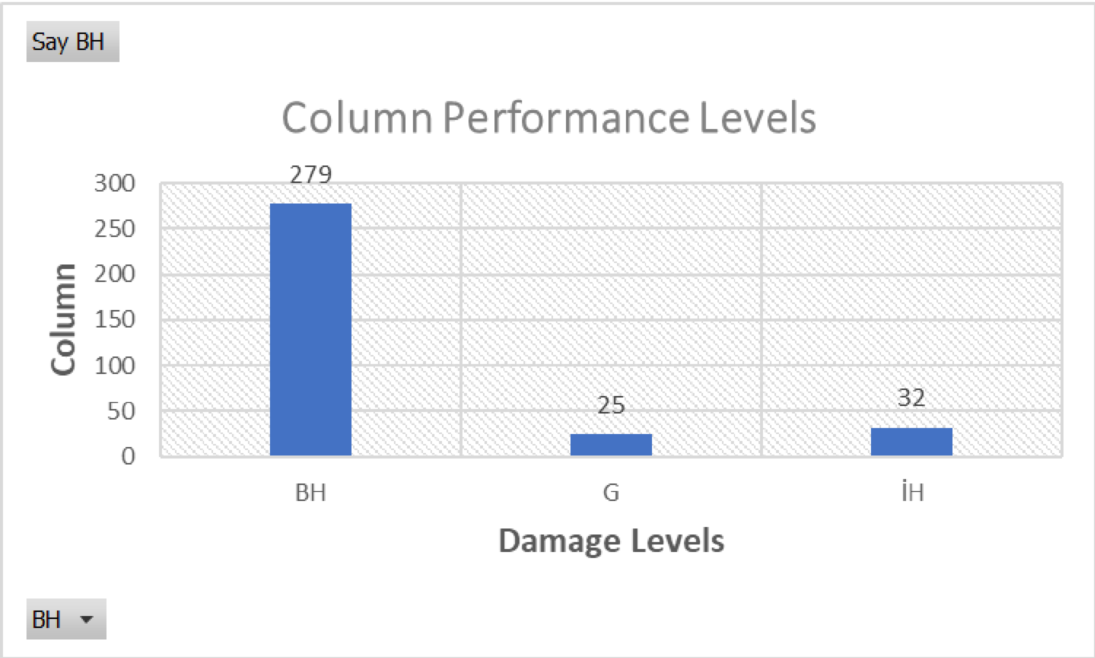

Figure 4.62: Analysis Results with Directivity Effect: Final Performance Levels of Column Elements

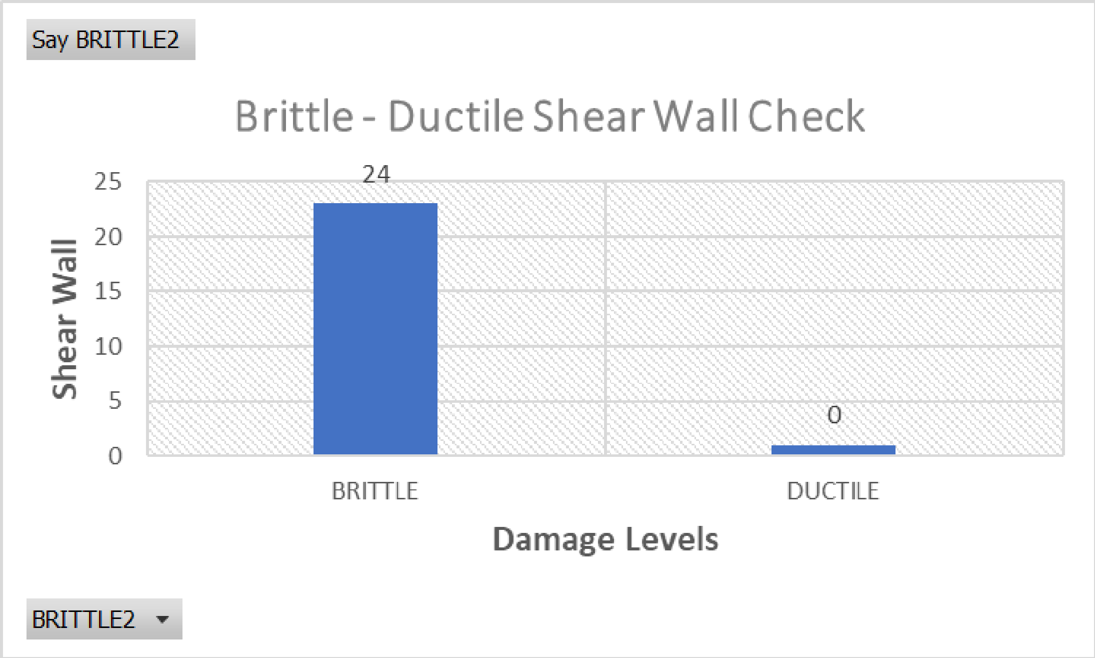

Figure 4.63: Analysis Results with Directivity Effect: Brittle-Ductile Element Verification for Shear Walls

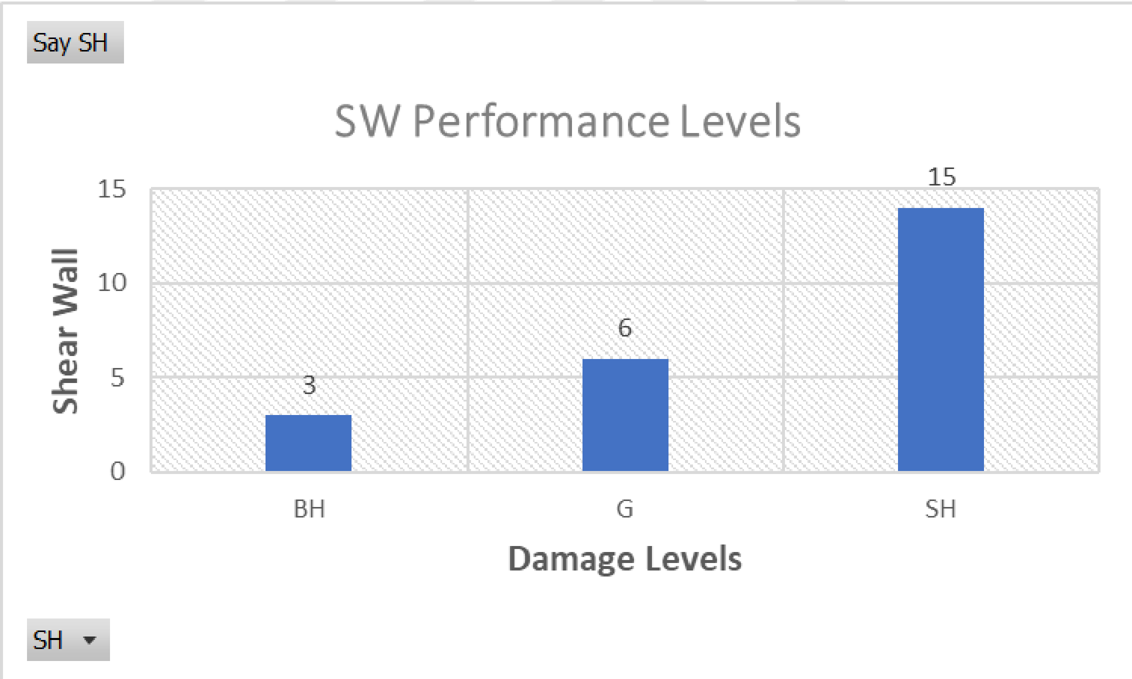

Figure 4.64: Analysis Results with Directivity Effect: Final Performance Levels of Shear Walls Elements

As a result of the calculations performed for shear wall elements, out of a total of 24 shear walls:

- All of the shear walls (100%) were classified as Brittle Element, indicating that even if the structure meets its performance target according to TBEC-2018, the shear capacities of these elements must be increased.
- 6 shear walls (25%) were classified in the Göçme Hasar level.
- 3 shear walls (12.5%) were classified in the Belirgin Hasar level (BH).

When the analysis results including the directivity effect are compared with the standard performance analysis outputs:

For Beams:

- An additional 56 beams (8.43%) were classified as brittle elements due to increased shear forces.
- 5 beams (0.77%) transitioned to the Belirgin Hasar (BH) performance level.

For Columns:

- An additional 104 columns (30.96%) were classified as brittle elements due to increased shear forces.
- 20 column (6.07%) transitioned to the Göçme damage level, and 20 columns (5.95%) transitioned to the İleri Hasar level.

For Shear Walls:

- 2 shear walls (8.4%) transitioned to the Göçme damage level.

The analysis results for Structure C – Residential Building are presented in this section. The natural vibration periods and mode shapes of the structure are provided below, **Table 4.10**.

Table 4.10: Building Natural Vibration Periods and Modal Analysis Results

Mode	Period	UX	UY	SumRZ
	sec			
1	1.945	0.0%	71.8%	2.5%
2	1.942	0.9%	2.4%	75.7%
3	1.592	72.9%	0.0%	76.6%
4	0.582	0.1%	0.0%	87.9%
5	0.552	0.0%	13.6%	87.9%
6	0.443	13.1%	0.0%	88.1%
7	0.298	0.1%	0.0%	92.9%
8	0.268	0.0%	5.2%	92.9%
9	0.207	5.5%	0.0%	93.0%
10	0.183	0.1%	0.0%	95.7%
11	0.163	0.0%	2.6%	95.7%
12	0.125	0.0%	0.0%	97.3%

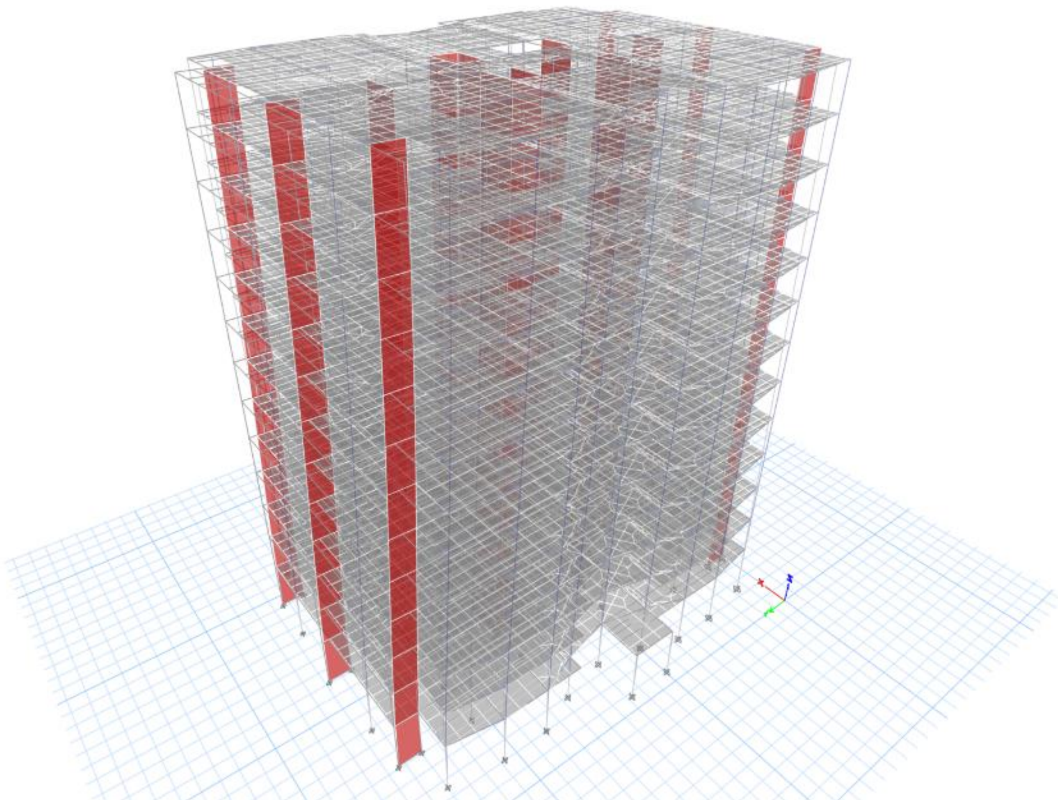

Figure 4.65: The first mode in the X-direction of the building at T= 1.945

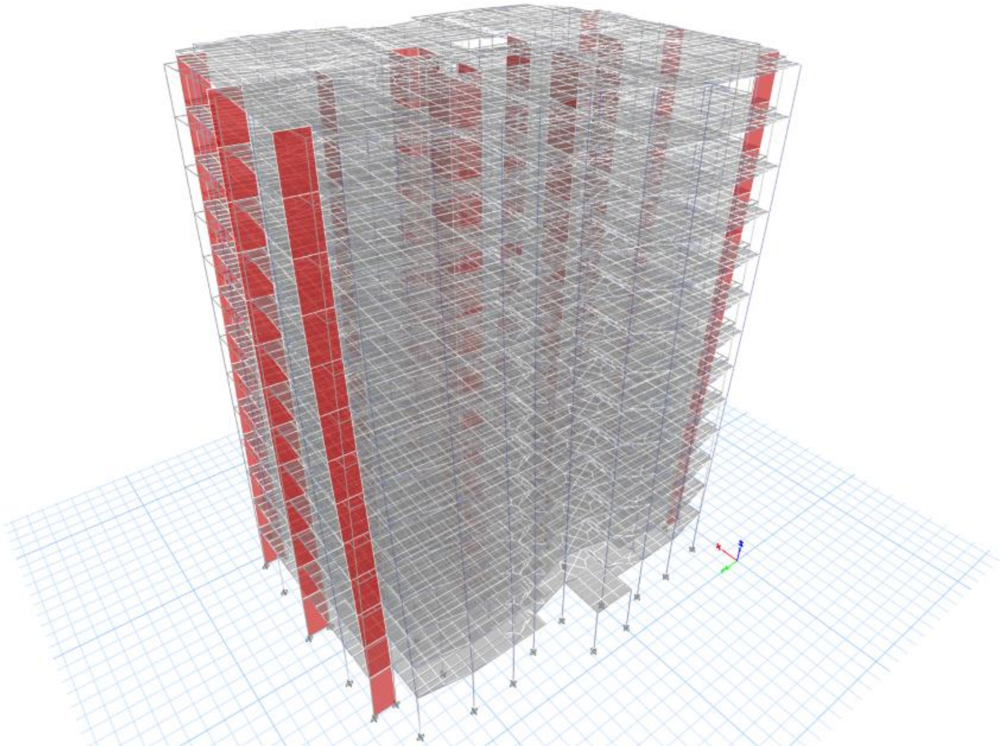

Figure 4.66: The second mode in the Z-rotation direction of the building at T = 1.941

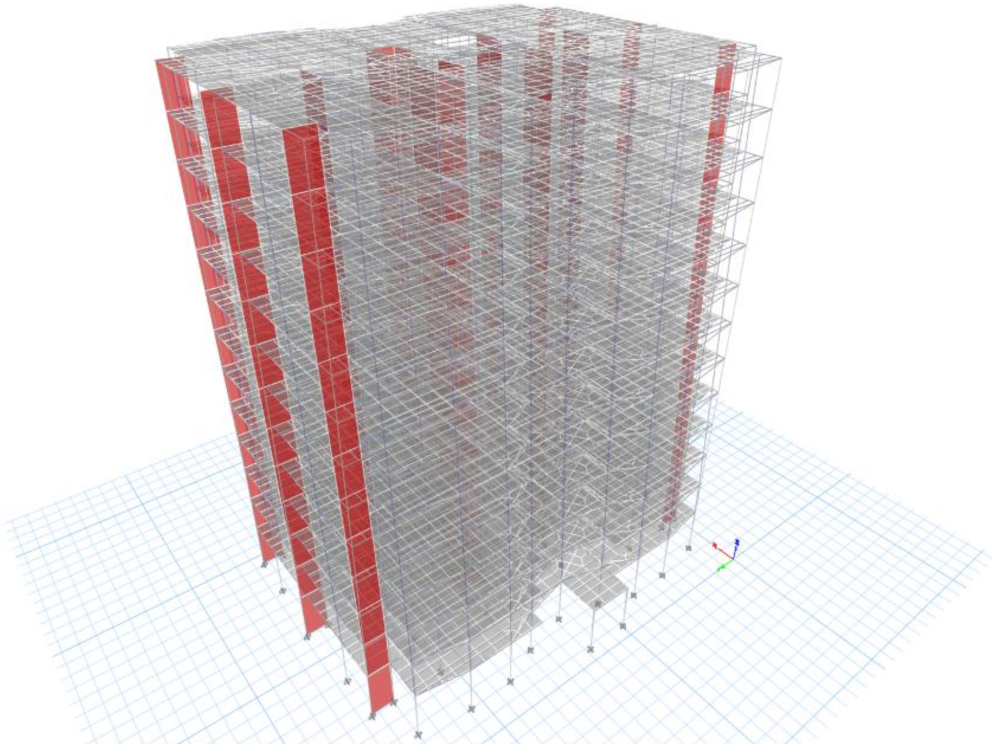

Figure 4.67: The third mode in the Y-direction of the building at T= 1.59

The displacement, inter story drifts, and base shear force values occurring in Structure A were obtained through 22 nonlinear time-history analyses performed using the analysis software. The values obtained from all earthquake records were evaluated considering the analysis outputs, and the average of the absolute maximum values from the 22 analyses were calculated.

As a result of the analysis of 11 pairs of earthquake records, the story displacement graphs obtained in the X and Y directions and their average values are presented in **Figure 4.68.**

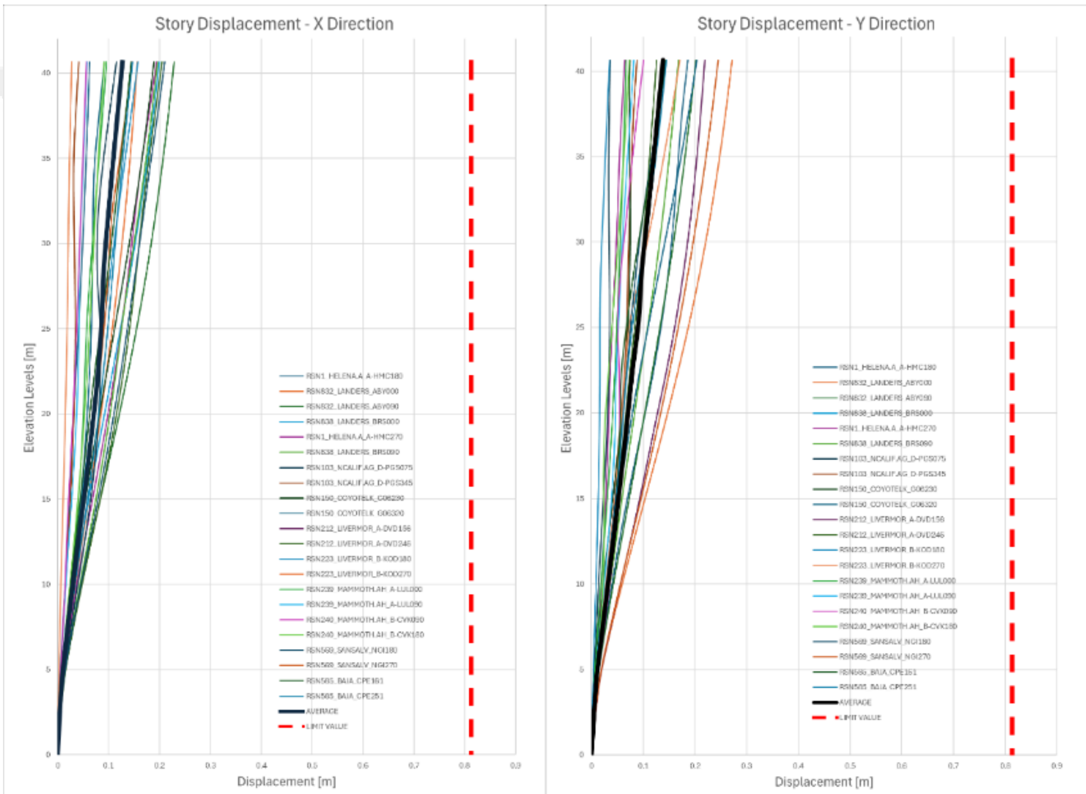

Figure 4.68: Displacement Outputs for X and Y Directions

As the average result, the peak displacement was calculated as:

0.1274/40.65 m = 0.31% in the X direction,

0.1384/40.65 m = 0.34% in the Y direction.

This result remains below the 2% limit value specified in internationally recognized codes such as FEMA 356 and ASCE 41-17.

As observed in the graphs, the structure exhibited a sudden displacement behavior between 25 and 30 meters. This change has been interpreted as a slenderness effect commonly observed in high-rise buildings.

The Inter story Drift Check for the Library Building was performed according to TBEC-2018, based on the values calculated using the following formula.

$$\frac{\delta_{i,max}^{(X)}}{h_i} \leq 0.008\,\kappa \quad (4.5)$$

As can be seen from the graphs:

- In the X direction, the average value remains below the limit, but the maximum value almost exceeds the limit in this direction, **Figure 4.69.**
- In the Y direction, the average value remains below the limit, but the maximum value exceeds the limit in this direction as well, **Figure 4.70.**

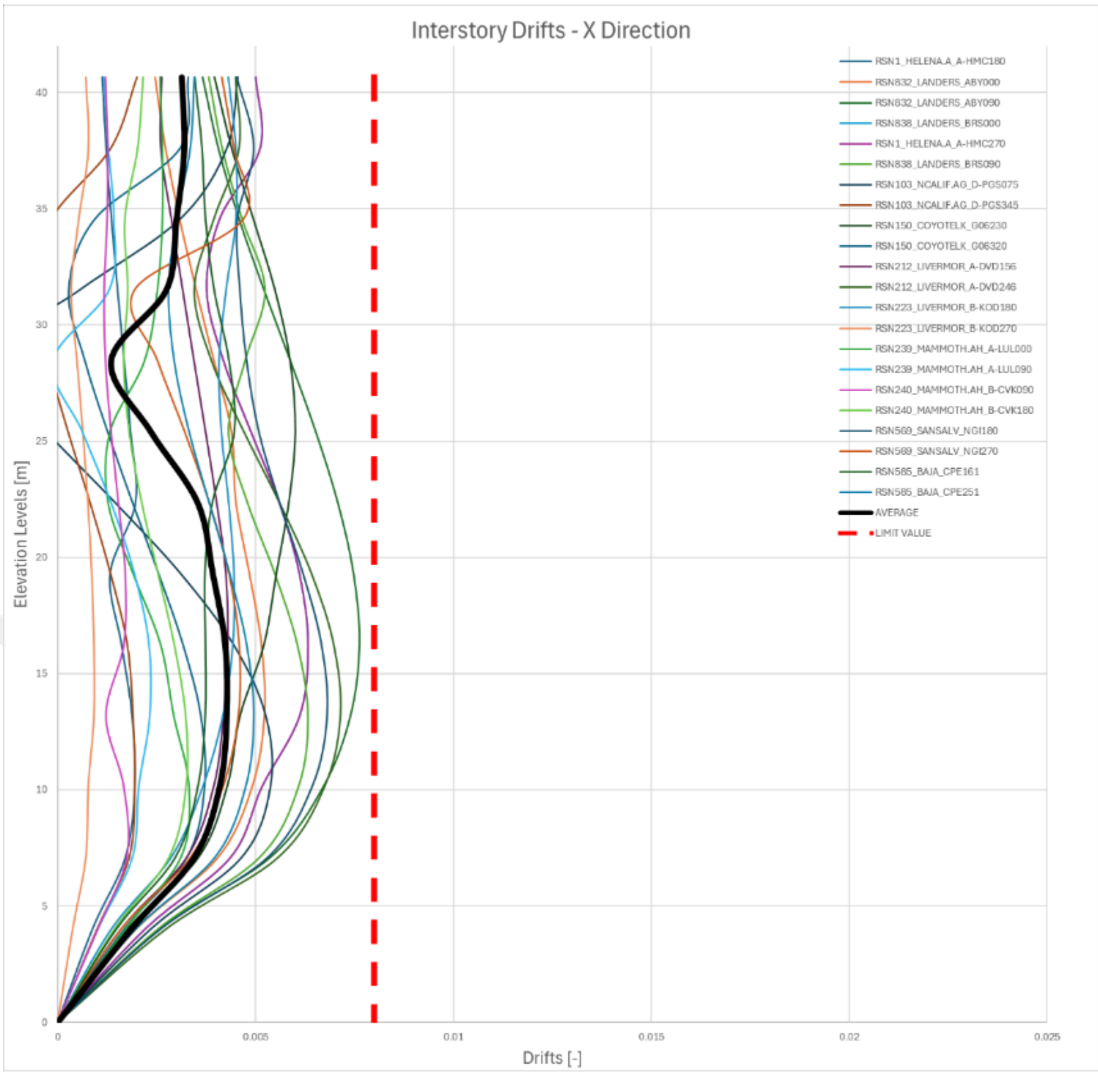

Figure 4.69: Inter story Drift Check for the X Direction

Another observation from the graph is that the first story height is 4.05 meters, while the upper stories have a height of 3.05 meters. This indicates that the building exhibits B2 – Stiffness Irregularity Between Adjacent Stories (Soft Story) as defined in TBEC-2018.

Similar to the displacement graphs, the interstory drift graphs also show a sudden change in the structure's behavior between 25 and 30 meters in height. This phenomenon has been interpreted as an effect of slenderness in high-rise buildings.

The base shear forces are provided in Table 4.11, and upon examining these results, it is observed that the highest base shear force values occurred under the influence of the "RSN 212 – Livermore 01" earthquake.

When analyzing the acceleration records of the 11 pairs of earthquakes, it was determined that the highest peak ground acceleration (PGA) values among all scaled ground motions were 0.74g and 0.96g, recorded during the "RSN 240 – Mammoth Lakes – 04" earthquake.

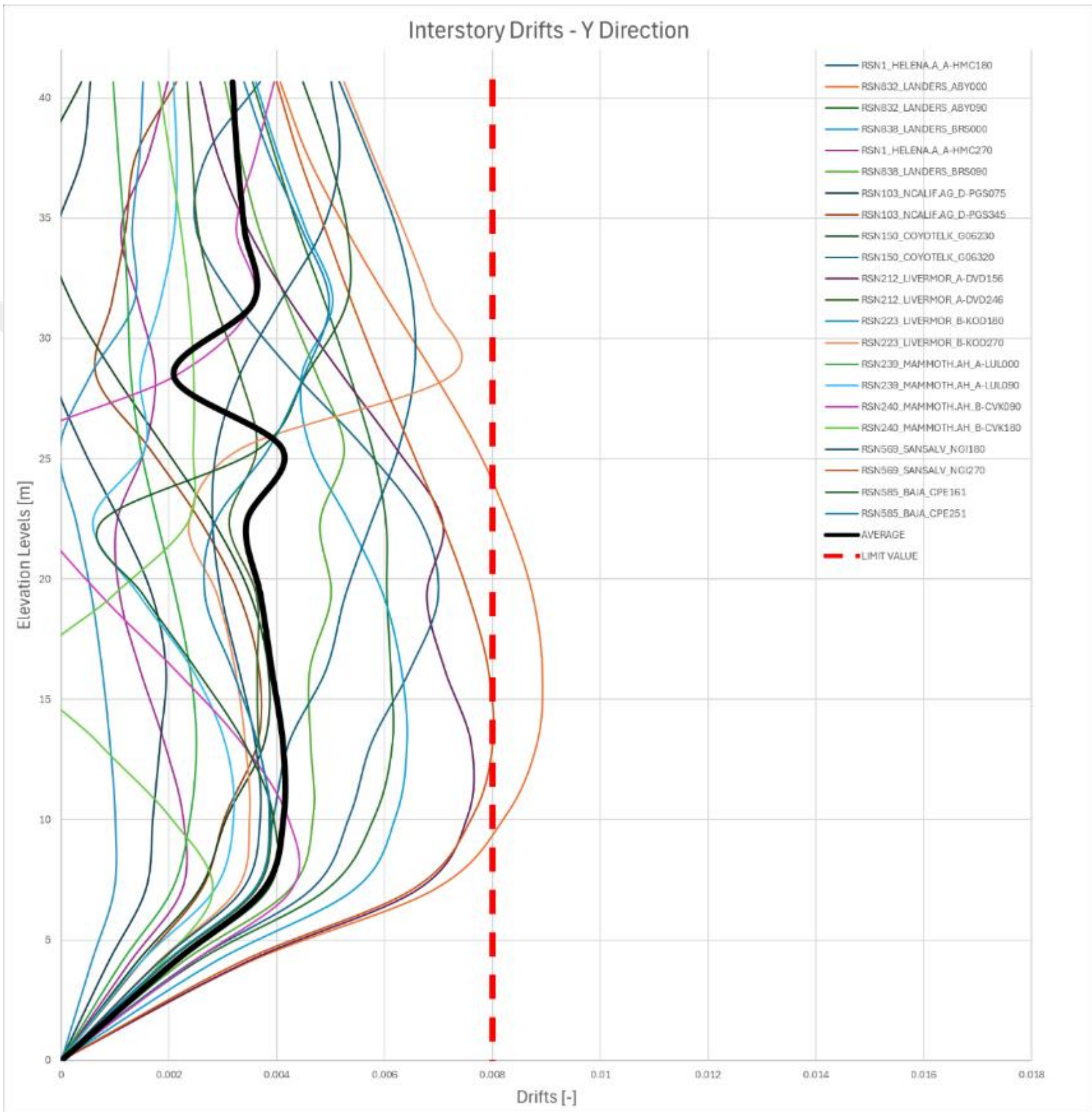

Figure 4.70: Inter story Drift Check for the Y Direction

The inconsistency between the base shear forces results and the earthquake acceleration records may indicate that the structure experienced a resonance condition under the " RSN 212 – Livermore 01" earthquake. This phenomenon can be validated by applying the Fast Fourier Transform (FFT) method to decompose the acceleration record in the time domain into its frequency components and comparing them with the structure's natural frequency.

The plastic hinge rotation values in frame elements were compared with the limit values specified in TBEC-2018 to assess the damage levels.

For columns and beams, the plastic hinge rotation limits corresponding to Göçmenin Önlenmesi (GÖ) were determined using the equations provided below. The limits for other performance levels are obtained by multiplying these values by specific factors relative to this performance level.

$$\theta_P^{(GÖ)} = \frac{2}{3}\left[(\phi_u - \phi_y)L_p\left(1 - 0.5\frac{L_p}{L_s}\right) + 4.5\,\phi_u\,d_b\right] \quad (4.6)$$

$$\theta_P^{(KH)} = 0.75\,\theta_P^{(GÖ)} \quad (4.7)$$

Table 4.11: Base Shear Forces in X and Y Directions from All Time History Analyses

Earthquake Name		X - Direction	Y - Direction
		[kN]	[kN]
RSN1_HELENA.A_A-HMC180	Max	9159.7355	9623.0274
RSN1_HELENA.A_A-HMC180	Min	-6592.3731	-14836.0309
RSN103_NCALIF.AG_D-PGS075	Max	24088.7343	4389.136
RSN103_NCALIF.AG_D-PGS075	Min	-26142.3831	-6293.5069
RSN150_COYOTELK_G06230	Max	14256.7966	6218.405
RSN150_COYOTELK_G06230	Min	-17629.6591	-9170.3701
RSN212_LIVERMOR_A-DVD156	Max	16114.7623	17519.1677
RSN212_LIVERMOR_A-DVD156	Min	-15612.0502	-20145.7451
RSN223_LIVERMOR_B-KOD180	Max	12818.825	3976.6961
RSN223_LIVERMOR_B-KOD180	Min	-12699.9311	-4550.8316
RSN239_MAMMOTH.AH_A-LUL000	Max	20743.511	7612.915
RSN239_MAMMOTH.AH_A-LUL000	Min	-19531.0572	-7900.0757
RSN240_MAMMOTH.AH_B-CVK090	Max	10937.3533	12021.2599
RSN240_MAMMOTH.AH_B-CVK090	Min	-12648.596	-17812.9861
RSN569_SANSALV_NGI180	Max	23571.9885	12387.8005
RSN569_SANSALV_NGI180	Min	-24566.8945	-12046.2673
RSN585_BAJA_CPE161	Max	14366.251	12594.0979
RSN585_BAJA_CPE161	Min	-14258.0702	-14282.1215
RSN832_LANDERS_ABY000	Max	18599.7658	19227.4501
RSN832_LANDERS_ABY000	Min	-14349.3804	-18916.3502
RSN838_LANDERS_BRS000	Max	15739.8818	17152.2371
RSN838_LANDERS_BRS000	Min	-17219.3196	-15848.113
RSN1_HELENA.A_A-HMC270	Max	22319.0203	7914.0976
RSN1_HELENA.A_A-HMC270	Min	-18721.3849	-8723.7919
RSN103_NCALIF.AG_D-PGS345	Max	10226.7982	10822.1982
RSN103_NCALIF.AG_D-PGS345	Min	-11782.9235	-9859.313
RSN150_COYOTELK_G06320	Max	13294.6218	10628.2441
RSN150_COYOTELK_G06320	Min	-17807.5489	-12025.6871
RSN212_LIVERMOR_A-DVD246	Max	26261.1146	10113.4902
RSN212_LIVERMOR_A-DVD246	Min	-23486.0281	-12428.9299
RSN223_LIVERMOR_B-KOD270	Max	4306.0374	11437.1094
RSN223_LIVERMOR_B-KOD270	Min	-3394.2127	-12893.2767
RSN239_MAMMOTH.AH_A-LUL090	Max	9485.6208	9324.8135
RSN239_MAMMOTH.AH_A-LUL090	Min	-11828.0013	-9522.6992
RSN240_MAMMOTH.AH_B-CVK180	Max	14761.5539	15562.1973
RSN240_MAMMOTH.AH_B-CVK180	Min	-12385.5313	-12460.3146
RSN569_SANSALV_NGI270	Max	14302.6608	19761.5867
RSN569_SANSALV_NGI270	Min	-13736.6451	-18759.8486
RSN585_BAJA_CPE251	Max	19063.7164	12228.2131
RSN585_BAJA_CPE251	Min	-20298.0463	-10447.5421
RSN832_LANDERS_ABY090	Max	22717.6919	13920.4633
RSN832_LANDERS_ABY090	Min	-20889.7713	-13155.2124
RSN838_LANDERS_BRS090	Max	24712.8788	13801.6363
RSN838_LANDERS_BRS090	Min	-20462.1883	-11212.5711

The plastic rotation values of all frame elements in the structure were compared with the limit values specified in the code, as defined by the equations provided above.

As a result of the calculations:

- Out of 1095 beams, 208 beams (18.99%) were classified as Brittle Element, indicating that, even if the structure meets its performance target according to TBEC-2018, the shear capacities of these elements must be increased.
- 56 beams (5.11%) were classified in the Göçme Hasar level.
- 9 beams (0.81%) were classified in the İleri Hasar level (İH).
- 805 beams (73.51%) were found to be at the Belirgin Hasar level (BH).

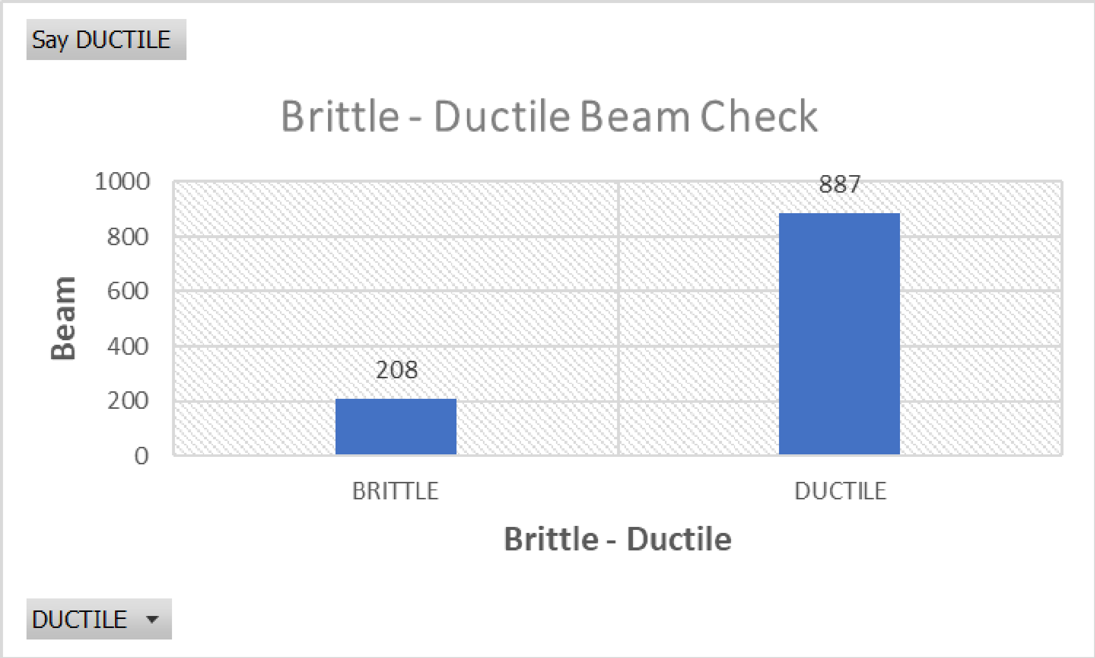

Figure 4.71: Brittle-Ductile Element Verification for Beams

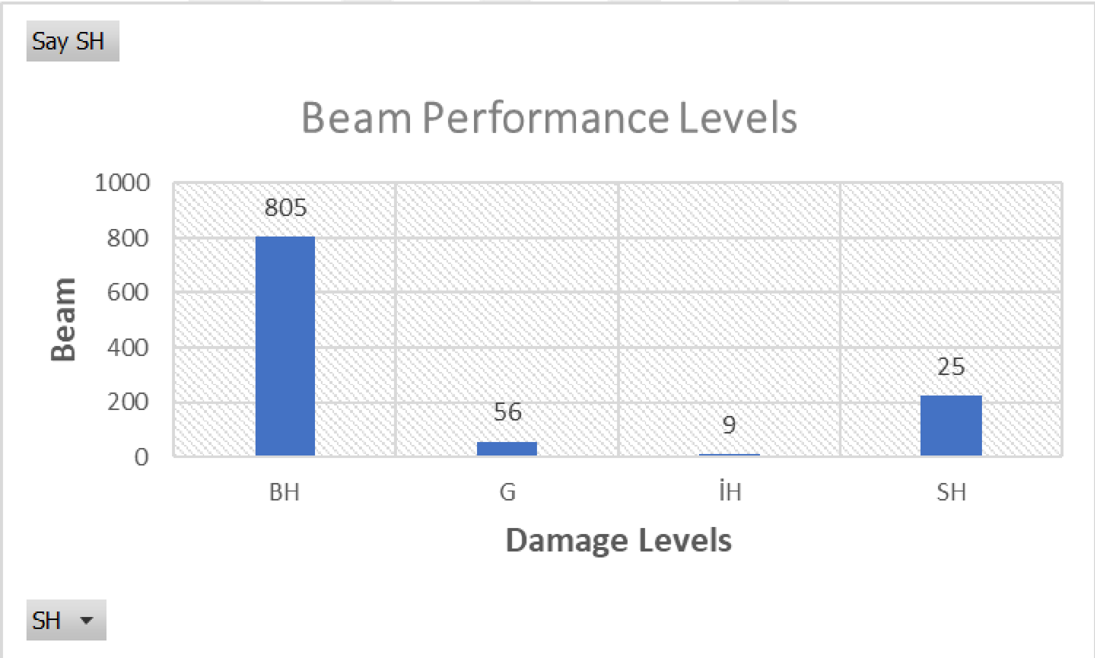

Figure 4.72: Final Performance Levels of Beam Elements

As a result of the calculations performed for column elements, out of a total of 470 columns:

- All 470 columns exhibited Ductile behavior in accordance with TBEC-2018 and did not require any additional increase in shear capacity.
- 410 columns (87.23%) were classified in the Belirgin Hasar level (BH).
- 60 column (12.76%) remained at the Sınırlı Hasar level (SH).

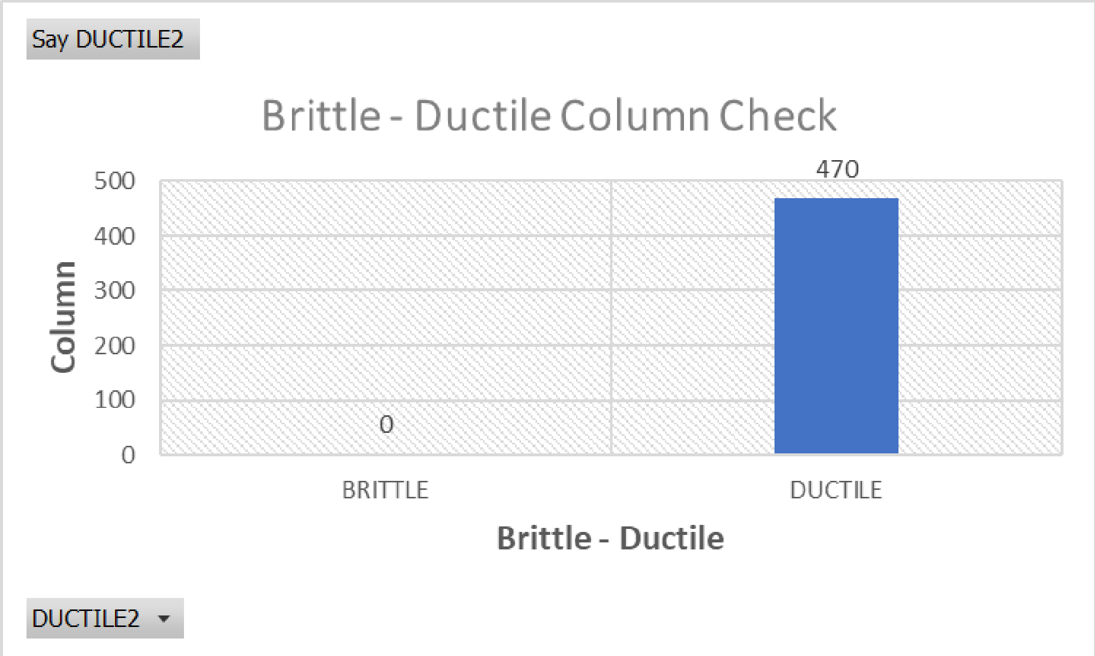

Figure 4.73: Brittle-Ductile Element Verification for Columns

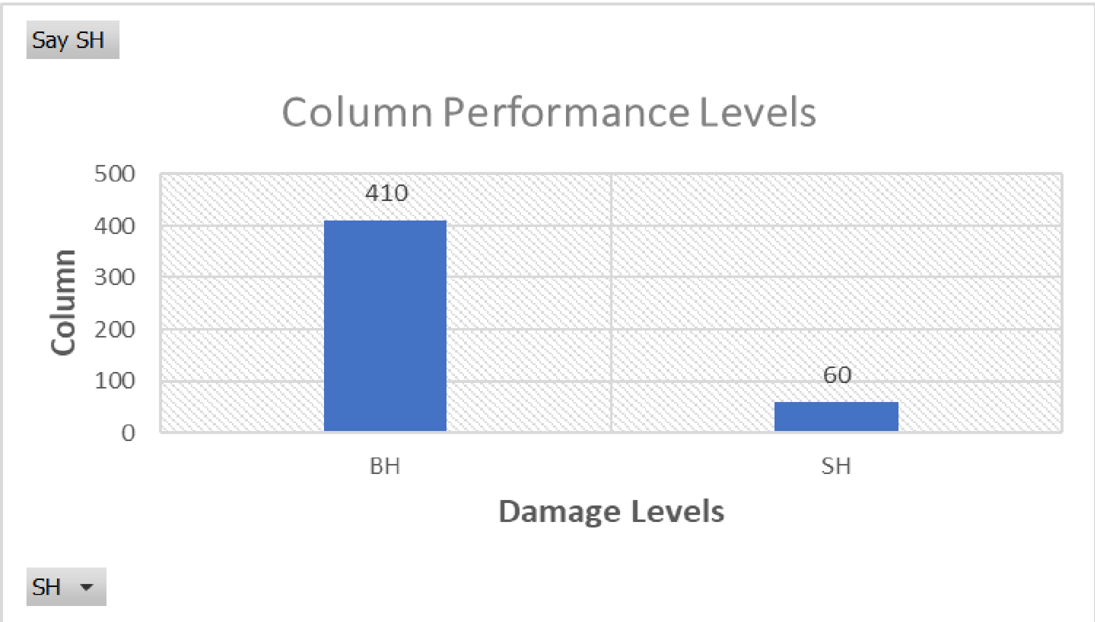

Figure 4.74: Final Performance Levels of Column Elements

For shear walls, the strain limits corresponding to the Göçmenin Önlenmesi (GÖ) performance level were determined using the equations provided below. In shear wall elements, the strains for concrete and steel were calculated separately and compared with the relevant limit values. The strain limits for other performance levels were obtained by multiplying the values corresponding to this performance level by specific factors.

$$\varepsilon_c^{(GÖ)} = 0.0035 + 0.04\sqrt{\omega_{we}} \leq 0.018 \qquad (4.8)$$

$$\varepsilon_s^{(GÖ)} = 0.4\ \varepsilon_{su} \qquad (4.9)$$

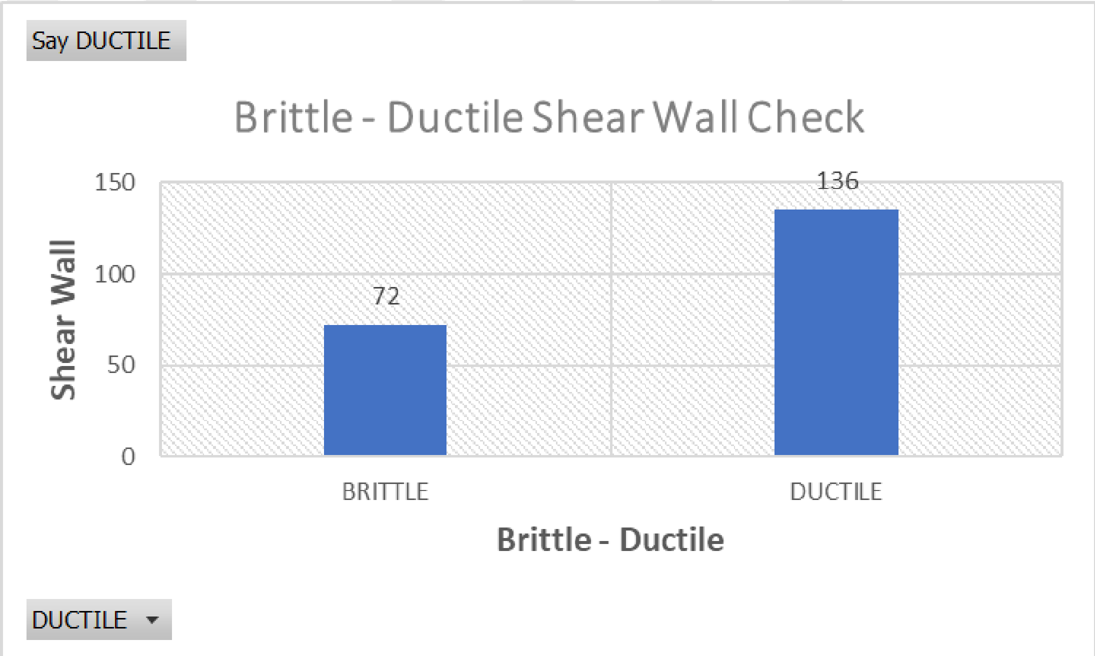

Figure 4.75: Brittle-Ductile Element Verification for Shear Walls

As a result of the calculations performed for shear wall elements, out of a total of 208 shear walls:

- 72 shear walls (34.61%) were classified as Brittle Element, indicating that even if the structure meets its performance target according to TBEC-2018, the shear capacities of these elements must be increased.
- 5 shear walls (2.4%) were classified in the İleri Hasar level (İH).
- 14 shear walls (6.7%) were classified in the Belirgin Hasar level (BH).

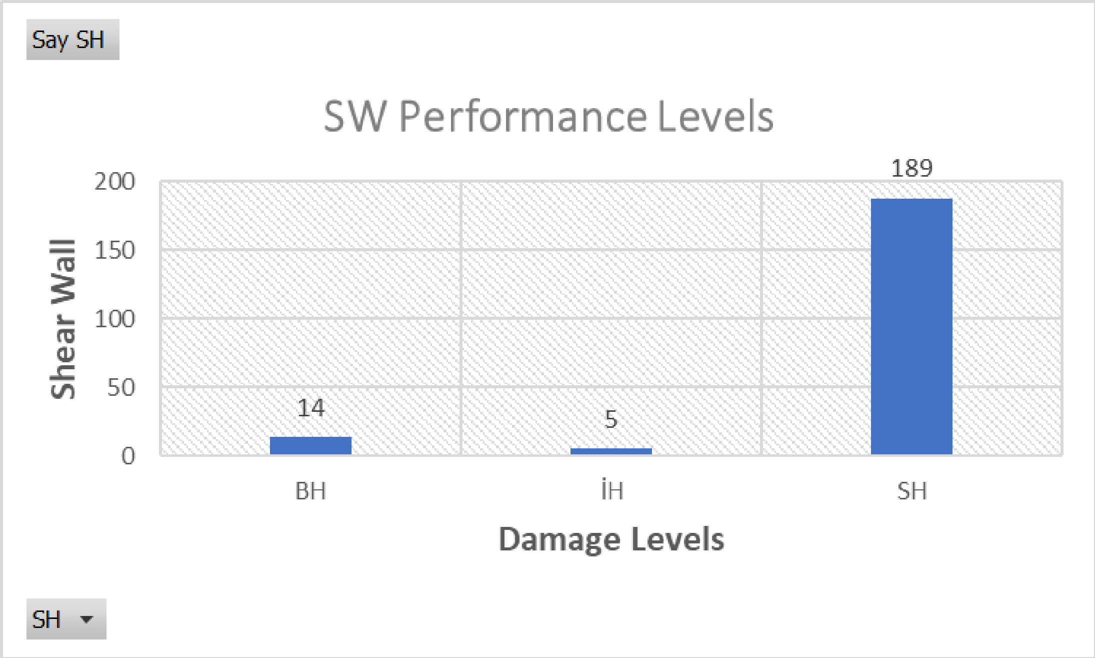

Figure 4.76: Final Performance Levels of Shear Wall Elements

Based on these damage level results, according to TBEC-2018, the performance level of the structure is in the "Göçme" condition. However, for this specific building, although it is classified under the "Göçme" condition, the structure can continue its service life at the "Kontrollü Hasar" performance level through a strengthening intervention limited to the beams.

Below, the brittle element outputs and the final performance level of Structure C, analyzed considering the directivity effect, are presented along with their respective comparisons as the results.

As a result of the calculations:

- Out of 1095 beams, 275 beams (25.11%) were classified as Brittle Element, indicating that, even if the structure meets its performance target according to TBEC-2018, the shear capacities of these elements must be increased.
- 921 beams (84.10%) were found to be at the Belirgin Hasar level (BH).
- 115 beams (10.50%) remained at the Sınırlı Hasar level (SH).
- 21 beams (1.91%) were classified in the Göçme Hasar level.
- 3 beams (0.27%) were classified in the İleri Hasar level (İH).

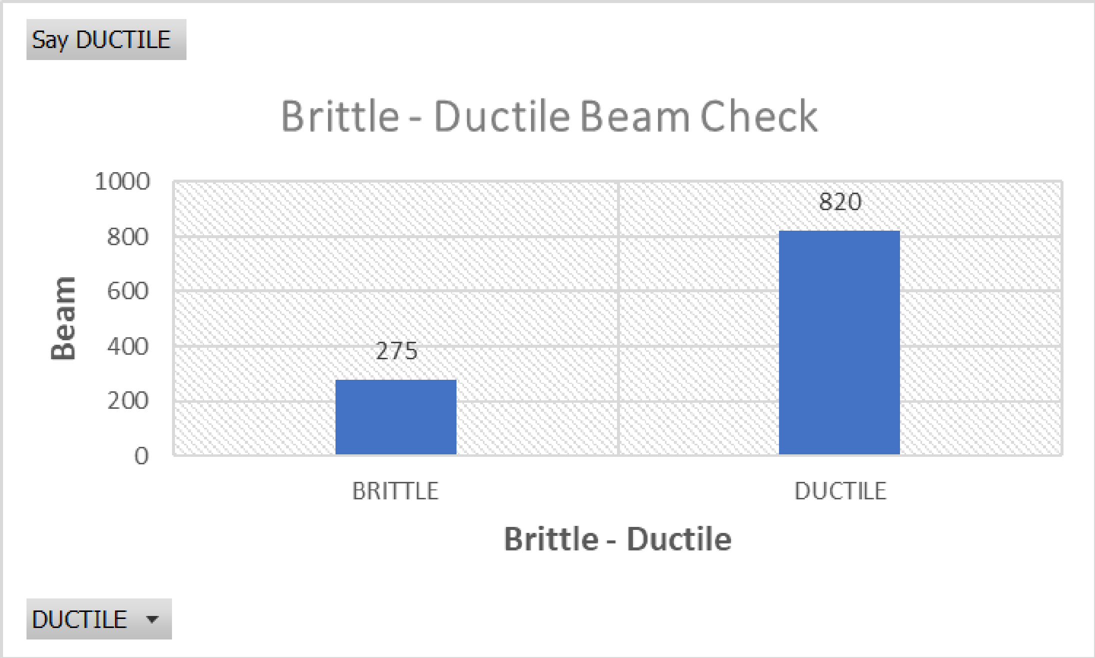

Figure 4.77: Analysis Results with Directivity Effect: Brittle-Ductile Element Verification for Beams

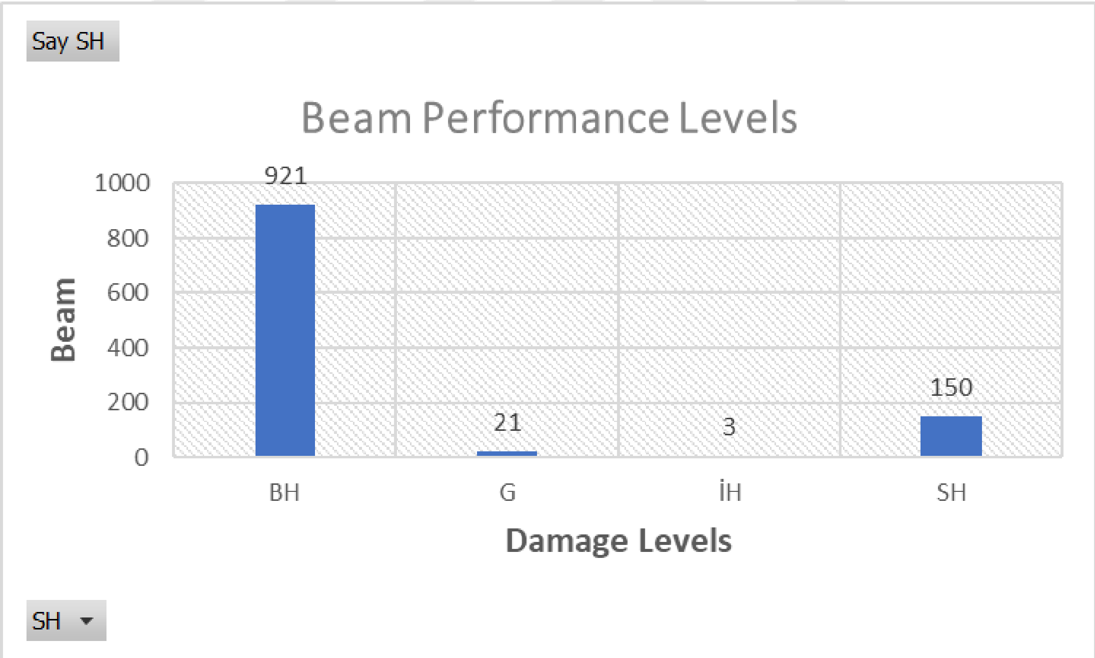

Figure 4.78: Analysis Results with Directivity Effect: Final Performance Levels of Beam Elements

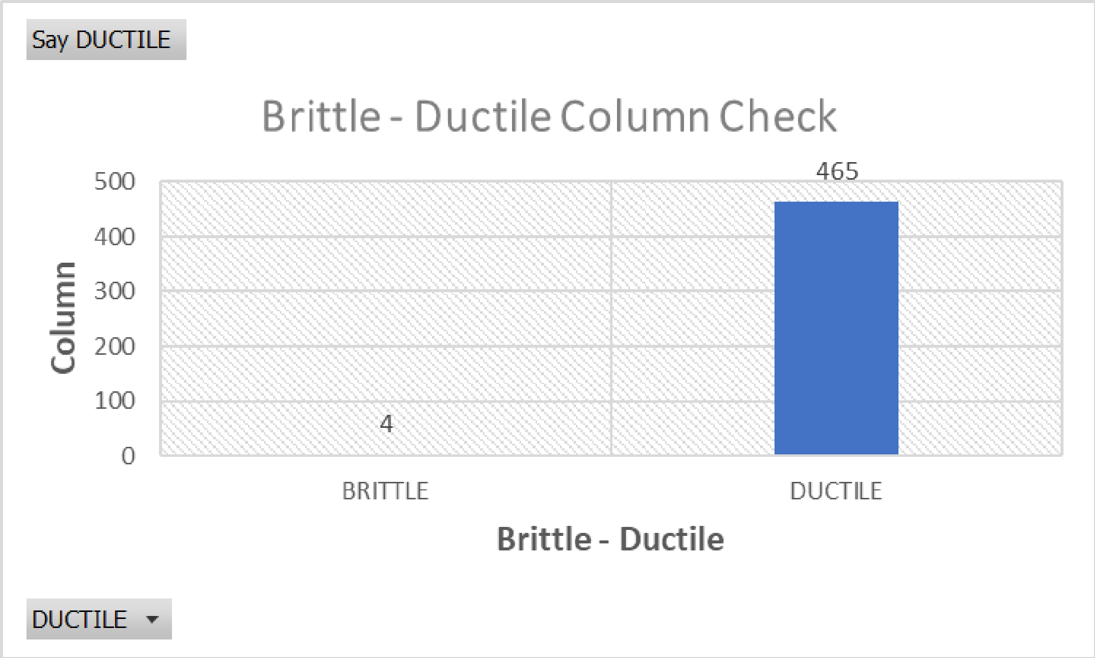

Figure 4.79: Analysis Results with Directivity Effect: Brittle-Ductile Element Verification for Columns

As a result of the calculations performed for column elements, out of a total of 470 columns:

- 4 columns (0.85%) were classified as Brittle Element, indicating that even if the structure meets its performance target according to TBEC-2018, the shear capacities of these elements must be increased.
- 410 columns (87.23%) were classified in the Belirgin Hasar level (BH).
- 60 beams (12.76%) remained at the Sınırlı Hasar level (SH).

As a result of the calculations performed for shear wall elements, out of a total of 208 shear walls:

- 81 shear walls (38.34%) were classified as Brittle Element, indicating that even if the structure meets its performance target according to TBEC-2018, the shear capacities of these elements must be increased.
- 16 shear walls (7.69%) were classified in the İleri Hasar level (İH).
- 7 shear walls (3.36%) were classified in the Belirgin Hasar level (BH).

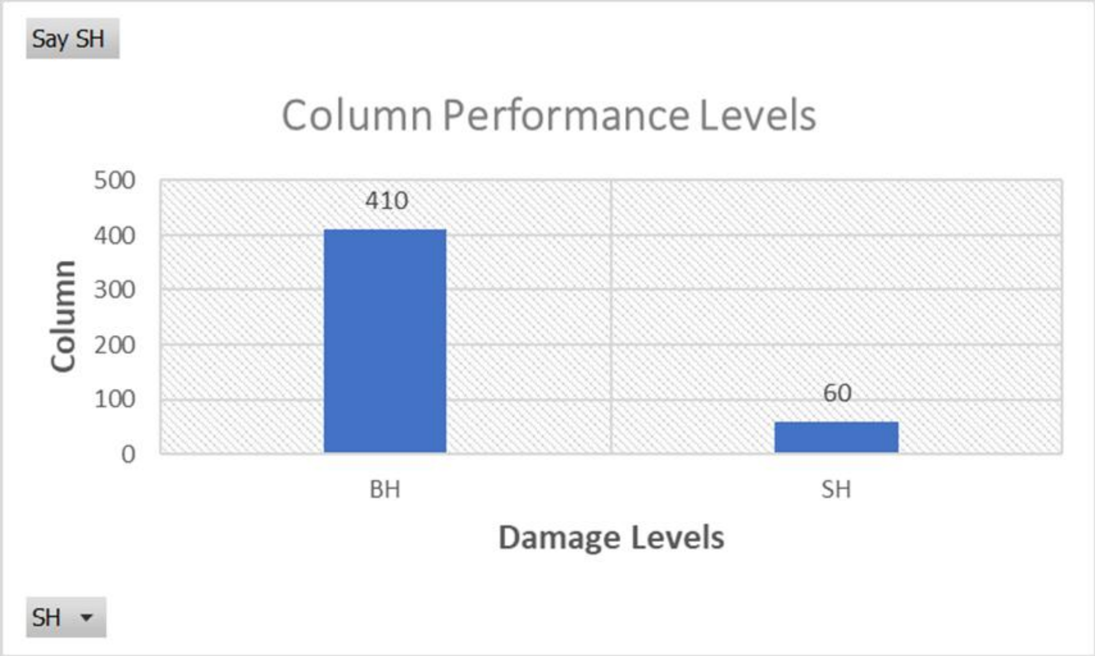

Figure 4.80: Analysis Results with Directivity Effect: Final Performance Levels of Column Elements

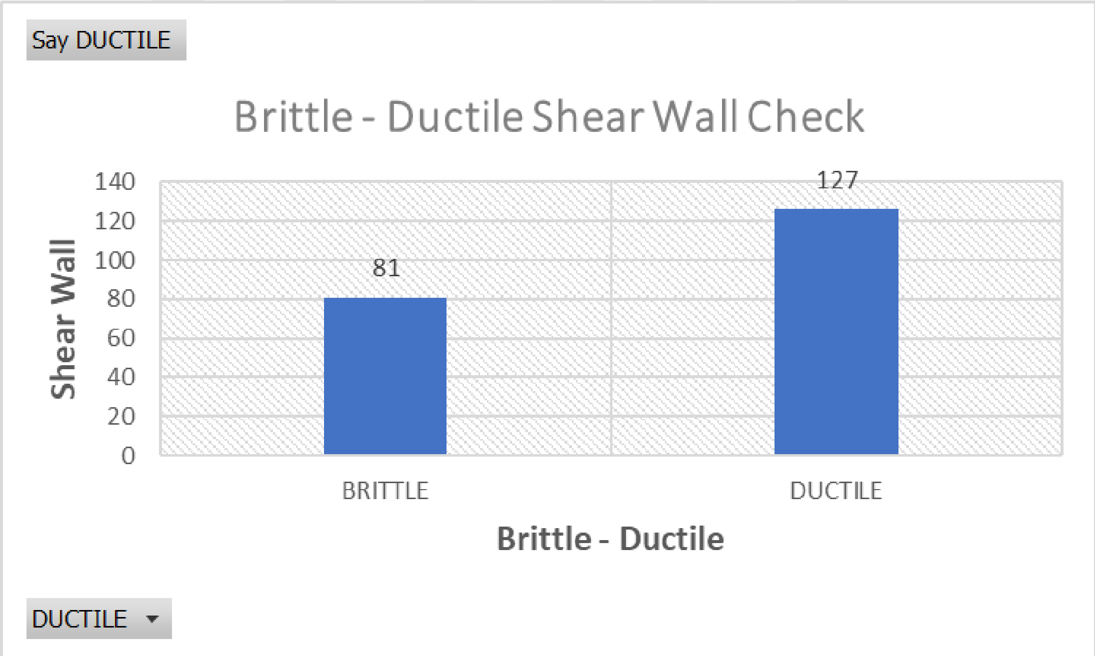

Figure 4.81: Analysis Results with Directivity Effect: Brittle-Ductile Element Verification for Shear Walls

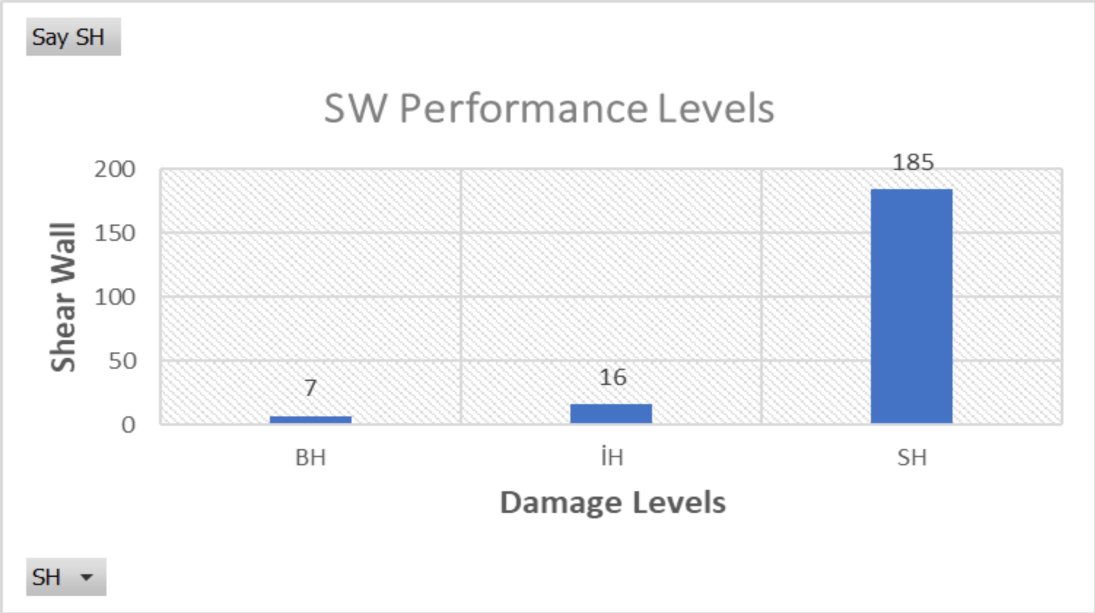

Figure 4.82: Analysis Results with Directivity Effect: Final Performance Levels of Shear Walls Elements

When the analysis results including the directivity effect are compared with the standard performance analysis outputs:

For Beams:

- An additional 67 beams (6.12%) were classified as brittle elements due to increased shear forces.
- At the Göçme Hasar level, 35 beams and 6 beams from the İleri Hasar level (İH) region have transitioned to the Belirgin Hasar level (BH) and Sınırlı Hasar level (SH), respectively.

For Columns:

- An additional 4 columns (0.85%) were classified as brittle elements due to increased shear forces.
- There has been no change in the performance levels.

For Shear Walls:

- An additional 9 shear walls (3.73%) were classified as brittle elements due to increased shear forces.
- 11 shear walls (5.29%) transitioned to the İleri Hasar level.

5. RESULTS

A literature review has revealed that there is seismic gap and uncertainty within the MOFZ fault zone, and that additional geophysical studies are required to resolve this uncertainty.

Although the local soil classification was provided as "ZD" in the reviewed articles, data obtained from AFAD's accelerometer records indicated that the actual soil classification should be "ZC", and the study was conducted based on this revised classification.

A probabilistic seismic hazard analysis (PSHA) was carried out using AFAD's earthquake catalog and the AFEAD fault map prepared for Eurasia. The results were compared with the DD-2 design spectrum derived for a selected location in Malatya city center, and the earthquakes were scaled according to the design spectrum.

Specifically, a higher acceleration response was obtained beyond the spectral period of 1.0 seconds, which may lead to inaccurate results in the design and assessment of high-rise buildings. Therefore, it would be appropriate to update the Interactive Seismic Hazard Map of Turkey—currently based on the latest MTA active fault map—in light of new fault data to be acquired through updated geophysical investigations.

The literature review also indicated that directional effects influenced earthquake records by an average of 13% due to local soil conditions. Based on this finding, the earthquake records were amplified accordingly.

For the building performance assessment analysis, 3 reinforced concrete building models were created in the selected analysis software based on the obtained data, and a load analysis was performed.

The developed building models were subjected to time-history functions, and an analysis was conducted.

As a result of the analysis, it was determined that for Structure A;

- The building exhibited a soft-story problem.
- The building was classified at the Göçme (G) performance level.

- The fact that the peak ground acceleration (PGA) acting on the structure and the maximum base shear force observed in the building originate from different earthquake loadings initially suggests the occurrence of a resonance effect.

In future studies, this phenomenon can be validated by applying the Fast Fourier Transform (FFT) method to decompose the acceleration record in the time domain into its frequency components and comparing them with the structure's natural frequency. In addition, implementing a strengthening intervention would be beneficial.

As is the case with the majority of the building stock in Turkey, this issue has also influenced the structural behavior of this building and has indirectly played a role in reducing its seismic performance. For this reason, revisions should be made to the current code provisions and legal regulations.

As a result of the analysis, it was determined that for Structure B;

- There is an existing building of this type of structure; however, two additional stories were virtually added to align it with the mid-rise building category. In fact, this scenario reflects a common issue observed particularly in the Anatolian region of Turkey, where unauthorized floor or mass additions are frequently made to existing buildings. Such modifications have adversely contributed to the structure being classified at the Göçme (G) performance level.

- Although the columns of the structure comply with the minimum dimensional requirements of current seismic codes, the low concrete strength of 10 MPa (C10) has significantly limited the shear capacity of the columns.

- Particularly on the lower floors, the columns along the longer façade have exceeded their shear capacities under unsymmetrical shear demands and were identified as brittle elements. This indicates that vertical members, while strong in one direction, can rapidly reach the "Göçme" mode when constructed with low concrete strength.

In buildings with this type of architectural layout, utilizing symmetric vertical load-bearing systems in both directions will lead to more reliable and structurally efficient outcomes.

As a result of the analysis, it was determined that for Structure C;

- The high-rise building, which has a higher concrete strength class compared to the other two buildings, exhibited better performance in terms of shear resistance.
- The fact that the building was designed with nearly equal number of reinforced concrete shear walls in both principal directions in plan contributed positively to its structural behavior and performance levels.
- Although the structure was classified at the Collapse performance level, continued use may be possible through a strengthening intervention focused on the beam elements.
- The sudden change observed between 25 and 30 meters in both displacement and interstory drift demands further investigation in future studies.

When comparing member performance levels at each structure, it was observed that as the number of stories increases, the influence of directivity effects becomes more evident. However, it was concluded that a well-configured structural system and the use of high-strength concrete can help mitigate this effect.

REFERENCES

Abrahamson, N. A., Silva, W. J., & Kamai, R. (2014). Summary of the ASK14 ground motion relation for active crustal regions. *Earthquake Spectra*, *30*(3), 1025–1055. https://doi.org/10.1193/070913EQS198M

Aochi, H., & Madariaga, R. (2003). The 1999 I ˙ zmit, Turkey, Earthquake: Nonplanar Fault Structure, Dynamic Rupture Process, and Strong Ground Motion. In *Bulletin of the Seismological Society of America* (Vol. 93, Issue 3).

Baker, J. W. (2007). Quantitative classification of near-fault ground motions using wavelet analysis. *Bulletin of the Seismological Society of America*, *97*(5), 1486–1501. https://doi.org/10.1785/0120060255

Baker, J. W. (2011). Conditional Mean Spectrum: Tool for Ground-Motion Selection. *Journal of Structural Engineering*, *137*(3), 322–331. https://doi.org/10.1061/(asce)st.1943-541x.0000215

Boore, D. M., Stewart, J. P., Seyhan, E., & Atkinson, G. M. (2014). NGA-West2 equations for predicting PGA, PGV, and 5% damped PSA for shallow crustal earthquakes. *Earthquake Spectra*, *30*(3), 1057–1085. https://doi.org/10.1193/070113EQS184M

Chiou, B. S. J., & Youngs, R. R. (2014). Update of the Chiou and Youngs NGA model for the average horizontal component of peak ground motion and response spectra. *Earthquake Spectra*, *30*(3), 1117–1153. https://doi.org/10.1193/072813EQS219M

Kohrangi, M., Vamvatsikos, D., & Bazzurro, P. (2019). Pulse-like versus non-pulse-like ground motion records: Spectral shape comparisons and record selection strategies. *Earthquake Engineering and Structural Dynamics*, *48*(1), 46–64. https://doi.org/10.1002/eqe.3122

Mavroeidis, G. P., & Papageorgiou, A. S. (2003). A Mathematical Representation of Near-Fault Ground Motions. In *Bulletin of the Seismological Society of America* (Vol. 93, Issue 3).

Moghimi, S., & Akkar, S. (2017). Effect of major seismological parameters on directivity dominant spectral amplification (COMPDYN 2017). *COMPDYN 2017 - Proceedings of the 6th International Conference on Computational Methods in Structural Dynamics and Earthquake Engineering*, *2*, 4509–4526. https://doi.org/10.7712/120117.5741.18397
Önal, M., & Ceylan, Ç. (2020). Correlations Between SPT, PMT and MASW on Quaternary Alluvial - Fluvial Sediments in Battalgazi, Malatya, Turkey. *NATURENGS MTU Journal of Engineering and Natural Sciences, Malatya Turgut Ozal University*, *1*(2), 39–53. https://doi.org/10.46572/nat.2020.15

Somerville, P. G., Smith, N. F., Graves, R. W., Services, W.-C. F., & Abrahamson, N. A. (n.d.). *Modification of Empirical Strong Ground Motion*

Attenuation Relations to Include the Amplitude and Duration Effects of Rupture Directivity.

Vassiliou, M. F., & Makris, N. (2011). Estimating time scales and length scales in pulselike earthquake acceleration records with wavelet analysis. *Bulletin of the Seismological Society of America*, *101*(2), 596–618. https://doi.org/10.1785/0120090387

Yıldız, D. Y., Coşkun, N. D., Uz, V., İssi, A., & Uz, B. (2023). Geological, petrographical, mineralogical, geochemical and gemological features of Malatya rubies. *Gospodarka Surowcami Mineralnymi / Mineral Resources Management*, *39*(4), 141–156. https://doi.org/10.24425/gsm.2023.148162

Yıldız, Ö. (2022). Seismic site characterization of Battalgazi in Malatya, Turkey. *Arabian Journal of Geosciences*, *15*(9). https://doi.org/10.1007/s12517-022-10170-x

Zelenin, E., Bachmanov, D., Garipova, S., Trifonov, V., & Kozhurin, A. (2022). The Active Faults of Eurasia Database (AFEAD): the ontology and design behind the continental-scale dataset. *Earth System Science Data*, *14*(10), 4489–4503. https://doi.org/10.5194/essd-14-4489-2022

BIOGRAPHY

Furkan KANLI is a civil engineer who graduated from Istanbul Kültür University with a focus on earthquake-resistant reinforced concrete structures. He has gained extensive experience in structural design, seismic assessment, and retrofit strategies through various roles in both consultancy firms and research institutions. Currently, he works at Orient Research Consulting Engineers, where he is responsible for structural analysis, retrofit design, and reporting in line with Turkish and American standards. Previously, he contributed to the seismic evaluation of existing structures at the Earthquake Engineering and Disaster Management Institute of Istanbul Technical University. In addition to his freelance projects involving residential structural design, he has worked on metro infrastructure and industrial building projects at firms such as Yapı Akademisi and Smart BIM Engineering. With strong analytical skills and proficiency in software like ETABS, SAP2000, and AutoCAD, Furkan continues to deliver resilient and code-compliant engineering solutions.

PUBLICATIONS AND PRESENTATIONS FROM THE THESIS

International Congress of New Horizons in Sciences, December 07, 2024 - December 08, 2024, İstanbul